Ligands Designed for Ruthenium Nitrosyl Transport

by

Carol F. Fortney

BS, University of Pittsburgh, 1998

MS, University of Pittsburgh, 2003

Submitted to the Graduate Faculty of

Arts and Sciences in partial fulfillment

of the requirements for the degree of

Doctor of Philosophy

University of Pittsburgh

2007

UNIVERSITY OF PITTSBURGH

FACULTY OF ARTS AND SCIENCES

This dissertation was presented

by

Carol F. Fortney

It was defended on

April 25, 2007

and approved by

Dr. David H. Waldeck, Professor, Department of Chemistry

Dr. Stéphane Petoud, Assistant Professor, Department of Chemistry

Dr. Catalina Achim, Assistant Professor, C. M. U. Department of Chemistry

Dissertation Advisor: Dr. Bodie E. Douglas, Professor Emeritus, Department of Chemsitry

Carol F. Fortney, PhD

University of Pittsburgh, 2007

Since the award of the Nobel Prize for the discovery that endothelium-derived relaxing factor is nitric oxide, there has been an enormous amount of research into its role in other physiological processes. Nitric oxide has been shown to be involved in neurotransmission, respiration and fighting infection, among many other functions. While nitric oxide is essential to life, its overproduction can be deadly. For example, toxic shock results from overproduction of nitric oxide during infection and can cause a fatal drop in blood pressure. Since many of nitric oxide's biological functions involve iron complexes, our initial goals were to investigate iron complexes that might be used as nitric oxide scavengers.

Since nitric oxide is also inhibits the growth of certain types of tumors, we are interested in developing ruthenium nitrosyl complexes that can transport nitric oxide to a tumor site and release NO photolytically. This document describes the preparation and characterization of several bis-carboxamido bis-pyridyl and bis-carboxamido bis-pyrazyl ligands. The deprotonated carboxamido group is expected to activate the RuNO moiety to photolytic loss of nitric oxide and then stabilize the ruthenium-solvent complex that remains after photolysis. The pyridyl/pyrazyl groups will enforce chelation. Systematic variation of the ligand backbone will provide insight into the factors that govern photolytic loss of nitric oxide. Characterization of some of the respective ruthenium nitrosyl complexes is discussed.

TABLE OF CONTENTS

LIST OF TABLES

LIST OF FIGURES

LIST OF SCHEMES

ACKNOWLEDGMENTS

I would like to express my gratitude to the chemistry department for providing the opportunity and resources for me to continue this research after Professor Shepherd passed away. Also, I would like to thank, Professor Bodie Douglas who stepped out of retirement to become my advisor. Along with committee members David Waldeck and Stéphane Petoud, Dr. Douglas provided the support and direction I needed to complete this degree. I am also grateful to Professor Catalina Achim for becoming a committee member on very short notice and to Professor Claudia Turro who kindly provided access to her photolysis instruments.

There are many others, in the department and outside of the department, whom I wish to thank for their assistance and encouragement. Some of those in the department are Professors George Bandik, Stephen Weber, Ken Jordan, Rob Coalson and Gilbert Walker. I could not have made it through the more challenging times without Professor Shepherd's sister and brother-in-law, Sandra and Bob Slates, and Professor Shepherd's good friends, Fu-Tyan and Fu-Mei Lin.

This dissertation is dedicated to the memory of Professor Rex E. Shepherd.

1.0 GENERAL INTRODUCTION

1.1 BACKGROUND RESEARCH

This introduction provides a background for the research discussed in this document. Much additional early work, also well directed toward current research goals, is reviewed in the appendix.

It is well established that the nitrosyl moiety, whether NO^+, $NO^\bullet$, or NO^-, is sensitive to the nature of the central metal and to the coordination environment,[1-4] and that the nitrosyl group exerts an influence on the reactivity of other ligands.[4-9] However, the factors that control nitrosyl behavior are incompletely understood. As a step toward designing ruthenium nitrosyl compounds intended for use in photodynamic therapy[10-12] and for use as antiviral agents,[13] we have prepared some ligands to help elucidate effects of the coordination environment on ruthenium-bound NO.

Related studies of ruthenium nitrosyl complexes include $[Ru(NO^+)]^{3+}$ and $[Ru^{II}(NO^+)Cl]^{2+}$ coordinated to *N*-(hydroxyethyl)ethylenediamine triacetate ($hedta^{3-}$),[14,15] bipyridine,[16,17] dipyridylamine,[18,19] imidazole donors,[20] peptide ligands such as diglycylhistidine and gly-gly-gly = triglycine,[21] the π-donating macrocycle dioxocyclam[22] (dioxocyclam = 1,4,8,11-tetraazacylcotetradecane-5,7-dione), methylated biimidazole[16] donors and the antitumor

agent bleomycin.[23] Studies that have lead to the current strategy of using tetradentate π-donors to facilitate photolytic loss of $NO^{\bullet}$ are reviewed briefly.

The investigation of ruthenium nitrosyl polyaminopolycarboxylates, including $[Ru^{II}(NO^{+})(hedta^{3-})]$ [($hedta^{3-}$ = *N*-(hydroxyethyl)ethylenediaminetriacetate)], provided the first comparison of $Ru^{II}NO^{+}$, $Ru^{II}NO^{\bullet}$, and $Ru^{II}NO^{-}$ complexes that have identical secondary ligand fields and a constant oxidation state for the central metal.[14] The thorough investigation of the $[Ru(NO)]^{3+}$ complex of bleomycin revealed that bleomycin's coordination preference depends on the metal's d^n count, as well as on the π-acceptor nature and the hydrogen bonding capacity of NO^{+} or its replacement. The study also illustrated that ruthenium nitrosyl agents can be tuned for cell selectivity.[23,24]

Studies of the different structural isomers[15] of $[Ru^{II}(NO^{+})(hedta)(H_2O)]$ showed that two nitrogen π-donating ligands cis to the nitrosyl group push electron density onto the nitrosyl moiety. Increased electron density on the nitrosyl group is evidenced by a decrease in the NO stretching frequency, an effect which has been correlated with a propensity to lose NO by photolysis.[13,24-27] Because amido groups also facilitate cell transport,[28-33] peptides such as triglycine (gly-gly-gly) and diglycylhistidine (gly-gly-his) were investigated as amido donor ligands.[21] Gly-gly-gly coordination to $[Ru(NO)Cl_3(H_2O)_2]$ occurred through the terminal amine and the amido group only at pH = 8.22. With gly-gly-his, 70 % of the coordination was due to the histidyl group, 20 % was due to the histidyl and amido chelate, and 10 % coordinated through the amine and the amido group at the gly-gly end of gly-gly-his. One conclusion from the peptide investigations was that, even though peptides are desirable ligands that can be tailored to target specific cell types, the ligands' failure to chelate fully under physiological conditions diminishes their potential as ligands for NO transport. If peptides are to be used as

transporter ligands, they may have to be connected to synthetic chelates at the Ru(NO) center via biocompatible linkers.

Since multiple coordination to peptides was found to be disfavored below pH = 7, the viability of the dioxocyclam (dioxocyclam = 1,4,8,11 -tetraazacyclotetradecane-5,7-dione) ligand[22] was investigated. The hypothesis was that the macrocyclic dioxocyclam ligand would enforce the desired bis-amine/bis-amide chelation. The [Ru(NO)(dioxocyclam)Cl] compound induced lower ν_{NO} (1845 cm^{-1}) than did the tetra-amino $[Ru(NO)(cyclam)]^{2+}$ (ν_{NO} = 1875 cm^{-1})[34] (cyclam = 1,4,8,11- tetraazacyclotetradecane), an effect that illustrates the significant shift of electron density to NO by the amido groups in dioxocyclam. This study provided additional evidence that amido ligands activate the nitrosyl group. The dioxocyclam complex, like that of cyclam, exhibits slow release of NO. The intent was to derivatize dioxocyclam at the methylene carbon between the two carbonyl groups with side chains that can increase the solubility and recognition; however, other strategies were adopted because the dioxocyclam ligand was too costly for use on a large scale.

Based on results obtained in an ESI-MS investigation of *cis*-$[Ru(NO)Cl(bpy)_2]^{2+}$, it was concluded that π-acceptor ligands, by competing with NO^+ for electron density, can weaken the Ru-NO bond, and assist the thermal and gas phase dissociation of $NO^{\bullet}$. On the other hand, π-donor ligands inhibit thermal and gas phase reactions by strengthening backbonding from Ru^{II} to NO.[24] The opposite applies to photolytic loss of $NO^{\bullet}$; π-donor ligands may facilitate photolytic loss of $NO^{\bullet}$ while π-acceptor ligands, such as N-heterocyclic ligands, inhibit photolytic loss of $NO^{\bullet}$ from ruthenium nitrosyl complexes because they can exhibit MLCT to the N-heterocyclic π-acceptor and ligand field (LF) excitations which are at lower energy than the MLCT-to-NO^+ state.[24,26,27,35]

Some observations from the studies described illustrate the rationale behind our selection of ligands and the use of ruthenium as the central metal ion. Ruthenium is the transition metal of choice for nitrosyl compounds designed for photodynamic therapy[27] because ruthenium complexes are known to accumulate in tumors[36-42] and because the strength of the Ru-NO bond[4] increases the probability that the complex will survive under physiological conditions. Nitrosyl photolability may be controlled by altering the π-donor/π-acceptor character of the ligand set. As one of the best π-donating groups, a deprotonated amido functionality should activate the nitrosyl moiety to photolabilization[27] by pushing electron density onto the nitrosyl group. The amido group's inclination toward water solubility and biocompatibility make chelated amido donors good ligands for transporting the ruthenium nitrosyl moiety through biological environments.[28-33] Our focus was on developing ruthenium nitrosyl complexes bearing tetradentate, bis-pyridyl/bis-carboxamido ligands, bis-pyrazyl/bis-carboxamido ligands and mixed carboxamido/phenolato ligands. The pyridyl/pyrazyl ligands exert a chelate effect[27,28,32,43,44]while the strong π-donating bis-amido/bis-phenolato donors should activate the $Ru^{II}(NO^{+})$ moiety toward photolysis, then stabilize the Ru^{III}-solvent complex formed upon photolysis.[3,27,45-48] Although the ligands described here were designed to examine the possibility of tuning the nitrosyl's photolability by modifications of the ligand set in the equatorial plane, we have also investigated ligands that will place a π-donor in a position trans to the nitrosyl group. It is well known that ligands trans to the nitrosyl group influence the behavior of the NO group by direct interaction with the π* orbitals of the NO group through the metal center.[35,49-55]

1.2 ENEMARK-FELTHAM NOTATI ON

Because early explanations for the behavior of metal nitrosyl complexes, which were based solely upon the oxidation state of the nitrosyl group, were inadequate, Enemark and Feltham developed a formalism that considers the Ru-NO moiety as a unit. Since the ruthenium nitrosyl complexes described in this document are formally of the $\{RuNO\}^6$ type in the Enemark-Feltham notation, this section will summarize the development and application of the Enemark-Feltham notation.[5,56-60]

In the 1930's Sidgwick recognized that, in bonding interactions with transition metals, nitric oxide, $NO^{\bullet}$, could lose an electron to form NO^+ or gain an electron to form NO^-. The valence bond structure of NO^+ has triple bond character (*sp* hybridized, linear), so Sidgwick proposed that NO^+ complexes would exhibit a linear MNO group. The valence bond structure for NO^- has double bond character (sp^2 hybridized, 120° bond angle), thus it was assumed that NO^- complexes would exhibit a bent MNO bond.[61,62] In fact, the first linear MNO complexes characterized in the 1930's were NO^+; later, in the 1960's, bent MNO^- groups were also characterized.[63,64] The available experimental evidence seemed to indicate that the charge on the NO group determined the MNO bond angle. After more transition metal nitrosyl complexes were characterized, it became clear that something other than the charge on NO determined the MNO bond angle. Recognizing that metal nitrosyl complexes are highly covalent, Enemark and Feltham developed a system that accounts for the MNO angle and the reactivity of MNO complexes based upon molecular orbital correlation diagrams.[5]

The Enemark-Feltham approach treats each MNO group as a covalently bound entity which is sensitive to ligand field effects. The method correlates molecular orbital orderings in

various geometries, and considers how the character of the HOMO affects the geometry of the MNO group. The MNO group is bent when the HOMO is antibonding and linear when the HOMO is bonding. In the Enemark-Feltham notation, $\{MNO\}^n$, n represents the total number of metal d and NO π^* electrons when NO is arbitrarily assigned as NO^+. The notation, which reflects the fact that there is significant mixing of metal d and π^* NO orbitals, allows for some generalizations.[5] For example, according to the Enemark-Feltham method, six-coordinate octahedral complexes with $\{MNO\}^6$ are expected to be linear based upon molecular orbital correlation diagrams. Exceptions occur and are understood by considering factors that influence the molecular orbital ordering, hence influence the MNO bond angle. The complexes described in this document are formally linear $\{RuNO^+\}^6$ complexes.

1.3 CHARACTERIZATION OF RUTHENIUM NITROSYL COMPLEXES

There are several characterization methods for ruthenium nitrosyl complexes in general and for determining the nature of the Ru-NO moiety. Some of the more common methods are described in this section.[27]

^1H and ^{13}C nuclear magnetic resonance spectroscopy are useful for determining the binding mode of the ligands. Upon coordination to the Ru-NO moiety, ^{13}C and ^1H NMR signals of the ligands exhibit an upfield shift. In general, the closer a proton or a carbon is to the electron withdrawing Ru-NO unit, the more downfield its signal. However, exceptions attributed to magnetic anisotropy, induced either by the Ru-NO unit or by the ligand, do occur. ^{15}N NMR spectroscopy is a direct indicator of the electronic nature of the nitrosyl nitrogen atom. With ^{15}N

dimethylformamide as the reference, a bent $^{15}NO^-$ has a shift between 700 and 600 ppm. A linear $RuNO^+$ ^{15}N signal usually appears around 260 ppm.

Infrared spectroscopy is also a powerful tool for characterizing ruthenium nitrosyl compounds. In general, the NO^- stretching mode absorbs around 1500 cm^{-1}; the NO^+ absorbs above 1800 cm^{-1}. The lower frequency observed for NO^- is due to backbonding into the NO π^* orbitals, which lowers the bond order and therefore the stretching frequency. It is important to realize that the stretching frequency does not correlate with the Ru-NO angle. There are both linear and bent $Ru\text{-}NO^+$ and $Ru\text{-}NO^-$ complexes. Thus, while infrared spectroscopy is useful for determining the electronic character of the NO moiety, it does not necessarily provide geometrical information.

The best way to determine the geometry of the RuNO moiety is by X-ray crystallography. An MNO group is considered to be linear if its MNO angle is between 165 and 180° and bent if its angle is less than 165°. Crystal structures are also useful for observing changes in the ligand brought about by coordination to Ru.

2.0 BIS-PYRIDINE CARBOXAMIDE LIGANDS

2.1 INTRODUCTION

Ruthenium is the metal center of choice because it makes a relatively strong Ru-NO bond that can survive in physiological conditions and because ruthenium complexes are known to accumulate in tumors.[36-42] NO lability can be tuned by alterations of the π-donor/π-acceptor character of the ligand set. Strong π-donors push electron density onto NO. Increased electron density then activates the Ru-NO moiety toward photolysis of $NO^{\bullet}$. Coordination of π-donors in the position *trans* to NO have the strongest effect on NO, however, π-donors coordinated cis to NO have also been shown to decrease the nitrosyl stretching frequency[35,49,50,52-55,65]. Chelated π-donors such as bis-phenolato and bis-carboxamido ligands, activate $Ru^{II}(NO^{+})$ toward photolysis by pushing electron density toward NO.[24,26,27] After photolysis the amido/phenolato donors then stabilize the Ru^{III}-solvent complex formed by photolabilization.[3,27,45-47] Finally, water solubility and biocompatibility make chelated amido donors useful as NO carriers through physiological environments.[28-33] The RuNO complexes might then be used in photodynamic treatment of colon cancer or skin cancer. Eventually side chains on the amido ligands or phenolato ligands can be selected to guide the complex toward specific targets.

The first set of ligands prepared consists of bis-pyridyl bis-carboxamido ligands. The carboxamido ligands will serve to activate the NO group toward photolysis, while the pyridyl

groups help maintain chelation under physiological conditions. The coordinating pyridine carboxamide environment is constant while the backbone of the ligand is varied. The first three ligands described have an aromatic backbone, which is either benzene, 2,3-diaminopyridine or 3,4-diaminopyridine. The nitrogen in the aromatic is intended to enhance solubility. The other two ligands have an ethane, propane backbone or a piperazine backbone. Backbone variability introduces structural as well as electronic differences in the coordination environment. Much of the report on *N*,*N*'-bis(2-pyridinecarboxamide)-1,2-benzene[25], *N*,*N*'-bis(2-pyridinecarboxamide)-1,2-ethane and -1,3-propane[66] has been published.

2.2 *N*,*N*′-BIS(2-PYRIDINECARBOXAMIDE)-1,2-BENZENE

2.2.1 Materials and Methods

Note:
A significant part of the material presented in this chapter is reproduced with permission from a publication in Inorganic Chemistry Communications, 7, Carol F. Fortney, Rex E. Shepherd, Synthesis and Characterization of a new {RuNO}^{6} complex, [Ru(NO)(bpb)Cl] (bpb = N,N'-bis(2-pyridinecarboxamide)-1,2-benzne dianion), 1065-1070, copyright Elsevier, 2004.

Trichloronitrosylruthenium dihydrate ($[Ru(NO)Cl_3(H_2O)_2]$) (**2.1**) was prepared using a modification of the procedure of Fletcher.[67] $[RuCl_3(H_2O)_3]$ (207.43 g/mol, 2.00g, 0.0096 mol, 1 equiv) was dissolved in HCl (1 M, 15.0-18.0 ml, > 1 equiv.) and heated to 100 °C in an oil bath. At 100 °C, an aqueous solution of $NaNO_2$ (68.9 g/mol, 1.99 g, 3 equiv.) was added dropwise over one hour. The dark red/black solution began to turn purple as NO_2 was released. After one hour the water was removed from the reaction mixture under vacuum (rotary evaporator, 90 °C). The remaining dark purple solid was dissolved in ethanol to separate the product from NaCl formed in the reaction. NaCl was removed via vacuum filtration. Ethanol was removed under vacuum (rotary evaporator, 65-70 °C.) The extremely hygroscopic purple solid was stored in a desiccator with Drierite.

***N*,*N*′-bis(2-pyridinecarboxamide)-1,2-benzene ($bpbH_2$) (2.2)** *N*,*N*′-bis(2-pyridine carboxamide)-1,2-benzene was prepared according to a literature procedure.[68] 1,2-diaminobenzene (10.43 g, 0.0964 mol, 1 equiv) in pyridine (~ 50.0 ml) was added to a stirred solution of picolinic acid (23.73 g, 0.0193 mol, 2 equiv) in pyridine (~ 120 ml). After triphenyl phosphite (50.7 ml, 0.1929 mol, 1 equiv) was added slowly, the reaction mixture was heated for

four hours in a water bath. Brown crystals formed overnight at room temperature. Pale pink crystals were obtained by recrystallization from ethylacetate. ^{1}H NMR (300 MHz, dimethyl sulfoxide-d_6): δ 10.7 (s, 2H, NH_2) 8.63 (dq, 2H, H-1); 8.15 (dt, 2H, H-4); 8.05 (td, 2H, H-3); 7.75 (td, 2H, H-5), 7.64 (qd, 2H, H-2), 7.29 (td, 2H, H-6). ^{13}C NMR (125 MHz, dimethyl sulfoxide-d_6): δ 162.74 (C=O), 149.42 (Pyridyl-*ipso*), 148.54 (C-1), 138.17 (C-3), 130.9 (Aryl-*ipso*), 127.1 (C-2), 125.66 (C-6), 125.29 (C-5), 122.42 (C4); GC-MS *m/z* 318.

Nitrosyl *N*,*N′*-bis(2-pyridinecarboxamido)-1,2-benzene chloride ruthenium(II) (2.3) Was prepared using an procedure adapted from Vagg.[69] $[Ru(NO)Cl_3(H_2O)_2]$ (0.861g, 0.0031 mol, 1 equiv) was added to a stirred solution of $bpbH_2$ (0.999 g, 0.0031 mol, 1 equiv) in an ethanol/water solution (95 %, ~60.0 ml, 65-70 °C). After 12 hours, a fine brown solid (0.452 g, 0.00094 mol, 30 %) was isolated by filtration, rinsed with ethanol, and dried in a 120 °C oven. ^{1}H NMR (300 MHz, dimethyl sulfoxide-d_6): δ 9.25 (d, 2H, H-1), 8.54 (td, 2H, H-5), 8.21 (td, H-3), 8.2 1(dd, 2H, H-4), 7.94 (dtd, 2H, H-2), 7.06 (td, 2H, H-6); ^{13}C NMR (125 MHz, dimethyl sulfoxide-d_6): δ 163.26 (C=O), 158.11 (Pyridyl-*ipso*), 152.49 (C-1), 143.71 (Aryl-*ipso*), 141.8 (C-3), 128.05 (C-2), 126.40 (C-4), 123.84 (C-6), 121.02 (C-5); IR (KBr): (ν_{NO} = 1867cm^{-1}); ESI-MS M + Na^+ 505.9 ($M^{+\bullet}$ = 482).

2.2.2 Results and Discussion

The ligand, *N*,*N*′-bis(2-pyridinecarboxamide)-1,2-benzene **(2.2)** has been prepared[68] previously and analyzed by X-ray crystallography.[70] The $\{Ru^{II}NO^{+}\}^{6}$ compound [Ru(NO)Cl(bpb)] **(2.3)** was obtained from the reaction between $[Ru(NO)Cl_3(H_2O)_2]$ and *N,N*′-bis(2pyridinecarboxamide--1,2-benzene) in 95% ethanol/H_2O at 75°C. Nuclear magnetic resonance spectroscopy (HH COSY, HMBC, and HMQC) allowed the unambiguous assignment of all ^{1}H and ^{13}C resonances. Figure 2.1 displays the labeling system; ^{1}H and ^{13}C chemical shifts for **2.2** and **2.3** are compared in Table 2.1. The free ligand's N-*H* resonance at δ 10.7 (s, 2 H) disappears upon exchange with D_2O. Disappearance of the amido N-H resonance upon coordination indicates that the ligand is deprotonated. The only proton resonances that do not exhibit a downfield shift upon coordination are the benzene meta protons, H-6, which shift slightly upfield. As expected, the most significant down field shifts correspond to H-1 and H-5, the protons ortho to the pyridyl nitrogen and ortho to the nitrogen substituent on the diamido benzene moiety, respectively.

The ^{13}C resonances are more diagnostic because their proximity to the chelating nitrogen increases their sensitivity to the electron withdrawing character of the RuNO moiety. By ^{13}C NMR the possibility that the amido functionality is bound to the metal center by the carbonyl oxygen can be eliminated because coordination there would generate a pronounced downfield shift of the ^{13}C resonance for the carbonyl carbon. The most noticeable downfield shifts correspond to the nitrogen bearing aryl-*ipso* carbon and the pyridyl-*ipso* carbon, which is bound to the coordinated pyridyl nitrogen. H-6, C-5, and C-6 all exhibit upfield shifts upon coordination.

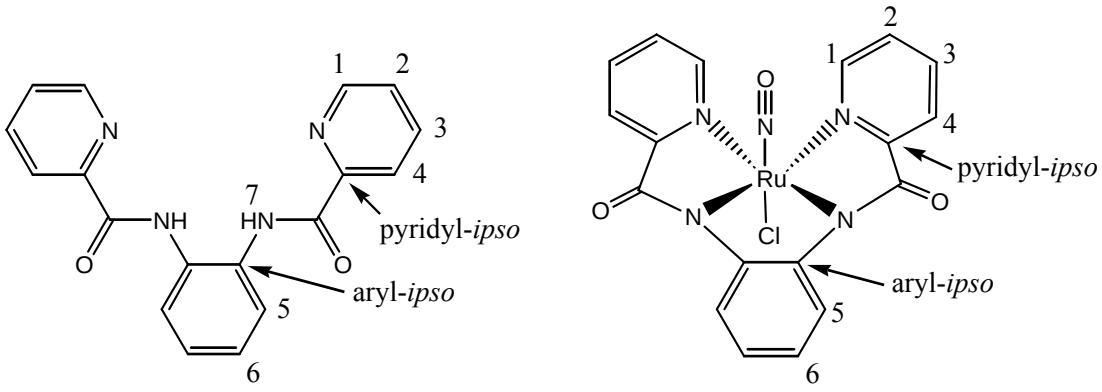

2.2 **2.3**

Figure 2.1-^{1}H and ^{13}C labeling scheme For 2.2 and 2.3

Table 2.1- Chemical shifts[a] for 2.2[b] and 2.3[c]

a. 300 MHz; dmso-d_6

b. *N,N'*-bis(2-pyridinecarboxamide)-1,2-benzene ($bpbH_2$)

c. [Ru(NO)(bpb)Cl] (bpb = *N,N'*-bis(2-pyridinecarboxamide)-1,2-benzene dianion)

* Not applicable

^{1}H	1	2	3	4	5	6	7			
2.2	8.63	7.64	8.05	8.15	7.75	7.29	10.7			
2.3	9.25	7.94	8.39	8.21	8.54	7.06	*			
^{13}C								**Ar-*ipso***	**Py-*ipso***	**C=O**
2.2	148.54	127.10	138.17	122.42	125.29	125.66	*	130.97	149.42	162.74
2.3	152.49	128.05	141.88	126.40	121.02	123.84	*	143.71	158.11	163.26

Scheme 2.1 summarizes the mass spectrometry data obtained for **2.3.** Compound **2.3** exhibits minimal solubility in methanol, so ESI-MS only allowed detection of a small amount of the neutral compound [Ru(NO)(bpb)Cl] plus Na^+ at *m/z* = 506 **2.3a**. Treatment of **2.3** with $AgNO_3$ produced the more soluble cation **2.3b**. Compound **2.3b**, with a methanol molecule, situated *trans* to the nitrosyl group, exists in equilibrium in solution with its deprotonated neutral form **2.3c**. Compound **2.3b** is detected, with loss of methanol, at m/z = 448. The neutral 2.**3c** is not detected by itself by ESI/MS. However, **2.3d**, (**2.3c** in the presence of K^+) is detected at m/z = 518. This confirms the conclusion from the first ESI/MS experiment with **2.3** and provides further evidence that all four nitrogen atoms are coordinated to the metal center.

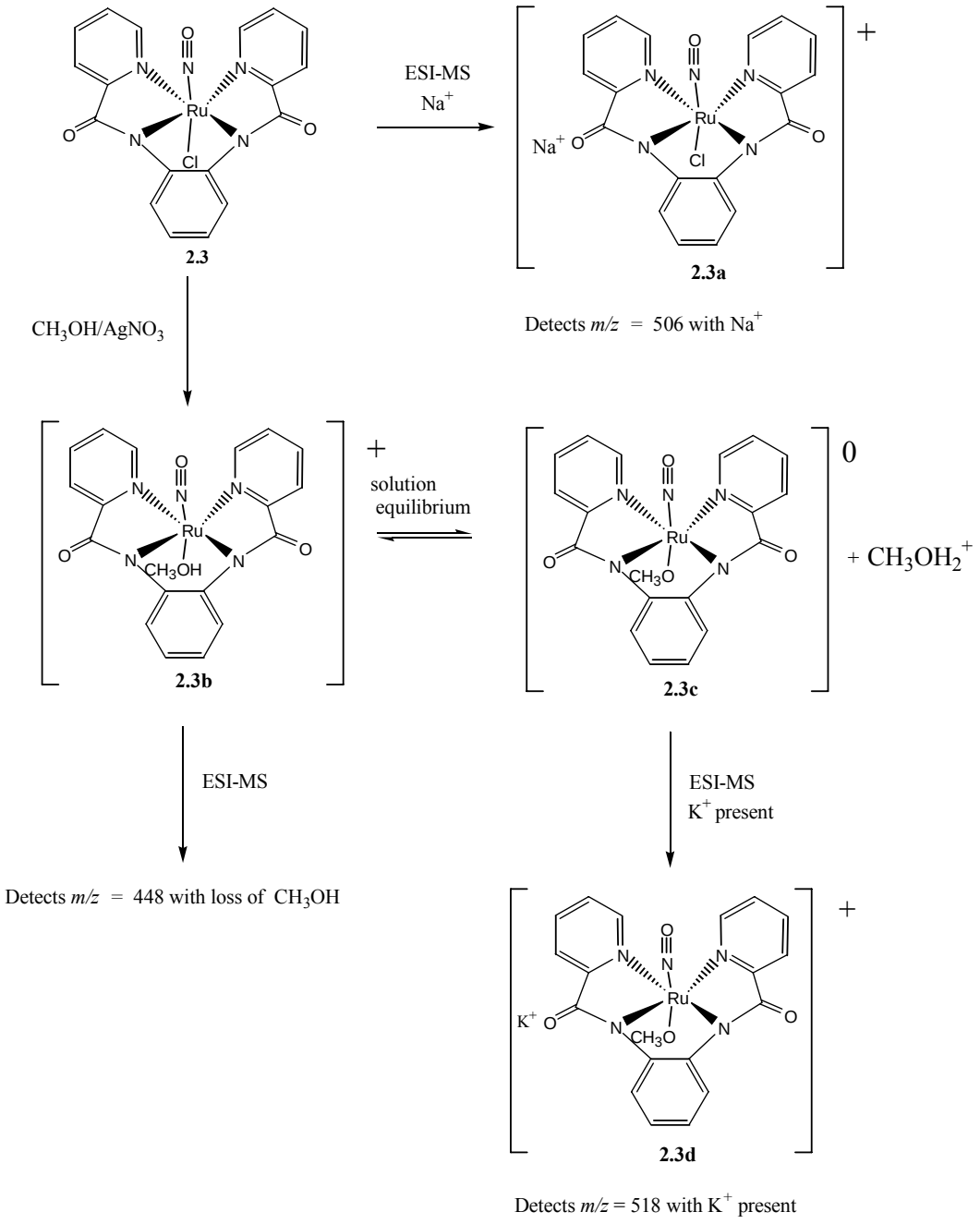

Scheme 1-ESI-MS data for [Ru(NO(bpb)Cl]

The infrared spectrum of **2.3** reveals that the nitrosyl group (ν_{NO} = 1867cm^{-1}) in [Ru(NO)(bpb)Cl] is activated, but to a lesser extent than in the ruthenium nitrosyl dioxocyclam complex (ν_{NO} =1845 cm^{-1}). The increased stretching frequency with respect to the dioxocyclam complex was anticipated because the amine donors of the dioxocyclam ligand have been replaced with π-accepting pyridyl donors in **2.3** therefore less electron density is available for back donation to the nitrosyl. The NO stretching frequency and the fact that this is a six coordinate {RuNO}^{6} complex suggest that **2.3** is formally a linear $Ru^{II}NO^+$ complex.

At the time the report of **2.3** was submitted for publication the Mascharak published a report of its synthesis, as well as the synthesis of derivatives. Our data are in good agreement with theirs. In addition a crystal structure of **2.3** confirmed that the RuNO moiety is linear and conclusions drawn from studies described in the introduction. Photochemical studies showed that [Ru(NO)(bpb)Cl] exhibits photolytic loss of NO under mild UV radiation.[26]

2.2.3 Conclusion

In summary, a six coordinate {RuNO}^{6} complex, [Ru(NO)(bpb)Cl] (**2.3)** was prepared and characterized by NMR spectroscopy, IR spectroscopy and ESI-MS. Compound **2.3** represents the first in a series of ruthenium nitrosyl bis-amido/bis-pyridyl and mixed amido/phenolato complexes being developed to elucidate the factors that regulate MNO character so that the RuNO group can be tuned for optimal photolytic activity.

2.3 *N*,*N*′-BIS(2-PYRIDINECARBOXAMIDE)-2,3-PYRIDINE

2.3.1 Materials and Methods

***N*,*N*′-bis(2-pyridinecarboxamide)-2,3-pyridine (2.4)** was prepared according to a literature procedure.[68] Triphenyl phosphite (d = 1.184 g/mL, 2.46 mL, 0.0094 mol) was added by pipette to a solution of picolinic acid (1.16 g, 0.0094 mol) and 2,3-diaminopyridine (0.513 g, 0.0047 mol) in dry pyridine (5.0 mL). After four hours of stirring in an oil bath at 100 °C the reaction mixture was allowed to sit at room temperature for several days until crystals formed. Clear crystals were collected by vacuum filtration. Recrystallization from dichloromethane afforded x-ray quality crystals. ^{1}H NMR (600 MHz, DMSO-d_6, δ): 10.91 (s, 1H, N-H (2)), 10.72 (s, 1H, N-H(1)), 8.74 (dd, 1H, H-17), 8.59 (dd, 1H, H-1), 8.42 (dd, 1H, H-10), 8.34 (dd, 1H, H-8), 8.19(dd, 1H, H-14), 8.15 (d, 1H, H-4), 8.08 (td, 1H, H15), 8.04 (td, 1H, H-3), 7.70 (m, 1H, H-16), 7.63 (m, 1H, H-2), 7.45 (dd, 1H, H-9); ^{13}C{H} (125 MHz, DMSO-$_{d6}$) δ): 163.58 (C-12, C=O), 162.51 (C-6, C=O), 148.91 (C-5, C-13), 148.77 (C-17), 148.62 (C-1), 144.71 (C-8), 142.96 (C-11), 138.26 (C-3, C-15), 132.68 (C-10), 128.33 (C-7), 127.44 (C-16), 127.32 (C-2), 122.64 (C-14), 122.36 (C-4), 122.32 (C-9); ESI-MS $M^{+\cdot}$ = 319

Reaction with $[Ru(NO)Cl_3(H_2O)_2]$: The reaction was run according to a modified literature procedure.[69] Trichloronitrosylruthenium (273.45 g/mol, 0.001 mol, 0.306 g) was added to an ethanol/water (95%, 40.0 mL) solution of *N*,*N*′-bis(2-pyridinecarboxamide)-2,3-pyridine (319.32 g/mol, 0.358 g, 0.001 mol, 1 equiv) with stirring. The reaction mixture was stirred for ten hours

at 85.0 °C. A brown precipitate was separated from the filtrate. X-ray quality crystals were obtained after volume reduction under vacuum (rotary evaporator 55 °C) and slow evaporation of solvent at ambient temperature. The yield was low and not obtained. The reaction will have to be scaled up to obtain NMR and IR data.

2.3.2 Results and Discussion

The ligand *N*,*N′*-bis(2-pyridinecarboxamide)-2,3-pyridine was characterized by ^{1}H NMR and ^{13}C NMR spectroscopy. Chemical shift assignments were made based upon HH COSY, HMQC, and HMBC spectra. The labeling scheme for the NMR assignments is shown in Figure 2.2. ^{1}H; ^{13}C NMR data are shown in Tables 2.2 and 2.3, respectively.

There are some differences between **2.2,** which has a benzene ring backbone, and **2.4.** The addition of a nitrogen atom in **2.4** has a long range effect, which differentiates the pyridyl arms from each other for **2.4**. The HH COSY spectrum (excluding N-H signals), shows the sets of pyridyl signals (Figure 2.3). For ligand **1.4**, there is only one set of pyridyl signals. The resonance forms of the pyridine ring in **2.4** places positive charge on the carbon atoms ortho and para to the pyridine nitrogen. For the 2,3-diaminopyridine ligand then, C-11 exhibits more of a positive character than does C-7 as shown by the ^{13}C NMR data. The signal for C-11 is at 142.96 ppm while that for C-7 is at 128.33 ppm. The corresponding carbon atoms in **1.4** show a single resonance at 130.97 ppm. The remaining ^{1}H and ^{13}C signals within **2.4** differ only slightly from each other.

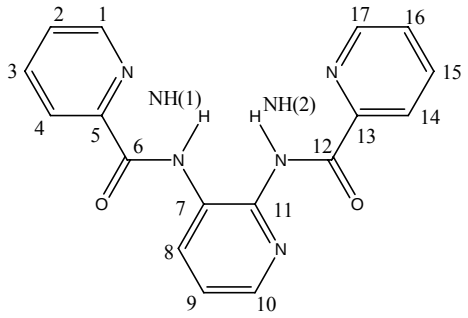

2.4

Figure 2.2- *N,N′*-bis(2-pyridinecarboxamide)-2,3-pyridine

Table 2.2-^{1}H NMR Data for *N,N′*-bis(2-pyridinecarboxamide)-2,3-pyridine

^{1}H	**1**	**2**	**3**	**4**	**8**	**9**	**10**	**14**	**15**	**16**	**17**	**N-H(1)**	**N-H(2)**
	8.59	7.63	8.04	8.15	8.34	7.45	8.42	8.19	8.08	7.70	8.74	10.72	10.91

Table 2.3-^{13}C NMR Data for *N,N′*-bis(2-pyridinecarboxamide)-2,3-pyridine

^{13}C	**1**	**2**	**3**	**4**	**5**	**6**	**7**	**8**	**9**	**10**
	148.62	127.32	138.26	122.36	148.91	162.51	128.33	144.71	122.32	132.68

11	**12**	**13**	**14**	**15**	**16**	**17**
142.96	163.58	148.91	122.64	138.26	127.44	148.77

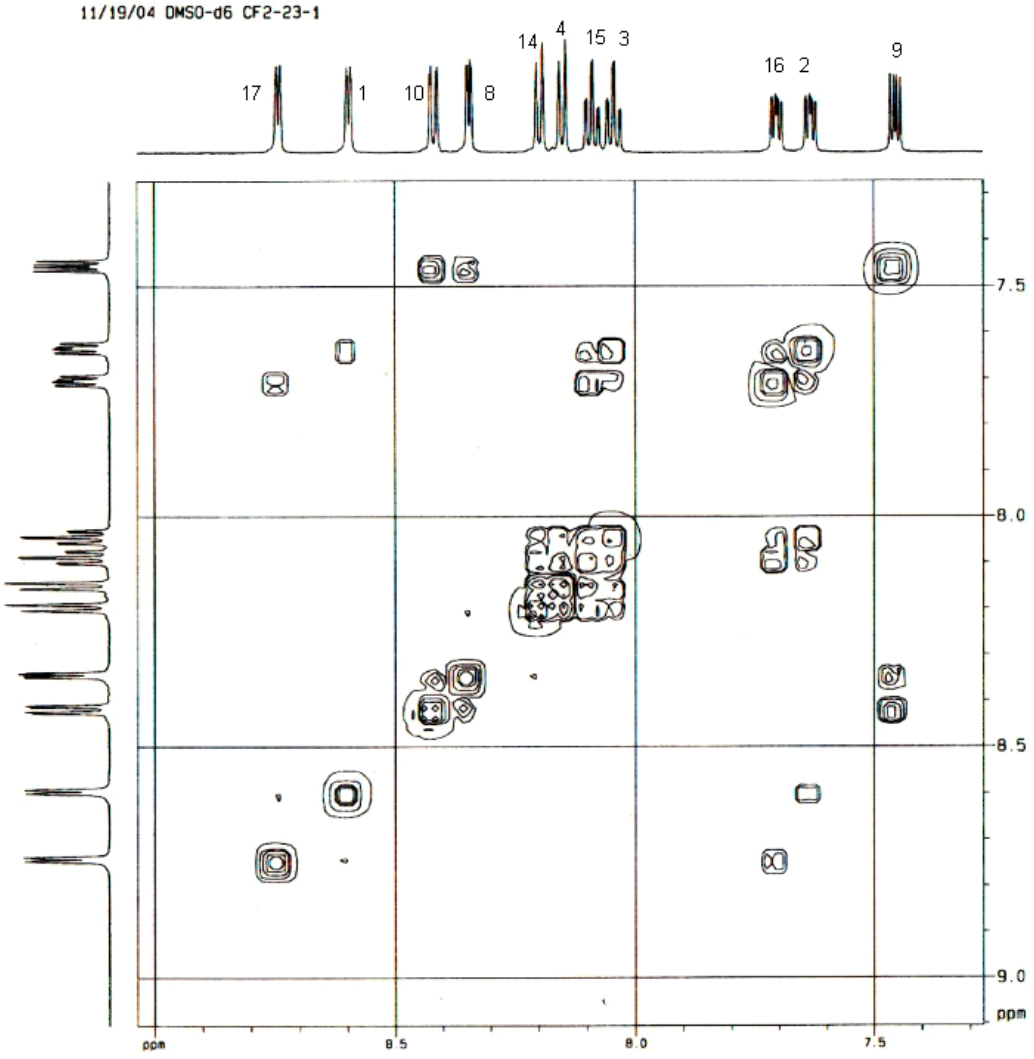

Figure 2.3-HH COSY of *N*,*N′*-bis(2pyridinecarboxamide)-2,3-pyridine

Figure 2.4 shows the crystal structure of **2.4.** Crystal intensity and collection data are reported in Table 2.4. Selected bond distances and angles are shown in Tables 2.5 and 2.6, respectively. The C(11)-C(7)-N(2) angle is 2° larger than that for C(7)-C(11)-N(4); there are no other remarkable differences between the pyridyl arms with respect to bond distances and bond lengths.

Table 2.4-Crystal data and refinements for 2.4 and 2.6

	2.4	**2.6**
Chemical Formula	$C_{17}H_{13}N_5O_2$	$C_{20}H_{19}Cl_3N_6O_{4.5}RuS_{1.5}$
Formula Weight	319.32	670.92
Temperature (K)	293(2)	150(2)
Wavelength (Å)	0.71073	0.71073
Crystal system	Monoclinic	Triclinic
Space group	P-2(1)/c	P-1
a (Å)	16.2399(9)	10.668(2)
b (Å)	11.5058(6)	16.519(3)
c (Å)	8.0877(4)	17.628(4)
α (°)	90	63.144(4)
β (°)	92.33(10)	84.309(5)
γ (°)	90	79.441(5)
Volume ($Å^3$)	1509.96(1)	2724.1(10)
Z	4	4
Density (calculated) Mg/m^3	1.405	1.636
Absorption Coefficient (mm^{-1})	0.097	1.025
F(000)	664	1344
Crystal Size (mm^3)	0.28 x 0.15 x 0.15	0.26 x 0.13 x 0.11
θ range for data collection (°)	2.17 to 24.99	1.94 to 25.00
Index Ranges	$-19 \le h \le 19$	$-12 \le h \le 12$
	$-13 \le k \le 13$	$-19 \le k \le 19$
	$-9 \le l \le 9$	$-20 \le l \le 20$
Reflections collected	11889	21758
Independent reflections	2650 [R(int) = 0.0260]	9583 [R(int) = 0.1160]
Completeness	99.9 % (θ=24.99°)	99.9 % (θ=25.00)
Data / restraints / parameters	2650/ 0 / 269	9583 / 0 / 634
Max. and min. transmissions	0.9856 and 0.9733	0.8956 and 0.7765
Refinement Method	Full-matrix least-squares on F^2	Full-matrix least-squares on F^2
Goodness-of-fit on F^2	1.343	1.101
Final R indices[$I > 2\sigma$ (I)]	R1 = 0.0469, wR2 = 0.1205	R1 = 0.1006, wR2 = 0.2187
R indices (all data)	R1 = 0.0574, wR2 = 0.1247	R1 =0.1646, wR2 = 0.2432
Largest diff. peak and hole (e $Å^3$)	0.155 and -0.144	3.606 and -1.583

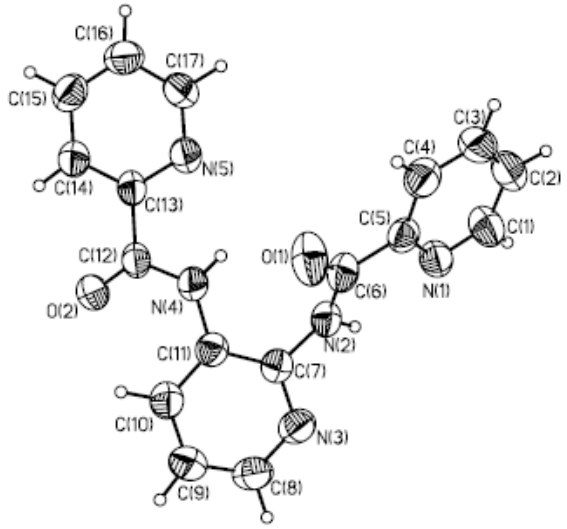

Figure 2.4-X-ray structure of 2.4

Table 2.5-Selected bond distances for 2.4

O(2)-C(12)	1.215(2)	O(1)-C(6)	1.221(2)	C(10)-C(11)	1.386(3)
N(4)-C(12)	1.349(2)	N(2)-C(6)	1.347(2)	C(9)-C(10)	1.372(3)
N(4)-C(11)	1.405(2)	N(2)-C(7)	1.413(2)	C(8)-C(9)	1.372(3)
N(4)-H(4N)	0.851(2)	N(2)-H(2N)	0.858(2)	N(3)-C(8)	1.332(3)
C(12)-C(13)	1.502(2)	C(5)-C(6)	1.494(3)	N(3)-C(7)	1.333(2)
N(5)-C(13)	1.333(2)	N(1)-C(5)	1.338(2)	C(7)-C(11)	1.393(2)
N(5)-C(17)	1.331(2)	N(1)-C(1)	1.331(2)	C(4)-H(4)	0.89(2)
C(16)-C(17)	1.371(3)	C(1)-C(2)	1.371(3)	C(14)-H(14)	095(2)
C(15)-C(16)	1.361(3)	C(2)-C(3)	1.355(3)		
C(14)-C(15)	1.376(3)	C(3)-C(4)	1.376(3)		
C(13)-C(14)	1.374(2)	C(4)-C(5)	1.375(2)		

Table 2.6-Selected bond angles for 2.4

C(3)-C(2)-C(1)	118.6(2)	C(15)-C(16)-C(17)	118.42(2)
C(2)-C(3)-C(4)	119.0(2)	C(16)-C(15)-C(14)	118.9(2)
C(3)-C(4)-C(5)	118.9(2)	C(13)-C(14)-C(15)	118.86(1)
C(4)-C(5)- N(1)	122.87(1)	N(5)-C(13)-C(14)	123.08(1)
C(5)- N(1)- C(1)	116.57(1)	C(17)- N(5)-C(13)	116.57(1)
C(13)-C(12)-O(2)	121.14(1)	O(1)-C(6)-C(5)	121.80(1)
N(4)-C(12)-C(13)	113.81(1)	N(2)-C(5)-N(2)	115.01(1)
C(12)- N(4)- C(11)	126.54(1)	C(6)- N(2)- C(7)	125.29(1)
C(10)-C(11)-N(4)	122.04(1)	N(3)-C(7)-N(2)	114.14(1)
C(7)-C(11)-N(4)	120.32(1)	C(11)-C(7)-N(2)	122.52(1)
C(11)-C(10)-C(9)	119.17(1)	C(8)-N(3)- C(7)	117.40(1)
C(10)-C(9)-C(8)	118.9(2)	N(3)-C(8)-C(9)	123.4(2)
O(2)-C(12)- N(4)	125.05(1)	O(1)-C(6)- N(2)	123.17(1)
C(10)-C(11)-C(7)	117.62(1)	N(3)-C(7)-C(11)	123.32(1)

While the tetradentate complex **2.5** shown in Figure 2.5 has not been isolated from the reaction mixture at this time, at least two other products were obtained from the reaction between **2.4** and $[Ru(NO)Cl_3(H_2O]$. The ^1H NMR spectrum, shown in Figure 2.6, indicates that one product is coordinated by only one carboxamido nitrogen, as there is only one N-H resonance in the spectrum. Assignment of ^1H signals await 2D analysis. Another product, for which the crystal structure was obtained, is shown in Figure 2.7.

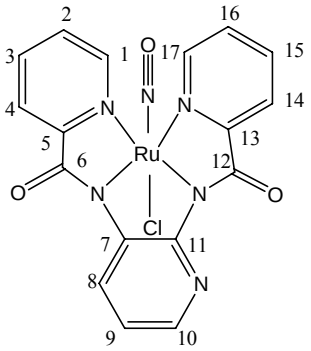

2.5

Figure 2.5-Tetradentate ruthenium nitrosyl complex

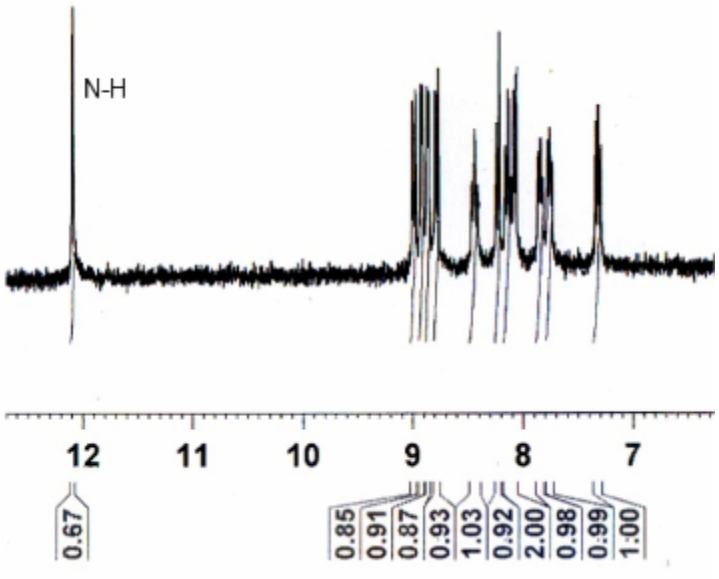

Figure 2.6-^1H NMR Spectrum of RuNO complex coordinated by one amido nitrogen

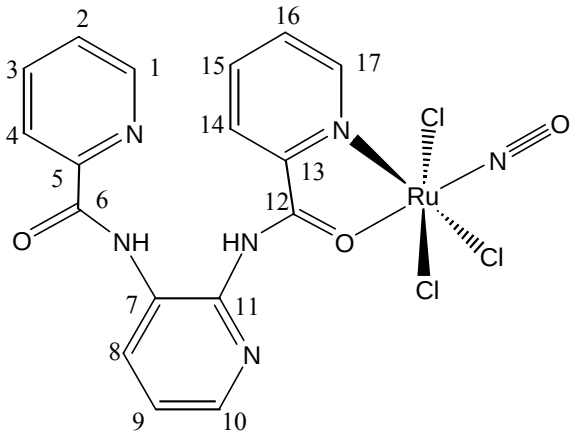

2.6

Figure 2.7-Product obtained from reaction mixture

In **2.6** the ligand binds axially through the carbonyl oxygen, which is trans to NO, and through a pyridyl nitrogen atom, in an equatorial position, trans to a chloride. The three chloride atoms are in the equatorial plane. There are two slightly different forms of this crystal as shown in Figure 2.8. Selected bond distances and angles are shown in Table 2.7.

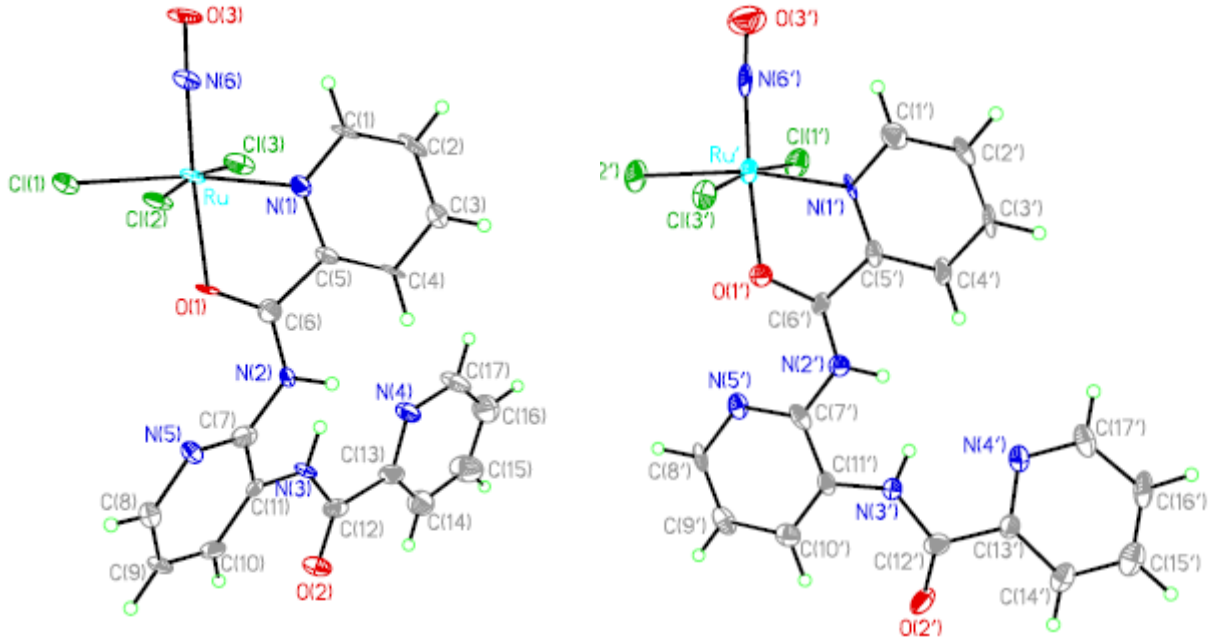

2.6 **2.6′**

Figure 2.8-Two forms of *trans*-O bound complex

Table 2.7- Selected bond distances (Å) and bond angles (°) for 2.6 and 2.6′

O(3)-N(6)	1.145(1)	O(3′)-N(6′)	1.139(1)
Ru-N(6)	1.733(9)	Ru′-N(6′)	1.727(1)
Ru-O(1)	2.054(7)	Ru′-O(1′)	2.031(7)
Ru-N(1)	2.067(8)	Ru′-N(1′)	2.061(8)
Ru-Cl(1)	2.350(3)	Ru′-Cl(2′)	2.351(3)
Ru-Cl(3)	2.361(3)	Ru′-Cl(1′)	2.363(3)
Ru-Cl(2)	2.369(3)	Ru′-Cl(3′)	2.366(3)
N(1)-C(1)	1.353(1)	N(1′)-C(1′)	1.342(1)
C(1)-C(2)	1.358(1)	C(1′)-C(2′)	1.365(1)
C(2)-C(3)	1.403(1)	C(2′)-C(3′)	1.368(1)
C(3)-C(4)	1.364(1)	C(3′)-C(4′)	1.369(1)
C(4)-C(5)	1.349(1)	C(4′)-C(5′)	1.372(1)
N(1)-C(5)	1.358(1)	N(1′)-C(5′)	1.340(1)
C(5)-C(6)	1.498(1)	C(5′)-C(6′)	1.489(1)
N(2)-C(6)	1.298(1)	N(2′)-C(6′)	1.263(1)
O(1)-C(6)	1.283(1)	O(1′)-C(6′)	1.301(1)
N(2)-C(7)	1.346(1)	N(2′)-C(7′)	1.344(1)
O(2)-C(12)	1.241(1)	O(2′)-C(12′)	1.219(1)
O(3)-N(6)-Ru	177.5(9)	O(3′)-N(6′)-Ru′	172.9(1)
N(6)-Ru-O(1)	175.7(4)	N(6′)-Ru′-O(1′)	174.6(4)
N(6)-Ru-N(1)	96.9(4)	N(6′)-Ru′-N(1′)	99.3(4)
N(6)-Ru-Cl(3)	91.4(3)	N(6′)-Ru′-Cl(1′)	88.93
N(6)-Ru-Cl(1)	91.9(3)	N(6′)-Ru′-Cl(2′)	91.1(3)
N(6)-Ru-Cl(2)	95.3(3)	N(6′)-Ru′-Cl(3′)	97.6(3)
O(1)-Ru-N(1)	78.8(3)	O(1′)-Ru′-N(1′)	78.2(3)
O(1)-C(6)-C(5)	118.8(1)	O(1′)-C(6′)-C(5′)	113.9(9)
N(1)-C(5)-C(6)	111.1(1)	N(1′)-C(5′)-C(6′)	115.0(9)
Ru-N(1)-C(5)	115.8(7)	Ru′-N(1′)-C(5′)	114.8(6)
O(1)-C(6)-N(2)	126.7(1)	O(1′)-C(6′)-N(2′)	128.4(1)
N(5)-C(7)-N(2)	123.61	N(5′)-C(7′)-N(2′)	122.3(1)
C(6)-O(1)-Ru	114.6(6)	C(6′)-O(1′)-Ru′	118.0(7)

The crystal structures for **2.6** and **2.6′** show that both are linear nitrosyl complexes with an N(6)-Ru-O(3) bond angle of 177.5(9) for **2.6** and 172.9(10) for **2.6′**. That the N(6′)-Ru′-O(3′) angle deviates from linearity more than the N(6)-Ru-O(3) angle follows from the fact that the Ru′-O(1′) is shorter than the Ru-O(1) bond. The oxygen atom, being trans to the strong π-accepting NO group, transfers electron denstiy through Ru^{II} toward NO. This transfer of electron density must be more efficient for **2.6′** than for **2.6** as evidenced by the shorter Ru′-O(1) and Ru′-N(6) bonds as well as the bending of the Ru-NO moiety.

For **2.6** and **2.6′** the Ru-Cl bond trans to N(1) of the pyridyl group is shorter than both of the other two Ru-Cl bonds. This difference in bond length is due to the π-accepting ability of the pyridyl group. The Ru-N(1) bond distances are about the same for **2.6** and **2.6′** However, the O(1)-C(5)-C(6) angle is 5° greater than that for O(1′)-C(5′)-C(6′) and the N(1)-C(5)-C(6) angle is 4° less than the N(1′)-C(5′)-C(6′) angle. The C(5)-N(1) distance for **2.6** is slightly larger than that for **2.6′.** The differences in bond distances and angles are interesting considering that the ligand is bound in the same fashion for both complexes.

2.3.3 Conclusion

The ligand *N*,*N*′-bis(2pyridinecarboxamide)-2,3-pyridine was characterized by ^{1}H NMR and ^{13}C NMR spectroscopy. Chemical shift assignments were made based upon HH COSY, HMQC, and HMBC spectra. For *N*,*N*′-bis(2-pyridinecarboxamide)1,2-benzene, **2.2,** which has a benzene ring backbone, the pyridyl arms are identical. For **2.4** the addition of a nitrogen atom in the aromatic backbone of the ligand has a long range effect which differentiates the pyridyl arms from each other. The differences between **2.2** and **2.4** translate into differences in coordination mode. A resonance form of the 2,3-dicarboxamido pyridine moiety places positive character on C-11 of the ligand. That positive character seems to compete for the lone pair of the attached nitrogen atom. This may explain the unusual coordination mode depicted by the crystal structures. A second product which appears to be bound through one carboxamido nitrogen was isolated and requires further characterization.

A serendipitous outcome of these unexpected results is that this new ligand has the potential to become a binuclear ruthenium nitrosyl carrier, similar to the binuclear complexes described in the appendix that Professor Shepherd prepared earlier in his career. Since the ligand is capable of coordinating through the carbonyl oxygen and one pyridyl group in one case and through at least one carboxamido nitrogen in the other, the rest of the ligand also might be able to bind to a second ruthenium center. The pendant half of the ligand could also serve as an anchoring site for a cell or protein.

During the ligand synthesis, a large amount of a second product was obtained. NMR and mass spectral data indicate that the extra product is the monosubstituted 1,2-diaminopyridine. It has not been determined whether the substitution has occurred at N(4) or (2). An interesting

extension of this project would be to test the coordination preference of the monosubstituted ligand.

The most intriguing characteristic of these new complexes is that the chloride ions are all in the equatorial plane. For all other complexes isolated in this series, two chloride ions are displaced and one remains trans to NO. It is not very likely that there was any $[Ru(NO)Cl_3(H_2O)_2]$ with H_2O trans to NO, being that NO prefers to have stonger π-donors trans to it. Perhaps, upon coordination, the complex isomerizes to place NO trans to the oxygen. That might explain the observation of two complexes with the same ligand coordination but with different conformations. The different conformations of the pendant ligand might be explained by crystal packing. Infrared analysis using KBr pellets should give two NO peaks for a sample with these structures. In solution, if the differences are attributed to packing, the complexes should become equivalent. Therefore, NMR spectroscopy should also be diagnostic once more sample is prepared.

2.4 *N,N′*-BIS(2-PYRIDINECARBOXAMIDE)-3,4-PYRIDINE

2.4.1 Materials and Methods

***N,N′*-bis(2-pyridinecarboxamide)-3,4-pyridine (2.7)** was prepared according to a literature procedure.[68] Triphenyl phosphite (d = 1.184 g/mL, 2.43 mL,.0093 mol) was added slowly to a stirred solution of picolinic acid (1.15 g, 0.0093 mol, 2 equiv) and 3,4-diaminopyridine (109.13 g/mol, 0.508 g, 0.0047 mol) in dry pyridine (5.0 mL). The reaction mixture was stirred for four hours in an oil bath at 100 °C. Crystals formed in the reaction after several days at ambient temperature. Clear crystals were collected by vacuum filtration. X-ray quality crystals were obtained by recrystallization from chloroform. ^{1}H NMR (500 MHz, DMSO-d_6, δ): 10.97 (s, 1H, N-H (1)), 10.79 (s, 1H, N-H(2)), 8.77 (d, 1H, H-1), 8.67 (s, 1H, H-10), 8.57 (d, 1H, H-17), 8.47 (d, 1H, H-9), 8.19 (m, 1H, H-4), 8.17 (m, 1H, H-14), 8.14 (d, 1H, H-8), 8.08 (m, 2H, H-15, H-3), 7.71 (m, 1H, H-2), 7.66 (m, 1H, H-16) ; ^{13}C{H} (125 MHz, DMSO-$_{d6}$) δ): 163.89 (C-6, (C=O)), 162.55 (C-12, (C=O)), 149.07 (C-5), 148.71 (C-1), 148.64 (C-17), 148.53 (C-13), 148.42 (C-10), 147.49 (C-9), 125.03 (C-11), 138.46 (C-15), 138.20 (C-3), 127.64 (C-16), 127.35 (C-2), 139.48 (C-7), 122.71 (C-14), 122.60 (C-4), 116.32 (C-8); ESI-MS $M^{+\cdot}$ = 319

Reaction with $[Ru(NO)Cl_3(H_2O)_2]$: The reaction was run according to a modified literature procedure.[69] An ethanol/water (95%, 3.0 mL) solution of trichloronitrosylruthenium (0.025 g, 0.092 mmol,) was transferred by pipette to an ethanol/water (95%, 15.0 mL, 80.0 °C) solution of *N,N′*-bis(2-pyridinecarboxamide)-3,4-pyridine (0.0295 g, 0.092 mmol). The reaction mixture was stirred for ten hours at 80.0 °C. A brown precipitate was removed from the reaction

mixture. The filtrate volume was reduced under vacuum (rotary evaporator 55 °C) and stored at ambient temperature for crystal formation.

2.4.2 Results and Discussion

The ligand **2.7** was isolated in undetermined, but low yield and characterized by NMR spectroscopy. The relatively low yield is attributed to formation of a monosubstituted side product based upon NMR spectroscopy. The labeling scheme for NMR data is shown in Figure 2.9; ^{13}C and ^{1}H NMR data are in Tables 2.8 and 2.9. Chemical shift assignments were made based upon HH COSY, HMBC, and HMQC spectra. The chemical shift assignments are similar to those of **2.4**. The pyridyl arms are differentiated by their position with respect to the nitrogen atom in 2,3-diaminopyridine backbone. The NMR signals for the pyridyl arm attached to C-7 resonate slightly downfied from those attached to C-11 because of the positive character placed on C-7 by the resonance forms of 2,3-diaminopyridine. This effect is illustrated by the ^{13}C chemical shift differences between C-7 (139.48 ppm) and C-11 (125.03 ppm). This difference (14.45 ppm) is almost exactly the same as the difference in chemical shift observed for C-7 and C-11 in **1.6** (14.63 ppm). While the chemical shift difference is essentially the same, the chemical shift values for C-7 and C-11, at 125.03 ppm and 139.48 ppm are about 3 ppm upfield from the chemical shifts of C-7 and C-11 of **1.6**, at 128.33 and 142.96 ppm, respectively. This illustrates that the resonance effect is stronger at the ortho position than at the para position. Crystals, fine needles, obtained after recrystallization were too thin for X–ray analysis.

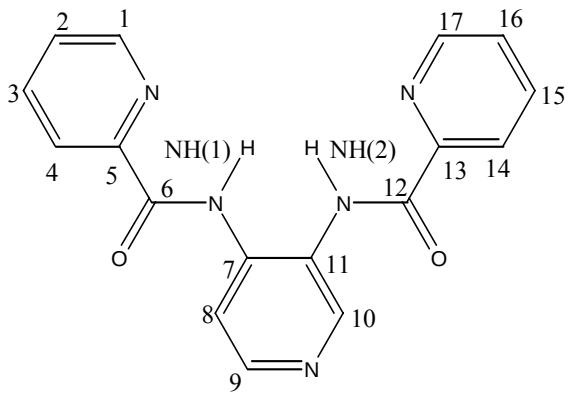

2.7

Figure 2.9-*N*,*N*′-bis(2-pyridinecarboxamide)-3,4-diaminopyridine

Table 2.8-^{1}H Resonances for *N*,*N*′-bis(2-pyridinecarboxamide)-3,4-pyridine

^{1}H	**1**	**2**	**3**	**4**	**8**	**9**	**10**	**14**	**15**	**16**	**17**	**N-H(1)**	**N-H(2)**
	8.77	7.71	8.08	8.19	8.14	8.47	8.67	8.17	8.08	7.66	8.57	10.97	10.79

Table 2.9-^{13}C Resonances for *N*,*N*′-bis(2-pyridinecarboxamide)-3,4-pyridine

^{13}C	**1**	**2**	**3**	**4**	**5**	**6**	**7**	**8**	**9**	**10**
	148.71	127.35	138.20	122.60	149.07	163.89	139.48	116.32	147.49	148.42

11	**12**	**13**	**14**	**15**	**16**	**17**
125.03	162.55	148.53	122.71	138.46	127.64	148.64

While the reaction with $[Ru(NO)Cl_3(H_2O)_2]$ was run, purification and complete NMR analysis are pending. Precipitate formation and color change, indicate that a reaction occurred. It is anticipated that this ligand will provide additional coordination modes different from the target complex, seen in Figure 2.10. The products are expected to be similar to those seen for **2.5**. However, if the same trend is followed, coordination is expected to occur through the O(1) and N(1) of **2.7**, rather than through O(2) and N(4) as seen in **2.5**.

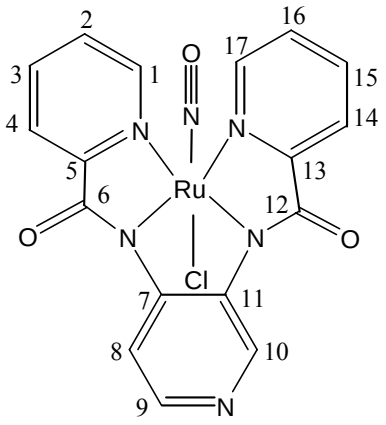

2.8

Figure 2.10-Tetradentate complex

2.4.3 Conclusion

The ligand *N*,*N*′-bis(2-pyridinecarboxamide)-3,4-diaminopyridine was synthesized and characterized by NMR spectroscopy and mass spectrometry. The relatively low yield is attributed to the formation of a monosubstituted side product. The NMR data are very similar to those obtained for **2.5**. The only observed difference being the placement of positive character on C-7 rather than C-11 for **2.7**. While products have not been isolated from the reaction between **2.7** and $[Ru(NO)Cl_3(H_2O)_2]$ they might be similar, but in opposite sense, to those obtained from the reaction between **2.5** and $[Ru(NO)Cl_3(H_2O)_2]$.

2.5 *N,N′*-BIS(2-PYRIDINECARBOXAMIDE)-1,2-ETHANE, -1,3-PROPANE

2.5.1 Materials and Methods

A significant part of the material presented in this chapter is reproduced with permission from a publication in Inorganic Chemistry Communications, 7, Carol F. Fortney, Steven J. Geib, Fu-tyan Lin, Rex E. Shepherd, Synthesis and Characterization of [Ru(NO)(bpp)Cl·2H$_2$O](bpp = N,N'-bis(2-pyridinecarboxamide)-1,3-propane dianion) and [Ru(NO)(bpe)Cl·2H$_2$O] (bpe = N,N'-bis(2-pyridinecarboxamide)-1,2-ethane dianion), 1065-1070, copyright Elsevier, 2005.

Materials and Measurements

[$RuCl_3 \bullet xH_2O$], $NaNO_2$, picolinic acid, 1,2-diaminopropane, 1,2-diaminoethane, pyridine, triphenylphosphite, chloroform and ethanol were obtained from Aldrich and used without further purification.

Instrumentation

^1H, $^{13}C\{^1H\}$ NMR, HMQC, HH COSY, and HMBC spectra were obtained on a Bruker AVANCE DRX 500 digital NMR spectrometer. Infrared spectra of KBr or KCl pellets were obtained on Perkin Elmer BX FT-IR spectrophotometer. Mass spectrometry was carried out on a Waters Q-TOF API US instrument using electrospray ionization or on a 571A HP GC-MS instrument.

Syntheses

Trichloronitrosylruthenium [$Ru(NO)(Cl_3)(H_2O)$] was prepared using a modification of the procedure of Fletcher et al.[67] [$RuCl_3 \bullet xH_2O$] (207.43 g/mol, 2.00 g, 0.0096 mol, 1 equiv) was dissolved in 1 M HCl (15.0-18.0 ml, > 1 equiv). The resulting solution was heated to 100° C in

an oil bath. At 100° C, an aqueous solution of $NaNO_2$ (68.9 g/mol, 1.99 g, 3 equiv.) was added dropwise over one hour. The dark red solution began to turn purple as NO_2 was released. After one hour, the water was removed from the reaction mixture under vacuum (rotary evaporator, 90 °C). The remaining dark purple solid was dissolved in ethanol to separate $[Ru(NO)(Cl_3)(H_2O)]$ from NaCl formed in the reaction. NaCl was removed via vacuum filtration. Ethanol was removed under vacuum (rotary evaporator, 65-70° C.) The extremely hygroscopic purple solid was stored in a desiccator with Drierite.

***N*,*N′*-bis(2-pyridine carboxamide)-1,2-ethane** ($bpeH_2$) (**2.9**) was prepared according to a modified literature procedure.[68] 1,2-diaminoethane (60.10 g/mol, d = 0.899 g/ml, 3.66 g, 0.060 mol, 1 equiv) in pyridine (~ 12.0 ml) was added to a stirred solution of picolinic acid (123.11 g/mol, 14.76 g, 0.119 mol, 2 equiv) in pyridine (~ 48.0 ml). After Triphenyl phosphite (310.29 g/mol, d = 1.184 g/ml. 31.5 ml, 0.119 mol, 2 equiv) was added slowly, the reaction mixture was heated for four hours in an oil bath (100° C). Pale yellow crystals formed overnight at room temperature. White crystals were obtained by recrystallization from chloroform. Yield : 14.06 g, 0.0520 mol, 87 % yield; ^{1}H NMR (500 MHz, DMSO-*d_6*): δ 8.95 (s, 2H, N*H_2*) 8.62 (d, 2H, H-1); 8.01 (d, 2H, H-4); 7.97 (td, 2H, H-3); 7.57 (td, 2H, H-5), 3.52 (m, 2H, H-5 & 6); (^{1}H NMR 500 MHz, $CDCl_3$) δ 8.52 (d, 2H, H-1), 8.37 (s, 2H, N*H_2*), 8.16 (d, 2H, H-4), 7.80 (td, 2H, H-3), 7.38 (td, 2H, H-2), 3.73 (m, 2H, H-5 & 6). ^{13}C {^{1}H} NMR (125 MHz, DMSO-*d_6*): δ 164.16 (C=O), 149.92 (Pyridyl-*ipso*), 148.31 (C-1), 137.66 (C-3), 126.39 (C-2), 121.81 (C-4), 38.84 (C-5 & 6); ^{13}C {^{1}H} NMR (125 MHz, $CDCl_3$ chloroform): δ 164.96 (C=O), 149.77 (Pyridyl-*ipso*), 148.10 (C-1), 137.25 (C-3), 126.14 (C-2), 122.21 (C-4), 39.51 (C-5 & 6).

Chloro-nitrosyl-*N,N′*-bis(2-pyridinecarboxamido)-1,3-ethane-ruthenium(II).

[Ru(NO)(bpe)Cl•$(H_2O)_2$] (**2.10**) was prepared using an adapted procedure from Vagg.[69] [Ru(NO)$Cl_3(H_2O)$] (0.500g, 0.002 mol, 1 equiv) was added to a stirred solution of **2.9 (**0.494 g, 0.0018 mol, 1 equiv) in an ethanol/water solution (95 %, ~60.0 ml, ~ 85° C). After 12 hours at reflux, a fine brown solid was obtained and removed by filtration. Upon reduction of the filtrate volume under vacuum (rotary evaporator, 30° C) an orange solid precipitated.. The solid was rinsed with small amounts of ethanol and dried at ~100° C. X-ray quality crystals were obtained from a concentrated solution of [Ru(NO)(bpe)Cl•$(H_2O)_2$] in ethanol. Yield 0.247g, 30 % yield; ^{1}H NMR (500 MHz, DMSO-*d_6*): δ 9.23 (d, 2H, H-1), 8.34 (td, 2H, H-3), 8.08 (d, H-4), 7.90 (dd, 2H, H-2), 4.02 (m, 2H, H-5′ & 6), 3.91 (m, 2H, H-5 & 6′); ^{13}C {^{1}H} NMR (125 MHz, DMSO-*d_6)*: δ 166.56 (C=O), 157.76 (Pyridyl-*ipso*), 152.40 (C-1), 141.44 (C-3) 127.70 (C-2), 125.53 (C-4), 51.62 (C-5 & 6); IR (KBr): ν_{NO} = 1825cm^{-1}; ESI-MS M + Na^+ 457.95 ($M^{+\bullet}$ = 434.77).

***N,N′*-bis(2-pyridine carboxamide)-1,2-propane (bppH$_2$) (2.11)** was prepared according to a literature procedure.[68] 1,2-diaminopropane (74.13 g/mol, d = 0.888 g/ml, 4.71 ml, 3.71 g, 0.050 mol, 1 equiv) in pyridine (~ 20.0 ml) was added to a stirring solution of picolinic acid (123.11 g/mol, 12.3 g, 0.099 mol, 2 equiv) in pyridine (~ 40 ml). After triphenyl phosphite (310.29 g/mol, d = 1.18 g/ml, 26.27 ml, 31.0 g, , 0.099 mol, 2 equiv) was added slowly, the reaction mixture was heated for 4 h in an oil bath ~ 100° C. A brown oil was obtained after solvent evaporation (rotary evaporator, ~80 °C). The oil was dissolved in chloroform (~ 50 ml), washed with water (~ 50 ml, 3 times), saturated sodium bicarbonate solution (~50 ml, 4 times), and finally with water (~ 50 ml, 3 times).

The chloroform solution was dried over magnesium sulfate and concentrated under vacuum (rotary evaporator, ambient temperature). A powdery white precipitate formed as the concentrated solution was added dropwise over one hour to diethyl ether (~ 70 ml, 0° C) with stirring. Recrystallization of the white precipitate from chloroform yielded white crystals. Yield: 6.75 g, 47 % yield) ^{1}H NMR (500 MHz, DMSO-d_6): δ 8.99 (t, 2H, NH_2) 8.61 (d, 2H, H-1), 8.03 (d, 2H, H-4), 7.95 (t, 2H, H-3); 7.57 (td, 2H, H-2), 3.34 (q, 4H, H-5), 1.75 (qn, 2H, H-6). ^{13}C{^{1}H} NMR (125 MHz, DMSO-d_6): δ 163.91 (C=O), 150.05 (Pyridyl-*ipso*), 148.31 (C-1), 137.68 (C-3), 126.35 (C-2), 121.79 (C-4), 36.29 (C-5), 29.42 (C-6); GC-MS *m/z* 284.

Chloronitrosyl-*N,N′*-bis(2-pyridinecarboxamido)-1,3-propane-ruthenium(II), [Ru(NO)(bpp)Cl•(H_2O)$_2$] **(2.12)** (448.86 g/mol, 0.080 g, 1.78 x 10^{-4} mol, 10 % yield), was prepared by the same procedure as described above for **2.9**. Recrystallization from an from DMSO provided X-ray quality crystals. ^{1}H NMR (500 MHz, DMSO-d_6): δ 9.24 (d, 2H, H-1), 8.38 (t, 2H, H-3), 8.18 (d, H-4), 7.91(t, 2H, H-2), 3.78 (m, 2H, H-5), 3.54 (t, 2H, H-5′), 2.10 (m, 2H, H-6′), 1.77 (q, 2H, H-6); ^{13}C{^{1}H} NMR (125 MHz, DMSO-d_6): δ 168.83 (C=O), 154.23 (Pyridyl-*ipso*), 150.21 (C-1), 141.67 (C-3), 127.31 (C-2), 125.20 (C-4), 46.23 (C-5), 30.19 (C-6); IR (KBr): (ν_{NO} = 1838 cm^{-1}); ESI-MS M + Na^+ 471.97.

2.5.2 Results and Discussion

Crystallographic Data Collection

X-ray quality crystals were obtained for **2.10** and **2.12** by slow evaporation of ethanol from the reaction mixture filtrate. Crystals of **2.12** were also obtained from DMSO after the reaction mixture filtrate was reduced in volume and taken up in DMSO. The crystal structure shown for **2.9** is from a crystal obtained in DMSO. Data collections were performed at room temperature on a Bruker Smart Apex CCD diffractometer using graphite-monchromated Mo K_α (λ = 0.71073 Å) radiation. Full crystallographic details are deposited in the Cambridge Structural Database (CCD 245015 and CDC245016). Crystal and intensity collection data are reported in Table 2.10.

Table 2.10-Crystal data and refinements for 2.10 and 2.12

	2.10	**2.12**
Chemical Formula	$C_{15}H_{18}ClN_5O_5Ru$	$C_{14}H_{16}ClN_5O_5Ru$
Formula Weight	484.86	470.84
Temperature (K)	293(2)	295(2)
Wavelength (Å)	0.71073	0.71073
Crystal system	Triclinic	Triclinic
Space group	P-1	P-1
a (Å)	7.6860(1)	7.3057(7)
b (Å)	11.180(2)	11.0170(1)
c (Å)	11.462(2)	11.7851(1)
α (°)	80.47(3)	79.900(2)
β (°)	74.99(3)	74.622(2)
γ (°)	72.58(3)	74.29(2)
Volume ($Å^3$)	903.6(3)	874.93(1)
Z	2	2
Density (calculated) Mg/m^3	1.767	1.787
Absorption Coefficient (mm^{-1})	1.054	1.086
F(000)	480	472
Crystal Size (mm^3)	0.37 x 0.34 x 0.21	0.38 x 0.18 x 0.13
θ range for data collection (°)	1.85 to 32.59	1.80 to 32.54
Index Ranges	$-11 \le h \le 11$	$-10 \le h \le 10$
	$-16 \le k \le 16$	$-16 \le k \le 16$
	$-17 \le l \le 17$	$-17 \le l \le 17$
Reflections collected	11590	11486
Independent reflections	6118 [R(int) = 0.0395]	5976 [R(int) = 0.0348]
Completeness	92.7 % (θ=32.59°)	94.2 % (θ=32.54°)
Data / restraints / parameters	6118 / 0 / 244	5976 / 0 / 235
Max. and min. transmissions	0.8091 and 0.6965	0.8717 and 0.6831
Refinement Method	Full-matrix least-squares on F^2	Full-matrix least-squares on F^2
Goodness-of-fit on F^2	1.167	1.092
Final R indices[$I > 2\sigma$ (I)]	R1 = 0.0790, wR2 = 0.2595	R1 = 0.0615, wR2 = 0.1487
R indices (all data)	R1 = 0.0886, wR2 = 0.2656	R1 = 0.0870, wR2 = 0.1606
Largest diff. peak and hole (e $Å^3$)	4.009 and -1.477	1.682 and -.0598

Crystal Structure Data

Figures 2.11 and 2.12 display the molecular structures of **2.10** and **2.12**, respectively. Tables 2.11 and 2.12 show selected bond lengths and angles for **2.10** and **2.12**, respectively. Both the pyridyl and deprotonated amido nitrogen atoms of the tetradentate bpe^{2-} and bpp^{2-} ligands coordinate to the ruthenium center in the equatorial plane to form a slightly distorted octahedral compound with axial chloride and nitrosyl substituents. The Ru-N amido and Ru-N pyridyl. The Ru-N-O angle in both compounds is linear, 177.0(4) for **2.10** and 177.5(6) for **2.12**. It follows that the N-O bond length for **2.10** (2.120(5) Å) is very similar to that for **2.12** (2.123(8) Å). That the Ru-NO (1.732(6) Å) and Ru-Cl (2.368(3)Å) bond lengths for **2.12** are slightly shorter than those in **2.10** (Ru-NO (1.742(4)) Å and Ru-Cl (2.383(1)) Å) may indicate that the NO group exerts a slightly stronger trans strengthening effect in **2.10** than in **2.12.** The longer Ru-Cl and Ru-N(5) bonds in **2.10** may also be due to the smaller bite angles of the bpe^{2-} ligand as discussed below.

For both complexes the ruthenium center is displaced toward the nitrosyl group from the plane defined by the nitrogen atoms (0.145 Å in **2.12** and 0.167 Å in **2.10)** due to the different bite angles of the ligands. More displacement is required to alleviate the steric interaction with the rings in **2.10** because the five member chelate ring has a smaller bite angle (84.2(1)°).[26,50] The smaller N(2)-Ru-N(3) angle in **2.10** also allows a larger N(1)-Ru-N(4) angle of 115.04(14) Å). The six member chelate ring in **2.12,** which has a bite angle of 95.4(3)°, forces a smaller N(1)-Ru-N(4) angle of 107.3(2)°. The smaller N(1)-Ru-N(4) in **2.12** causes the pyridyl groups to tip out of the plane slightly more in **2.12** than in **2.10** to minimize steric interaction between H-1 and H-14. Tilting of chelated pyridyl groups has been observed by others.[26] Both pyridyl rings involving N(1) on **2.10** and **2.12** exhibit less of a tilt than do those involving N(4).

The carbon-carbon bonds in the 5 member ring formed by the diamide in **2.10** exhibit typical bond lengths and angles. The N(5)-Ru-N(2) angle is 98.48(17) ° while the N(5)-Ru-N(3) angle is a little less at 96.35(16)°. The six member ring formed upon chelation of the bpp^{2-} ligand exhibits angles that are little larger than those of a six member ring. The largest deviation from the typical value of 112° is the C(8)-C(9)-N(3) angle which is 115.87°. In **2.12** the N(5)-Ru-N(2) and N(5)-Ru-N(3) angles, at 95.9(3)° and 93.7(3)°, repectively, deviate less from 90° than do those in **2.10**.

Finally, as Figure 2.13 shows, there are short close contacts between the chloride ion and the hydrogen atom on the pyridyl ring that is para to the nitrogen of the heterocyle. This interaction is great enough to pull the hydrogen atoms attached to C-10 in **2.10** and C-12 in **2.12** slightly out of the plane of the rest of the hydrogen atoms.

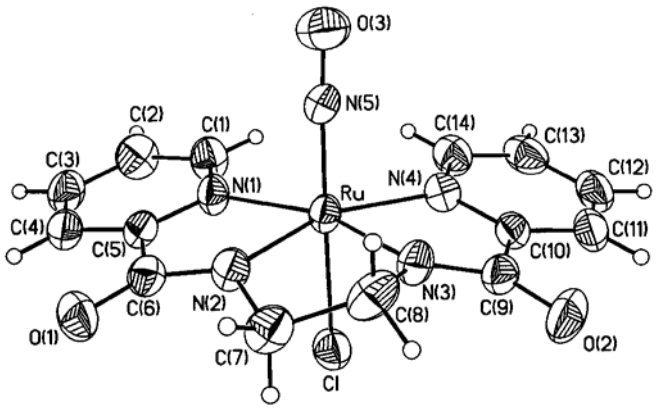

2.10

Figure 2.11-Molecular structure of [Ru(NO)(bpe)Cl]

Table 2.11- Selected bond distances (Å) and bond angles (°) for 2.10

O(3)-N(5)	1.140(5)	O(2)-C(9)	1.238(5)
Ru-N(5)	1.742(4)	O(1)-C(6)	1.231(5)
Ru-Cl	2.383(1)	N(2)-C(7)	1.471(6)
Ru-N(1)	2.118(3)	C(7)-C(8)	1.532(8)
Ru-N(4)	2.127(4)	N(3)-C(8)	1.456(6)
Ru-N(3)	1.980(3)	N(3)-C(9)	1.315(6)
Ru-N(2)	1.983(4)	N(2)-C(6)	1.329(6)
O(3)-N(5)-Ru	177.0(4)	N(3)-Ru-N(4)	79.51(1)
N(5)-Ru-Cl	174.2(1)	N(3)-Ru-N(1)	162.6(1)
N(5)-Ru-N(1)	92.53(1)	N(2)-Ru-N(4)	161.1(1)
N(5)-Ru-N(4)	92.81(1)	C(8)-N(3)-Ru	112.5(3)
N(5)-Ru-N(3)	96.39(1)	N(3)-C(8)-C(7)	110.4(4)
N(5)-Ru-N(2)	98.48(1)	C(7)-N(2)-Ru	113.4(3)
N(3)-Ru-N(2)	84.20(1)	N(2)-C(7)-C(8)	109.3(4)
N(1)-Ru-N(4)	115.0(1)	N(3)-C(9)-C(10)	112.2(4)
N(2)-Ru-N(1)	79.70(1)	N(2)-C(6)-C(5)	112.7(4)

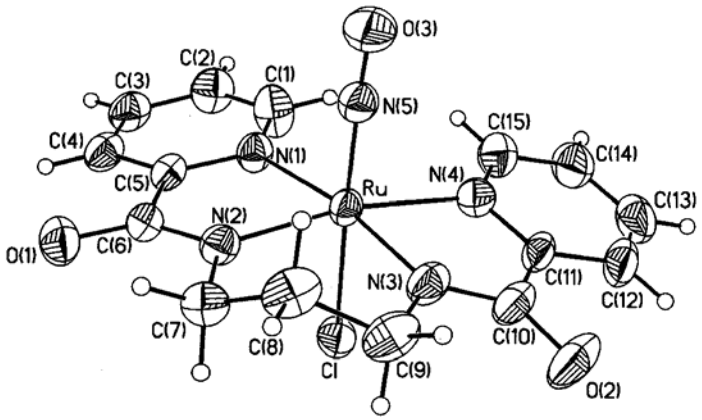

2.12

Figure 2.12-X-ray structure of [Ru(NO)(bpp)Cl]

Table 2.12- Selected bond distances (Å) and angles (°) for 2.12

O(3)-N(5)	1.143(8)	O(1)-C(6)	1.246(8)
Ru-N(5)	1.732(6)	O(2)-C(10)	1.252(9)
Ru-Cl	2.368(2)	N(2)-C(6)	1.321(9)
Ru-N(1)	2.129(5)	N(3)-C(10)	1.298(1)
Ru-N(4)	2.147(7)	N(2)-C(7)	1.460(9)
Ru-N(3)	2.039(6)	C(7)-C(8)	1.517(1)
Ru-N(2)	2.034(6)	C(8)-C(9)	1.522(1)
		N(3)-C(9)	1.468(1)
O(3)-N(5)-Ru	177.5(7)	N(3)-Ru-N(4)	77.9(3)
N(5)-Ru-Cl	176.4(2)	N(3)-Ru-N(1)	171.1(2)
N(5)-Ru- N(1)	93.2(3)	N(2)-Ru-N(4)	169.0(2)
N(5)-Ru- N(4)	93.3(3)	N(2)-C(7)-C(8)	112.6(6)
N(5)-Ru- N(3)	93.7(3)	C(7)-C(8)-C(9)	115.8(7)
N(5)-Ru- N(2)	95.9(3)	C(9)-N(3)-Ru	123.4(5)
N(2)-Ru- N(3)	95.4(3)	C(7)-N(2)-Ru	123.5(5)
N(1)-Ru- N(4)	107.3(2)	N(3)-C(10)-C(11)	114.1(6)
N(2)-Ru- N(1)	78.3(2)	N(2)-C(6)-C(5)	113.5(6)

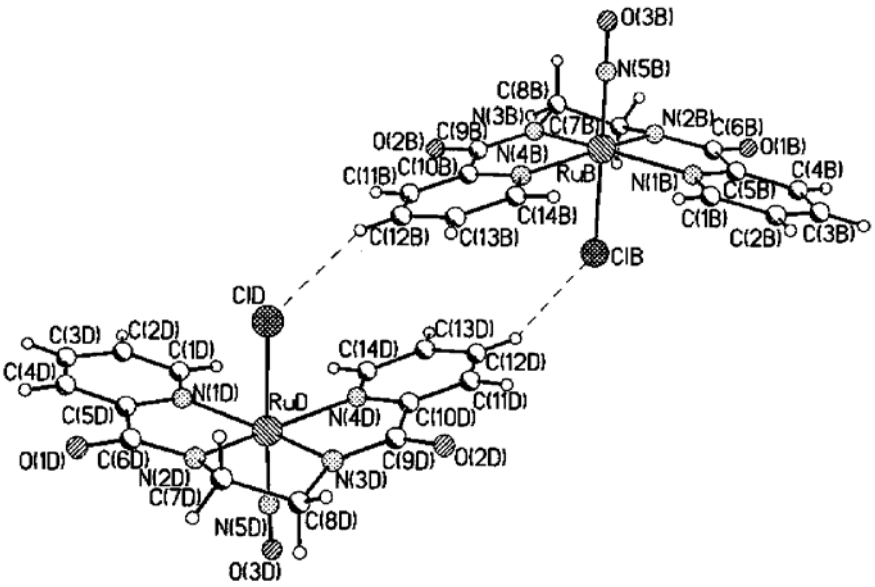

2.10

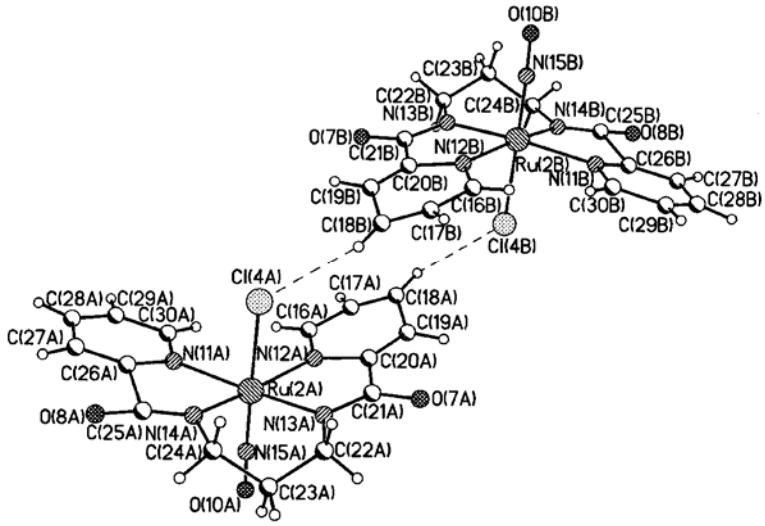

2.12

Figure 2.13-Close contacts in the crystal lattices of 2.10 and 2.12

Infrared Data

The infrared spectrum of a pure sample of **2.10** in KBr showed a split nitrosyl peak with one peak at 1852 cm^{-1} and the other at 1825 cm^{-1}. Split NO peaks have been observed for complexes having only one NO group. For example, splitting of the absorbance associated with the NO stretching mode has been observed for *cis*-$[RuCl(en)_2(NO)]Cl_2$, $[RuBr(en)_2(NO)]Br_2$, $[RuI(en)_2(NO)]I_2$,[55] $[Ru(NH_3)_5(NO)]Cl_3 \bullet H_2O$,[71]and *mer*-$[RuX_3(en)(NO)]$ where X = Cl, Br, and I.[72] For the complex ions the splitting has been attributed to an interaction between the counterion and the NO group.[2,71] For neutral complexes, the splitting has been explained by a slight difference in the conformation of the ethylenediamine ligand induced in sample preparation.[55] Unexpected peaks in infrared spectra, particulary with KBr pellets, have also been attributed to reactions with KBr and to interactions with KBr.[73] To eliminate the possibility of interaction with KBr as the cause of the extra NO stretch, a spectrum was obtained using a KCl pellet. In this case (Figure 2.14a) exhibited only one NO stretch at 1825 cm^1 and a shoulder of another at 1850 cm^{-1}. This result suggests that bromide might displace chloride when the sample is prepared in KBr. Hence, only one NO peak is observed when the sample is prepared in KCl. However, the Ru-Cl bond is quite strong, especially when it is trans to NO. Moreover, if Br^- had displaced Cl^- the peak that should remain when the spectrum is obtained in KCl should be the one with the highest stretching frequency. Since the lower frequency peak remains, exchange with bromide was not the cause of the splitting. Another spectrum of the same KCl pellet of **2.10** obtained after several days of being exposed to air (Figure 2.14b) showed two NO peaks of equal intensity. The extra peak along with an increase in the intensity of the peak representing the O-H stretching mode suggested that water might be the cause of the splitting. A final IR spectrum (Figure 2.14c), obtained after the same KCl pellet was stored for two days at 120° C to remove

the water, exhibited only one NO peak at 1825 cm^{-1} and lacked the O-H peak. Therefore it was concluded that water is the cause of the split NO peak. Only one NO peak was observed in the infrared spectrum of **2.12** at 1868 cm^{-1}. Given their similar N-O bond lengths the stretching frequency for **2.12** seemed a little high compared to that for **2.10**. To test whether the peak was actually two overlapping peaks, the KBr pellet of **2.12** was dried at 120 °C. Figure 2.15 shows that after about three hours drying, the peak representing the NO stretching frequency had shifted to 1838 cm^{-1} as the water peak decreased in size. A peak at about 1384 cm^{-1} is characteristic of all RuNO compounds derived from $[Ru(NO)Cl_3(H_2O)_2]$ is observed in the spectra for both compounds and is assigned to the Ru-NO bending mode.[22]

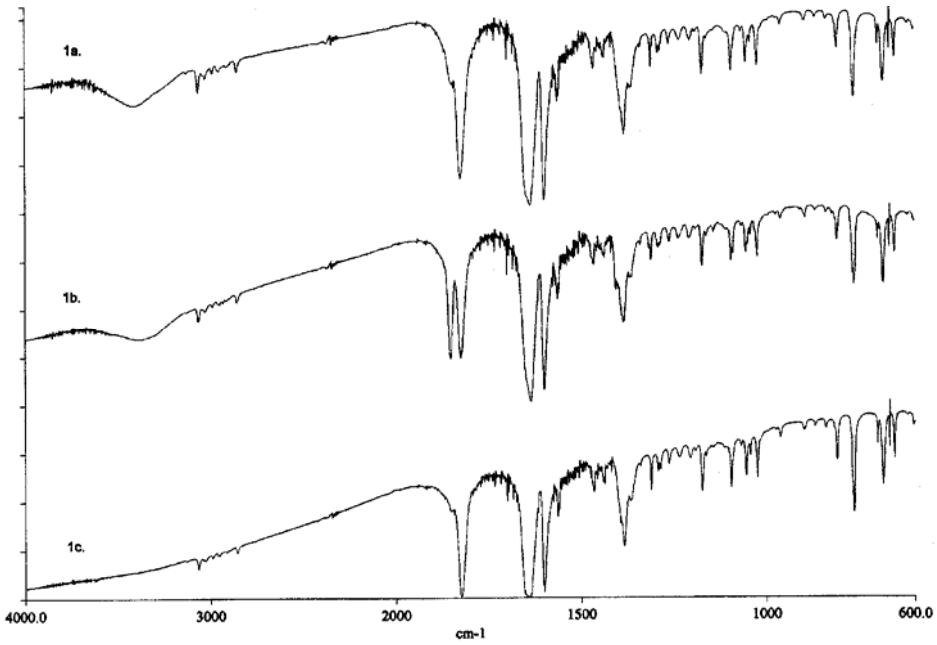

Figure 2.14- IR spectrum of $[Ru(NO)(bpe)(H_2O)_2]$ KCl pellet
a. immediately after preparation; b. after several days in air at ambient temperature c. after two days in 120° C oven

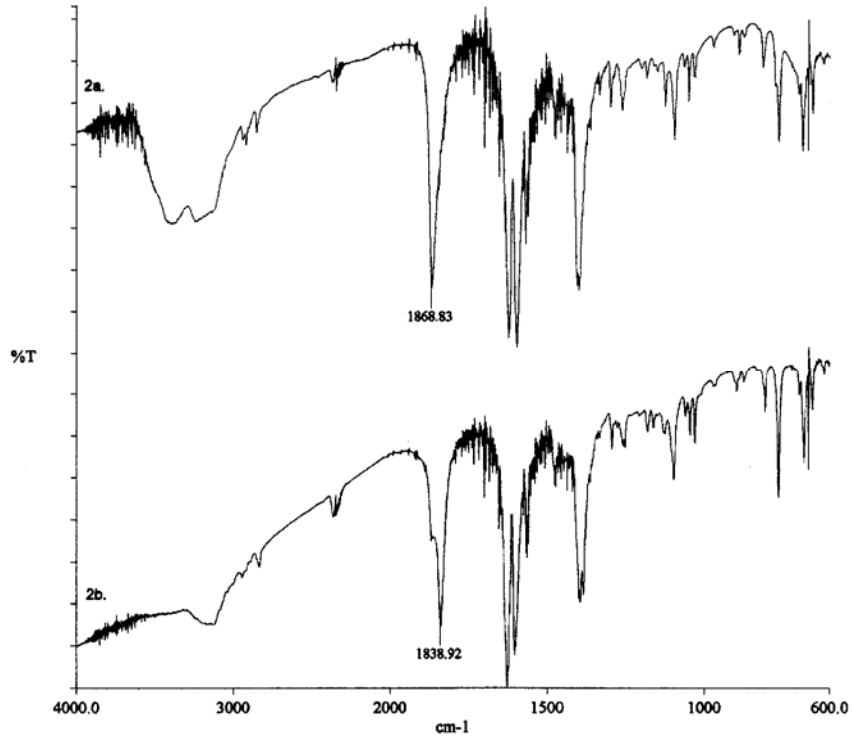

Figure 2.15- a. Fresh [Ru(NO)(bpp)Cl] KBr pellet; b. After 3 hours at 120° C

NMR Data

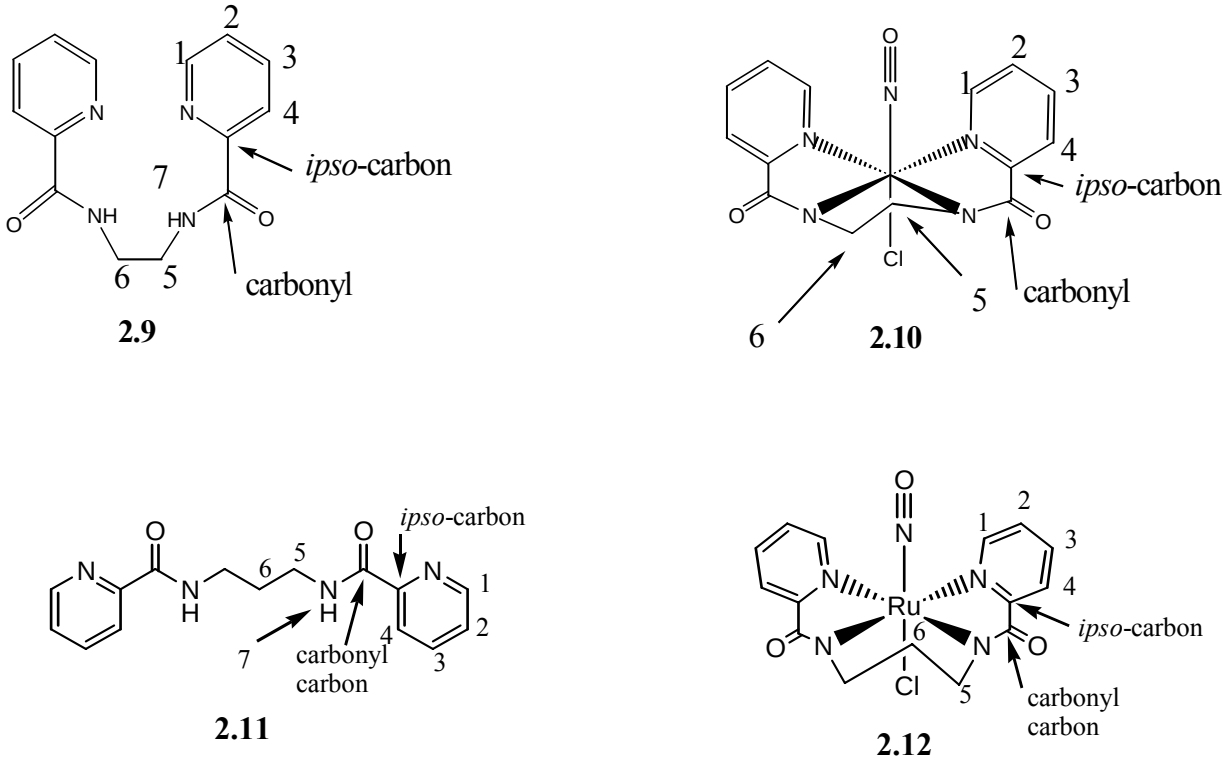

Figure 2.16-Numbering schemes for 2.9, 2.10, 2.11, and 2.12

Table 2.13-^{1}H and ^{13}C Chemical Shifts[a] for 2.9[b], 2.10[c], 2.11[d], and 2.12[e]

^{1}H	1	2	3	4	5	5′ [f]	6	6′ [f]	7		
2.9	8.62	7.57	7.97	8.01	3.52	*	3.52	*	8.95		
2.10	9.23	7.90	8.34	8.08	3.91	4.02	4.02	3.91	*		
2.11	8.61	7.57	7.95	8.03	3.34	*	1.75	*	8.99		
2.12	9.24	7.91	8.38	8.18	3.78	3.54	1.77	2.10	*		
^{13}C										**Py-*ipso***	**C=O**
2.9	148.31	126.39	137.66	121.81	38.48	*	38.48	*	*	149.92	164.16
2.10	152.40	127.70	141.44	125.53	51.62	*	51.62	*	*	157.76	166.56
2.11	148.31	126.35	137.68	121.79	36.29	*	29.42	*	*	150.05	163.91
2.12	150.21	127.31	141.67	125.20	46.23	*	30.19	*	*	154.23	168.83

a. 500 MHz for ^{1}H; 125 MHz for ^{13}C; dmso-d_6

b. *N,N′*-bis(2-pyridinecarboxamide)-1,2-ethane ($bpeH_2$)

c. [Ru(NO)(bpe)Cl] (bpp = *N,N′*-bis(2-pyridinecarboxamide)-1,2-ethane dianion)

d. *N,N′*-bis(2-pyridinecarboxamide)-1,2-propane ($bppH_2$)

f. Prime indicates methylene proton oriented toward the Ru-NO moiety

* Not applicable

Figure 2.16 shows the numbering schemes for **2.9**, **2.10**, **2.11** and **2.12.** The ^{1}H and ^{13}C NMR data, obtained in DMSO-d_6, are shown in Table 2.13. ^{1}H and ^{13}C assignments are based on the HH COSY and HMQC spectra. The HH COSY and HMQC spectra for the pyridyl resonances of **2.9** are shown in Figures 2.17 and 2.18, respectively. Figure 2.17 depicts the correlations between H-2, H-3 and H-1, between H-3 and H-4, and between H-1 and H-2. A correlation (not shown) also exists between the ethylene protons at 3.52 ppm and and the amide protons at 8.95 ppm.

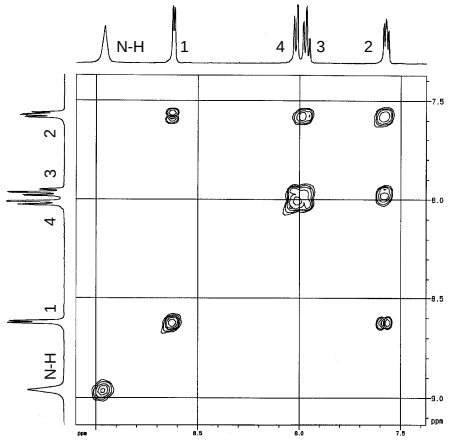

Figure 2.17- Pyridyl region of HH COSY spectrum of 2.11

The HMQC spectrum in Figure 2.18 shows the correlation of each proton resonance with its respective carbon resonance. Quaternary carbon signals at 149.77 ppm and 164.96 ppm in the HMQC spectrum are assigned to the pyridyl-*ipso* carbon and the carbonyl carbon, respectively, based upon the HMBC spectrum.[74] The most downfield ^{13}C signal that exhibits a proton correlation, appears at 148.10 ppm and corresponds to H-1. H-1 is also the most downfield doublet by virtue of its proximity to the electron-withdrawing the pyridyl nitrogen. The next most downfield doublet, H-4, correlates with the second most upfield ^{13}C resonance. This might be rationalized by considering the magnetic anisotropy induced by the ring current as well as the different resonance forms of the pyridine ring.[75,76] Except for the extra carbon and proton signals associated with the extra methylene carbon in **2.11,** the NMR data for **2.11** i**s** almost exactly the same as that for **2.9.**

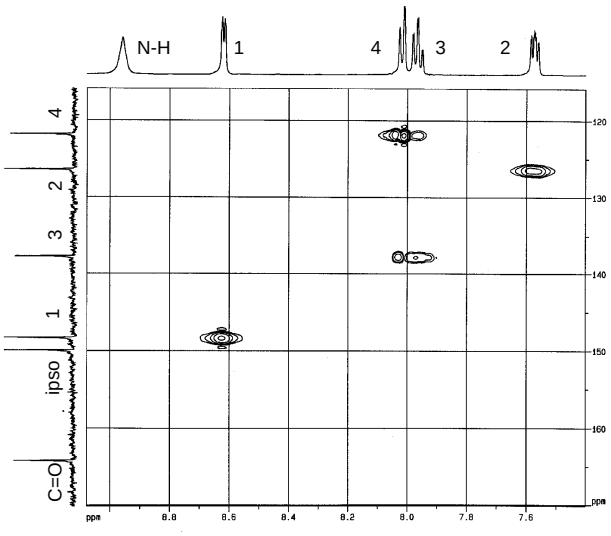

Figure 2.18-Pyridyl region of HMQC spectrum of 2.11

Table 2.13 compares the ^{1}H and ^{13}C data for **2.9**, **2.10**, **2.11** and **2.12**. The lack of an N-H signal in the ^{1}H NMR spectra for **2.10** and **2.12** indicates that each ligand coordinates in its deprotonated form. Due to the electron withdrawing nature of the Ru-NO center,[22] all proton and carbon resonances shift downfield upon coordination to ruthenium. The ethylene carbon atoms are undifferentiated in the ^{13}C spectrum of **2.10**, however the protons associated with them, H-5 and H-6, are differentiated by their proximity to the nitrosyl group.[72,77] Figure 2.19 illustrates how the ethylene protons' signal splits into two downfield-shifted multiplets upon formation of **2.10**. The most downfield multiplet at 4.02 ppm is assigned to H-5′, the axial proton on carbon 5, and to H-6, the equatorial proton on C-6. The signal at 3.90 ppm represents H-5 and H-6′, which are on the chloride face of the compound and farthest from the NO group. It might be helpful to refer to the crystal structure of **2.10** in Figure 2.11; but be aware of the different numbering scheme.

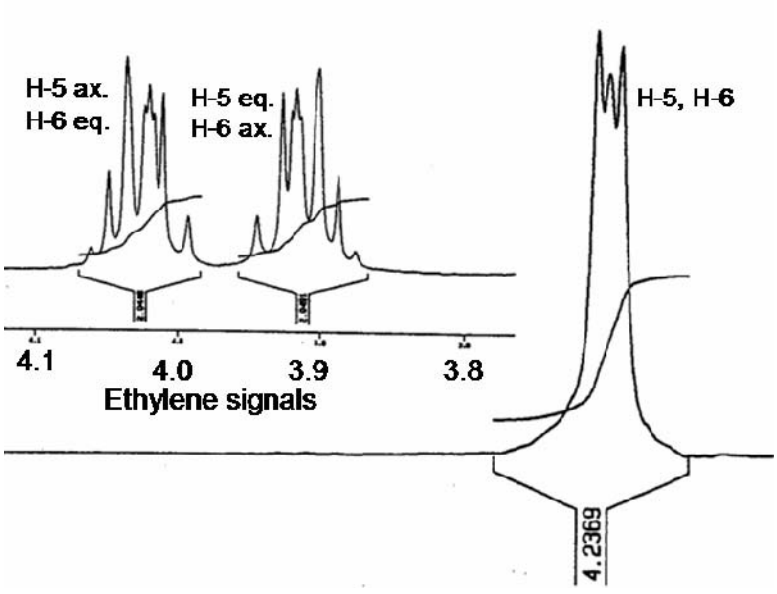

Figure 2.19- ^{1}H NMR signal for ethylene protons of 2.9 and 2.10

In **2.9** the protons on C-5, which are bonded to the amido nitrogens, are identical; however, they are in different environments than those on the central methylene carbon, C-6. Thus the spectrum exhibits a triplet at 3.34 ppm for protons labeled H-5 and a multiplet at 1.75 ppm for protons labeled H-6. Coordination of **2.9** causes both methylene signals to shift downfield and split into two groups of two signals. One of the signals, a doublet of doublets, at 3.78 ppm, has been assigned to the protons that are directed toward the nitrosyl group; the other signal, an apparent triplet at 3.54 ppm has been assigned to those oriented toward the chloride. The central methylene resonance is also split into two multiplets. Again, the most downfield shifted signal at 2.10 ppm has been assigned to the proton which is directed toward the nitrosyl group while the negligibly shifted resonance at 1.77 ppm is assigned to the proton directed away from the NO group.

As previously mentioned, all ^{1}H and ^{13}C signals shift downfield upon coordination. However, there are some interesting differences in the magnitude of the shift for **2.10** and **2.12.** For **2.10** both carbons which are bonded to the amido nitrogen atoms (C-5) resonate 13.14 ppm more downfield than those of the free ligand. This compares to a downfield shift of 9.94 ppm for the analogous carbon atoms in **2.12**. Also, C-1 and the pyridyl *ipso* signals are more affected upon coordination in **2.10** than they are in **2.12**. For **2.10** for C-1 shifts 4.09 ppm, while that for **2.12** C-1 shifts only 1.9 ppm. A difference of similar magnitude is seen for the pyridyl *ipso* carbon which is downfield shifted 7.84 ppm in **2.10** and only 4.18 ppm for **2.12**. The carbonyl signal, on the other hand, is less responsive to coordination in **2.10** than it is in **2.12**. In **2.10** the carbonyl carbon ^{13}C signal shifts downfield 2.40 ppm while in **2.12** it shifts 4.92 ppm.

2.5.3 Conclusion

The $\{RuNO\}^6$ compounds, [Ru(NO)(bpe)Cl•$2H_2O$)] and [Ru(NO)(bpp)Cl•$2H_2O$], are distorted octahedral compounds with the chloride ligand trans to a linearly bound NO group. The ^1H and ^{13}C spectra suggest that the compounds maintain the same coordination geometry in solution as they do in the solid state. The crystal structure reveals that all of the ruthenium-nitrogen bonds in the equatorial plane are shorter for **2.10** than for **2.12.** Accordingly ^{13}C and ^1H NMR analyses shows that carbons bonded to nitrogen and their respective protons are more downfield shifted in **2.10** than in **2.12** upon coordination. An exception is the ^{13}C signal of the carbonyl carbon which is less downfield shifted in upon coordination of **2.10** than it is upon coordination of **2.12**.

The nitrosyl stretching frequencies of 1825 cm^{-1} for **2.10** 1838 cm^{-1} for **2.12** are in good agreement with literature values for similar compounds.[1,26,55,78] That the NO stretching frequencies of **2.10** and **2.12** are less than that for the [Ru(NO)(bpb)Cl] compound (1867 cm^{-1}) indicates that more electron density is pushed on to the NO group by the bpe^{2-} and bpp^{2-} ligands than by the bpb^{2-} ligand.

The infrared spectrum of **2.10** exhibited a distinctly split NO peak. Split NO peaks have been observed and attributed to interactions with counter ions, to slight variations in NO and ligand conformation, to the solvent when the sample is prepared in solution, and with reactions with KBr in KBr pellets.[73,79] The split NO peak exhibited by **2.10** is attributed to hydrogen bonding interaction with water in the KBr pellet. Drying the KBr pellet of **2.12** revealed that there was a split NO peak for **2.12** as well. Drying of a KBr pellet of [Ru(NO)(bpb)Cl] removed water but the NO peak remained unchanged. This can indicate that the nitrosyl oxygen

atoms in **2.10** and in **2.12** exhibit a higher basicity, therefore an increased propensity to hydrogen bond,[73] compared to that in [Ru(NO)(bpb)Cl] **(1.5)**.

2.6 *N*,*N*′-BIS(2-PYRIDINECARBOXAMIDE)-1,4-PIPERAZINE

2.6.1 Materials and Methods

***N*,*N*′-bis(2-pyridinecarboxamide)-1,4-piperazine (2.13)** was prepared according to a literature procedure.[68] Triphenyl phosphite (d = 1.184 g/mL, 30.40 mL, 0.116 mol) was added slowly to a solution of picolinic acid (14.29 g, 0.116 mol) and 1,4 piperazine (5.00 g, 0.0580 mol) in dry pyridine (47.0 mL). After four hours of stirring at 100 °C the reaction mixture was allowed to sit at room temperature for several days until crystals formed. White crystals were collected by vacuum filtration. Recrystallization several times from dimethylsulfoxide yielded X-ray quality crystals. ^{1}H NMR (300 MHz, DMSO-d_6, δ): 8.58 (dd, 2H, H-1), 7.93 (m, 2H, H-3), 7.61 (m, 2H, H-4), 7.48 (m, 2H, H-2), 3.75 (s, 2H, H-8), 3.66 (m, 2H, H-7), 3.53 (m, 2H, H-6), 3.44 (s, 2H, H-5); ^{13}C{H} (125 MHz, DMSO-$_{d6}$ δ): 166.86 (C=O), 153.63 (Py-*ipso*), 148.40 (C-1), 148.31 (C-1′), 137.46 (C-3, C-3′), 124.78 (C-4), 123.40 (C-2), 46.83 (C-5), 46.24 (C-6), 41.95 (C-7), 41.40 (C-8); ESI-MS M^+ 298

Reaction with [Ru(NO)Cl$_3$(H$_2$O)$_2$]: The reaction between **2.13** and [Ru(NO)Cl$_3$(H$_2$O)$_2$] was run according to a modified literature procedure.[69] Trichloronitrosylruthenium (0.0018 mol, 0.500 g) was added to a ethanol/water (95%, 40.0 mL) solution of *N*,*N*′-bis(2-pyridinecarboxamide)-2,4-piperazine (0.447 g, 0.0015 mol, 1 equiv) with stirring. The reaction mixture was stirred for ten hours at 85.0 °C. A brown precipitate was isolated from the reaction mixture.

The filtrate was left for slow evaporation of solvent at room temperature for crystal formation. The color change and precipitate formation indicate that a reaction has occurred. However, isolation and characterization of the products is pending.

2.6.2 Results and Discussion

The ligand *N*,*N*′-bis(2-pyridinecarboxamide)-1,4-piperazine **(2.13)** was prepared and characterized by ^{13}C and ^{1}H NMR spectroscopy. The labeling scheme for NMR chemical shift assignments is shown in Figure 2.20. ^{1}H and ^{13}C NMR assignments can be seen in Tables 2.13 and 2.14, respectively. The respective ^{1}H signals for each pyridyl moiety exhibit the same chemical shift values. The aryl portion of the ^{1}H NMR spectrum can be seen in Figure 2.21 .The ^{13}C signals are approximately the same for each pyridyl moiety, C-1 for one pyridyl moiety resonates at 148.40 while C-1′ resonates at 148.31; two very closely spaced signals also occur for C-3 and C-3′.

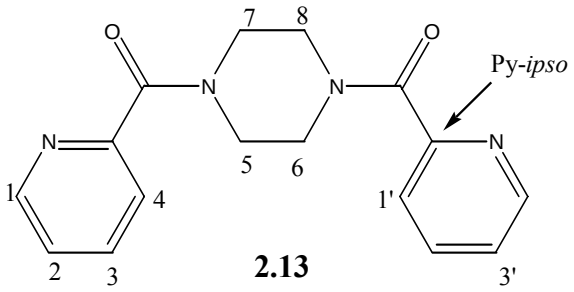

2.13

Figure 2.20-*N*,*N*′-bis(2-pyridinecarboxamide)-1,4-piperazine

Table 2.14-^{1}H NMR Data for *N*,*N*′-bis(2-pyrazinecarboxamide)-1,4-piperazine

^{1}H	1	2	3	4	5	6	7	8
2.13	8.58	7.48	7.93	7.61	3.44	3.53	3.66	3.75

Table 2.15-^{13}C NMR Data for *N*,*N*′-bis(2-pyrazinecarboxamide)-1,4-piperazine

^{13}C	1	2	3	4	Py-*ipso*	C=O	5	6	7	8
2.13	148.40	124.78	137.46	46.83	153.63	166.86	46.83	46.24	41.95	41.48

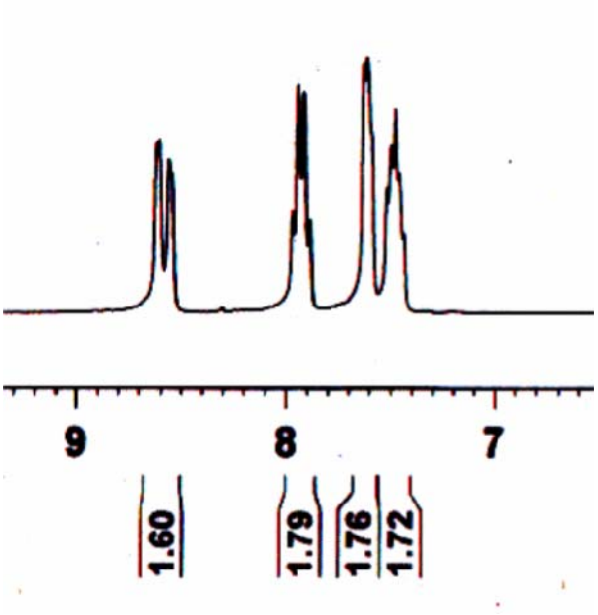

Figure 2.21-Aryl region of ^{1}H NMR spectrum of 2.13

The X-ray structure of *N*,*N*′-bis(2-pyridinecarboxamide)-1,4-piperazine can be seen in Figure 2.22. Crystal intensity and collection data are reported in Table 2.16. Selected bond distances and angles are shown in Table 2.17. There is some variation in bond angles for the piperazine ring. The N(2)-C(9)-C(10) angle is larger than the N(3)-C(8)-C(7) angle while the C(9)-C(10)-N(3) angle is slightly larger than the N(2)-C(8)-C(7) angle. The angles that include the pyridine nitrogen also vary slightly with the N(4)-C(12)-C(11) angle being larger than the corresponding N(1)-C(5)-(6) angle.

Table 2.16-Crystal data and refinements for 2.13

	2.13
Chemical Formula	$C_{144}H_{176}N_{32}O_{24}$
Formula Weight	2995.65
Temperature (K)	150(2)
Wavelength (Å)	0.71073
Crystal system	Triclinic
Space group	P-1
a (Å)	10.4724(9)
b (Å)	18.2261(15)
c (Å)	19.9367(14)
α (°)	90
β (°)	108.922(4)
γ (°)	90
Volume ($Å^3$)	3599.7(5)
Z	1
Density (calculated) Mg/m^3	1.382
Absorption Coefficient (mm^{-1})	0.206
F(000)	1584
Crystal Size (mm^3)	0.27 x 0.22 x 0.22
θ range for data collection (°)	1.55 to 27.50
Index Ranges	$-13 \le h \le 13$ $-23 \le k \le 23$ $-25 \le l \le 25$
Reflections collected	34838
Independent reflections	8264 [R(int) = 0.0260]
Completeness	100 % (θ=27.50°)
Data / restraints / parameters	8264/ 0 / 469
Max. and min. transmissions	0.9560 and 0.9464
Refinement Method	Full-matrix least-squares on F^2
Goodness-of-fit on F^2	0.934
Final R indices[$I > 2\sigma(I)$]	R1 = 0.0753, wR2 = 0.1797
R indices (all data)	R1 = 0.1450, wR2 = 0.2100
Largest diff. peak and hole (e $Å^3$)	1.465 and -0.266

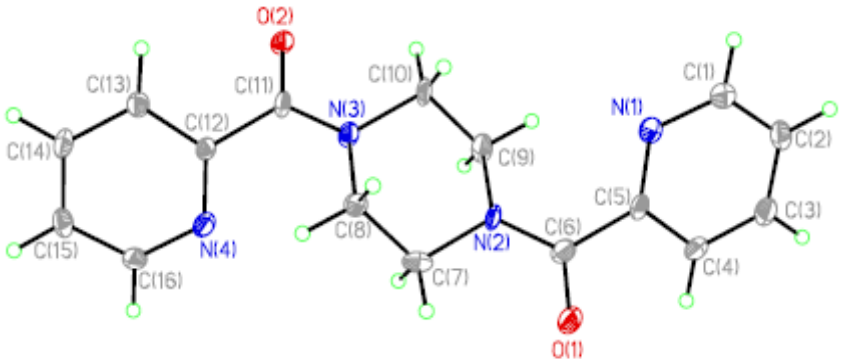

2.13

Figure 2.22-X-ray structure of *N*,*N*′-bis(2-pyridinecarboxamide)-1,4-piperazine

Table 2.17-Selected Bond Lengths and Angles for 2.13

O(1)-C(6)	1.232(5)	O(2)-C(11)	1.232(5)
N(3)-C(11)	1.344(5)	N(2)-C(6)	1.342(5)
N(3)-C(8)	1.472(5)	N(2)-C(9)	1.457(5)
C(7)-C(8)	1.512(5)	C(9)-C(10)	1.482(6)
N(2)-C(7)	1.485(5)	N(3)-C(10)	1.484(5)
C(11)-C(12)	1.513(5)	C(5)-C(6)	1.510(6)
N(4)-C(12)-C(11)	119.2(3)	N(1)-C(5)-C(6)	117.7(3)
N(3)-C(11)-C(12)	119.4(4)	N(2)-C(5)-C(6)	119.5(4)
N(3)-C(8)-C(7)	108.9(3)	C(9)-C(10)-N(3)	109.4(4)
N(2)-C(8)-C(7)	108.8(3)	N(2)-C(9)-C(10)	110.6(4)
C(16)-N(4)-C(12)	117.2(3)	N(1)-C(5)-C(6)	117.7(3)

Although the tetradentat compound (**2.14)** shown in Figure 2.24 has not been isolated. A color change, precipitate formation and preliminary NMR data from the reaction between **2.13** and $[Ru(NO)Cl_3(H_2O)_2]$ suggest the formation of at least one new species. The aryl region of the 300 MHz NMR spectrum of the reaction mixture is shown in Figure 2.25.

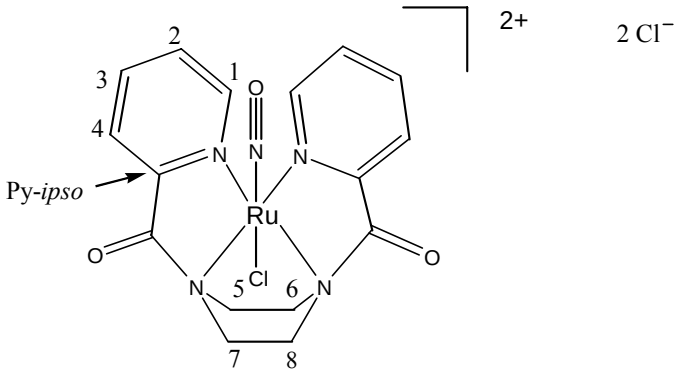

Figure 2.23-Tetradentate RuNO complex

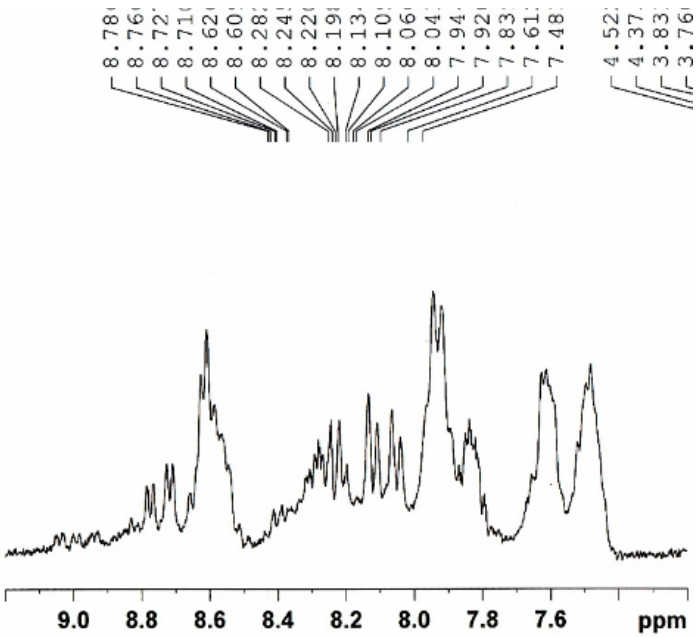

Figure 2.24-^{1}H NMR Spectrum of reaction mixture from 2.13 with $[Ru(NO)Cl_3(H_2O)_2]$

2.6.3 Conclusion

The ligand, *N*,*N*′-bis(2-pyridinecarboxamide)-1,4-piperazine has been synthesized and characterized by NMR spectroscopy and X-ray crystallography. Preliminary NMR results suggest formation of at least one new species upon reaction of $[Ru(NO)Cl_3(H_2O)_2]$ with **2.13**.

2.7 GENERAL CONCLUSION

The ligands *N*,*N*′-bis(2pyridinecarboxamide)-1,2-benzene, *N*,*N*′-bis(2pyridinecarboxamide)-2,3-diaminopyridine, *N*,*N*′-bis(2pyridinecarboxamide)-3,4-diaminopyridine, *N*,*N*′-bis(2pyridinecarboxamide)-1,2-ethane, *N*,*N*′-bis(2pyridinecarboxamide)-1,3-propane, and *N*,*N*′-bis(2pyridinecarboxamide)-1,4-piperazine were prepared and characterized by ^{13}C and ^{1}H NMR spectroscopy and/or X-ray crystallography. The ligands were allowed to react with $[Ru(NO)Cl_3(H_2O)_2]$ to form complexes that might facilitate RuNO transport through the body. The carboxamido groups were included to enhance solubility, activate the nitrosyl moiety to photolytic loss of $NO^{\bullet}$ and then stabilize the Ru^{III}-solvent complex that remains after photolysis. The pyridyl arms are intended to ensure chelation to the Ru^{II} center.

The first ligand, *N*,*N*′-bis(2pyridinecarboxamide)-1,2-benzene, coordinated to the RuNO center in the equatorial plane as expected. The complex is formally $\{Ru^{II}NO^{+}\}^6$ as determined by the NO stretching frequency of 1867 cm^{-1}. A crystal structure of the ruthenium nitrosyl complex obtained by the Mascharak group reveals a linear nitrosyl with an Ru-N-O angle of 172.37(14)°. Photochemical experiments confirmed photolysis $NO^{\bullet}$ under UV light.[26]

The second ligand, *N*,*N*′-bis(2-pyridinecarboxamide)-2,3-diaminopyridine, differs from *N*,*N*′-bis(2pyridinecarboxamide)-1,2-benzene, in that the aromatic backbone is 2,3-diaminopyridine, rather than 1,2 diamino benzene. Introduction of the pyridine moiety changes the reactivity of the ligand such that coordination to Ru^{II} occurs through a carbonyl oxygen atom and through one pyridine nitrogen. The uncoordinated ligand is pendant. X-ray crystallography reveals that the two RuNO complexes result from the same coordination mode. One complex has an Ru-N-O angle of 177.5(9) the other, 172.9(10). Another interesting feature about the complexes that result from this binding mode is the chloride ions are in the equatorial plane. For all of the other complexes characterized in this series, a chloride atom is trans to NO. Unfortunately, no IR data are available at this time. However, the slight difference in N-O bond for each isomer suggests that each will exhibit unique N-O stretching frequency, at least in the solid state. It remains to be seen if this coordination mode will facilitate NO transport and photolysis. Regardless, there are some possible benefits to this coordination mode. The uncoordinated portion of the ligand is available to either coordinate to another Ru-NO moiety or even to a different metal. The pendant carboxamido and pyridyl groups might also provide a means to anchor the complex to a biologically active site. Another product which seems to be coordinated through only one carboxamido nitrogen and one pyridyl group has also been isolated. This complex also offers the potential to coordinate to another metal center or to some bioliogically active site. Although the tetradentate coordinated complex has not been isolated, its presence in the reaction mixture has not been ruled out. If it is isolated the difference in the electron-donating abilities of the carboxamido nitrogen atoms are likely to introduce some interesting reactivity to the complex. Isolation of complexes with various coordination modes will reveal much about this ligand's influence on the Ru-NO moiety.

The third ligand, *N*,*N*′-bis(2pyridinecarboxamide)-3,4-diaminopyridine, was characterized by ^{13}C and ^{1}H NMR spectroscopy. The ligand exhibits the same differences in ^{13}C NMR chemical shift for the carboxamido bearing nitrogen atoms but in the opposite sense. Unfortunately, the product from the reaction between the ligand and $[Ru(NO)Cl_3(H_2O)_2]$ were not isolated in time for this report. However, if the complex follows the same trend at the 2,3-diaminopyridine derivative then similar coordination modes that reflect the difference in position of the pyridine nitrogen in the ligand backbone might be observed.

The fourth ligand, N,N′-bis(2pyridinecarboxamide)-1,2-ethane, has an alkyl backbone instead of an aromatic backbone. A crystal structure was obtained for the RuNO complex. The complex exhibits a linear Ru-NO bond with and angle of 177.0(4)° and N-O bond length of 1.140(5). The N-O infrared stretching frequency is 1825 cm^{-1}.

The fifth ligand, *N*,*N*′-bis(2pyridinecarboxamide)-1,3-propane, has an additional carbon in the the alkyl backbone and introduces some variation in the bite angles with respect the ethane derivative. The crystal structure of the RuNO complex reveals a linear Ru-N-O angle and N-O bond distance similar to the ethane derivative. The N-O infrared stretching frequency at 1838 cm^{-1} is higher than that of the ethane derivative and might be a function of bite angle. The protons on the backbone of the alkyl derivative seem to be good reporters of the magnetic anisotropy presented by the Ru-NO moiety. The ^{1}H NMR signals for the protons on the backbone each alkyl derivative are differentiated by their position with respect to the central metal. Derivatization at the central carbon might provide more information and also provide an anchoring site for biological molecules.

A crystal structure for the final ligand in this series, *N*,*N*′-bis(2pyridinecarboxamide)-1,4-piperazine was obtained. While the product(s) from the reaction between the ligand and

$[Ru(NO)Cl_3(H_2O)_2]$ were not isolated, ^1H NMR analysis suggest formation of at least one new product. If tetradentate coordination occurs, the orientation two piperazine ethylene chains should provide more information about the magnetic anisotropy about the Ru-NO moiety as well as provide sites for derivatization. Comparison of NMR data for the Ru-NO complex and the ligand will provide information about the distortion introduced to the ligand upon coordination.

In summary, the reaction between $[Ru(NO)Cl_3(H_2O)_2]$ and the ligands described yield complexes that may facilitate Ru-NO transport to tumor cells. Slight variations in the ligand backbone in some cases seems exert a strong influence of the ligand's coordination preference. The differences in coordination mode should translate into a different influence on photolytic activity. Based up the IR stretching frequencies of the NO moiety, the complexes that have been characterized seem to donate electron density to differing degrees to the Ru-NO moiety. Photolysis data can now be correlated with these differences in the coordination environment. Comparison the difference in the NMR spectra of the Ru-NO complex and the photolysis product can also provide interesting insights into the nitrosyl group's influence on the ligand.

3.0 BIS-PYRAZINE BIS-CARBOXAMIDO LIGANDS

In order to systematically vary the ligand environment, another set of ligands, with the same benzene, 2,3-diaminopyridine, 3,4-diaminopyridine, diaminoethane, 1,3-diaminopropane and 1,4-piperazine backbones was prepared with pyrazine instead of pyridine. Pyrazine is less of a σ base than is pyridine due to the extra nitrogen in the pyrazine ring. In addition, pyrazine is a more efficient π acceptor for the same reason. This variation will allow a comparison of the influence on NO photolability for pyrazine and pyridine. Incorporation of pyrazine also may change solubility and allow for bridging coordination between other metal centers. Recently pyrazine bridged ruthenium nitrosyl complexes were shown to release NO under visible light.[80]

3.1 *N*,*N*′-BIS(2-PYRAZINECARBOXAMIDE)-1,2-BENZENE

3.1.1 Materials and Methods

***N*, *N*′ -bis(2-pyrazinecarboxamide)-1,2-benzene (3.1)** was prepared according to a modified literature procedure.[68] 1,2-Diaminobenzene (2.00 g, 0.0184 mol) was added to a stirred solution of pyrazine carboxylic acid (4.55 g, 0.369 mol) in dry pyridine (18.0 mL). After triphenyl phosphite (310.29 g/mol, d = 1.184 g/mL, 9.69 mL) was added slowly, the reaction mixture was

stirred at 100 °C in an oil bath for four hours. White crystals were obtained after the reaction mixture was left standing at ambient temperature overnight. Recrystallization from chloroform afforded X-ray quality crystals. ^{1}H NMR (500 MHz, DMSO-d_6): δ 10.7 (s, 2H, N-H(1), N-H(2)), 9.30 (s, 2H, H-3), 8.91 (d, 2H, H-2), 8.75 (d, 2H, H-1), 7.75 (m, 2H, H-4), 7.33 (m, 2H, H-5). ^{13}C{^{1}H} ^{1}H NMR, DMSO-d_6): δ 161.84 (C=O), 148.02 (C-2), 144.29 (Pz-*ipso*), 143.93 (C-3), 143.39 (C-1), 130.61(Ar-*ipso*), 126.35 (C-5), 125.98 (C-4); ESI-MS $M^{+\cdot}$ = 320

Chloro-nitrosyl-*N,N′*-bis(2-pyrazinecarboxamido)-1,2-benzene (3.2) was prepared according to a modified literature procedure.[69] Trichloronitrosylruthenium (0.0018 mol, 0.500 g) was added to a stirred solution of *N,N′*-bis(2-pyrazinecarboxamide-1,2-benzene in an ethanol/water solution (95%, ~50.0 mL). The reaction mixture was stirred at 65.0-70.0 °C for twelve hours. A fine brown precipitate was filtered from the reaction mixture and rinsed with ethanol. ^{1}H NMR (500 MHz, DMSO-d_6): δ 9.43 (m, 2H, H-2), 9.34 (s, 2H, H-3), 9.26 (d, 2H, H-1), 8.53 (m, 2H, H-7), 7.09 (m, 2H, H-8,); ^{13}C{^{1}H} ^{1}H NMR, DMSO-d_6): δ 162.45 (C-5), 151.25 (Pz-*ipso*), 149.27 (C-1), 147.22 (C-3), 146.27 (C-2), 143.38 (Ar-*ipso*), 124.22 (C-8), 121.03 (C-7); ESI-MS $M^{+\cdot}$ = 320

3.1.2 Results and Discussion

Table 3.1 shows the ^{1}H and ^{13}C assignments for **3.1** and **3.2**; the labeling scheme is in Figure 3.1. ^{1}H and ^{13}C assignments were made based upon HH COSY, HMQC, and HMBC spectra. Disappearance of the amide N-H upon coordination indicates chelation by the phenylenediamine moiety. The upfield shift of the pyrazyl ^{1}H resonances and all but C-2 of the ^{13}C resonances

indicate coordination of the pyrazyl groups. The most affected protons on the pyrazyl ring correspond to H-1 and H-2; H-3 is barely affected. The most significantly affected protons are H-4 which are adjacent to the nitrogen-bearing carbons on the benzene ring. H-5 protons exhibit a slight upfield shift.

The ^{1}H and ^{13}C spectra for the ligand, **3.1**, are very similar to that of the pyridine analogue, **2.2**. The pyrazine ^{1}H resonances are more downfield than the corresponding pyridyl resonances for **2.2;** the aryl ^{1}H resonances are almost exactly the same. As expected, the ^{13}C chemical shift values are more sensitive to the additional nitrogen atom in the pyrazine ring. All pyrazine ^{13}C resonances, except for the pyrazine-*ipso* carbon are downfield with respect to the corresponding pyridyl resonances. The pyrazine-*ipso* carbon is actually more shielded than the corresponding carbon in **2.2**. The aryl ^{13}C resonances and the carbonyl resonance are about the same for **3.1** and **2.2.**

The RuNO complex, **3.2**, is also similar to the pyridine analogue, **2.3**. ^{1}H resonances for **3.2** are slightly downfield from the corresponding pyridyl resonances for **2.3**. The major difference is seen for H-2. H-2 for **3.2** resonates at 9.43 ppm; H-2 for **2.3** gives a signal at 7.94 ppm. A similar difference is seen for the ligands. Again, the ^{13}C NMR spectrum is more sensitive to the changes introduced by the nitrogens in the pyrazine ring. C-1 of Complex **2.3** resonates at 152.49 ppm while the corresponding resonance for **3.2** appears at 149.27. However, the downfield shift for C-1 of **3.2** is greater than that for **2.3** upon coordination to RuNO. The pyrazine *ipso* carbon in **3.2** is less downfield shifted upon coordination than is the pyridine *ipso*. That C-2 of **3.2** resonates 18.22 ppm downfield from C-2 of **2.3** is attributed to the adjacent pyrazine nitrogen. A similar difference is seen between the ligands. However, C-2 for **3.2** shifts

upfield 1.75 ppm upon coordination while C-2 for **2.3** shifts downfield only 0.95 ppm. All other changes in ^{13}C resonances are of similar magnitude and in the same direction.

The crystal structure for **3.1** is shown in Figure 3.2. Crystal intensity and collection data are shown in Table 3.2. Selected bond lengths and angles are presented in Table 3.3. As of this time, no crystal structure has been obtained for the complex **3.2**. The crystal structures for **2.2** and for **2.3** have been published by others.[26,70] Since a crystal structure for **3.2** has not been obtained the crystal structure of **3.1** will not be discussed here.

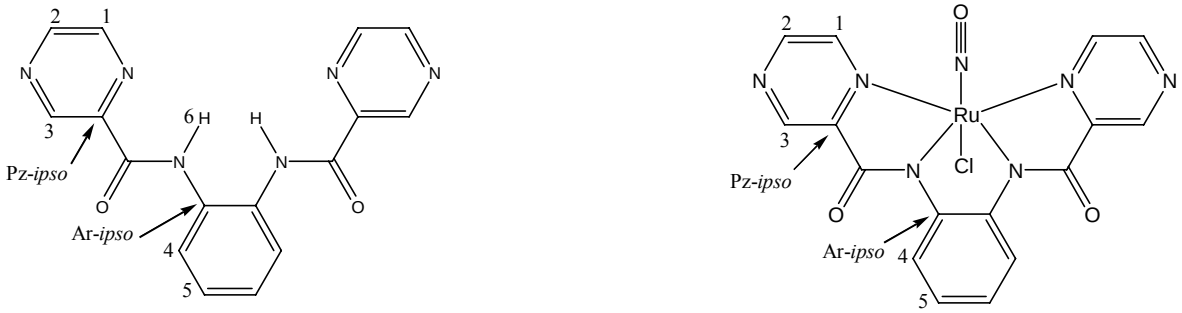

3.1 **3.2**

Figure 3.1-*N*,*N′*-bis(2-pyrazinecarboxamide)-1,2-benzene and RuNO complex

Table 3.1-^{1}H and ^{13}C NMR data for 3.1 and 3.2

^{1}H	**1**	**2**	**3**	**4**	**5**	**N-H**			
3.1	8.75	8.91	9.30	7.75	7.33	10.7			
3.2	9.26	9.43	9.34	8.53	7.09	*			
^{13}C							Ar-*ipso*	Pz-*ipso*	C=O
3.1	143.39	148.02	143.93	125.64	126.01	*	130.61	144.29	161.84
3.2	149.27	146.27	147.22	121.03	124.22	*	143.38	151.25	162.45

Table 3.2-Crystal data and refinements for 3.1

	3.1
Chemical Formula	$C_{16}H_{12}N_6O_2$
Formula Weight	320.32
Temperature (K)	295(2)
Wavelength (Å)	0.71073
Crystal system	Monoclinic
Space group	P2(1)/c
a (Å)	11.4639(11)
b (Å)	9.5090(9)
c (Å)	14.6602(14)
α (°)	90
β (°)	110.687(2)
γ (°)	90
Volume ($Å^3$)	1495.1(2)
Z	4
Density (calculated) Mg/m^3	1.423
Absorption Coefficient (mm^{-1})	0.100
F(000)	664
Crystal Size (mm^3)	0.37 x 0.34 x 0.12
θ range for data collection (°)	1.90 to 25.00
Index Ranges	$-13 \le h \le 13$ $-11 \le k \le 11$ $-17 \le l \le 17$
Reflections collected	11775
Independent reflections	2641 [R(int) = 0.0448]
Completeness	100 % (θ=25.00°)
Data / restraints / parameters	2641/ 0 /265
Max. and min. transmissions	0.9881 and 0.9639
Refinement Method	Full-matrix least-squares on F^2
Goodness-of-fit on F^2	1.229
Final R indices[$I > 2\sigma(I)$]	R1 = 0.0619, wR2 = 0.1364
R indices (all data)	R1 = 0.0926, wR2 = 0.1453
Largest diff. peak and hole (e $Å^3$)	0.151 and -0.213

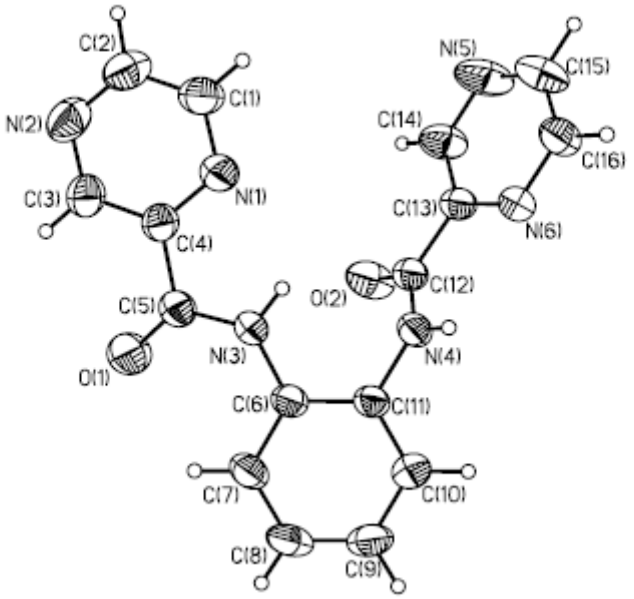

Figure 3.2-*N*,*N*′-bis(2-pyrazinecarboxamide)-1,2-benzene

Table 3.3-Selected bond lengths and angles for 3.1

O(1)-C(5)	1.215(3)	O(2)-C(12)	1.203(3)	O(1)-C(5)-N(3)	123.2(3)
N(3)-C(5)	1.349(3)	N(4)-C(12)	1.342(3)	O(2)-C(12)-N(4)	125.2(3)
C(4)-C(5)	1.491(3)	C(12)-C(13)	1.493(4)	O(1)-C(5)-C(4)	121.4(2)
N(3)-C(6)	1.431(3)	N(4)-C(11)	1.405(3)	O(2)-C(12)-C(13)	121.1(3)
N(1)-C(1)	1.331(3)	N(6)-C(16)	1.331(4)	N(1)-C(4)-C(5)	118.5(2)
N(1)-C(4)	1.325(3)	N(6)-C(13)	1.330(3)	N(6)-C(13)-C(12)	118.5(2)
C(1)-C(2)	1.367(4)	C(15)-C(16)	1.363(4)	N(3)-C(5)-C(4)	115.4(2)
N(2)-C(2)	1.312(4)	N(5)-C(15)	1.326(4)	N(4)-C(12)-C(13)	113.7(2)
N(2)-C(3)	1.334(4)	N(5)-C(14)	1.329(4)	C(3)-C(4)-C(5)	119.5(3)
C(3)-C(4)	1.373(4)	C(13)-C(14)	1.380(4)	C(14)-C(13)-C(12)	120.0(3)
C(6)-C(11)	1.395(3)	C(8)-C(9)	1.364(4)	C(11)-C(6)-N(3)	119.9(2)
C(10)-C(11)	1.390(4)	C(6)-C(7)	1.380(4)	C(6)-C(11)-N(4)	118.2(2)
C(7)-C(8)	1.384(4)	C(9)-C(10)	1.371(4)	C(6)-C(7)-C(8)	120.2(3)
				C(8)-C(9)-C(10)	120.8(3)
				C(10)-C(11)-C(6)	118.6(3)

3.1.3 Conclusion

The pyrazine analogue of *N*,*N*′-bis(2-pyridinecarboxamide)-1,2-benzene (**2.2**), *N*,*N*′-bis(2-pyrazinecarboxamide)-1,2-benzene (**3.1**) was prepared and characterized by ^{1}H NMR and ^{13}C NMR spectroscopy and X-ray crystallography. The corresponding ruthenium nitrosyl complex was prepared (**3.2**). NMR data indicate that the ligand coordinated through the pyrazine nitrogen atoms and the deprotonated carboxamido nitrogen atoms in the equatorial plane. Comparison of the NMR data for the ligand and complex to the pyridine suggests that the pyrazine moiety introduces some variations that will require further analysis to explain.

3.2 *N,N′*-BIS(2-PYRAZINECARBOXAMIDE)-2,3-PYRIDINE

3.2.1 Materials and Methods

***N,N′*-bis(2-pyrazinecarboxamide)-2,3-pyridine (3.3)** was prepared according to a modified literature procedure.[68] Pyrazinecarboxylic acid (1.23 g, 0.010 mol) was dissolved in dry pyridine (~ 5.0 mL). To the picolinic acid solution was added 2,3-diaminopyridine (109.13 g/mol, 0.548 g, 0.005 mol) and triphenyl phosphite (d = 1.184 g/mL, 2.63 mL, 0.010 mol). The reaction mixture was stirred at 100 °C for four hours. Upon standing at room temperature for 5 days the reaction mixture produced crystals in a thick dark brown mixture. An attempt to isolate the crystals by vacuum filtration failed because the viscous pyridine solution clogged the frit. The product crystals were taken up in dichloromethane and combined with the filtrate. Most of the viscous brown portion of the reaction mixture remained on the frit. After the filtrate volume was reduced by rotary evaporation (~ 40 °C) the filtrate was added dropwise to diethyl. A yellow precipitate was isolated by vacuum filtration. The filtrate was left at room temperature for a second crop. The procedure was repeated until no more product precipitated. The product was obtained in low but undetermined yield. ^{1}H NMR (600 MHz, dimethylsulfoxide-d_6): δ 11.09 (s, 1H, N-H (2)), 10.63 (s, 1H, N-H(2)), 9.31 (d, 2H, H-15, H-1), 8.95 (d, 1H, H-14), 8.91 (d, 1H, H-2), 8.82 (td, 1H, H-13), 8.74 (td, 1H, H-3), 8.38 (dd, 1H, H-9), 8.36 (dd, 1H, H-7); ^{13}C{^{1}H} ^{1}H NMR, dimethyl sulfoxide-d_6): δ 162.70 (C-11), 161.66 (C-5), 148.26 (C-14, C-2), 145.26 (C-9), 144.11 (C-12), 144.06 (C-4), 143.88 (C-15), 143.82 (C-1), 143.61 (C-13), 143.50 (C-3), 127.85 (C-6), 133.48 (C-7), 142.92 (C-10), 122.50 (C-8); ESI-MS $M^{+\cdot}$ = 321

Reaction with $[Ru(NO)Cl_3(H_2O)_2]$: The reaction between **3.3** and $[Ru(NO)Cl_3(H_2O)_2]$ was carried out according to a modified literature procedure.[69] Trichloronitrosylruthenium (0.135g, 0.00049 mol) was added to ethanol/water solution (95%, ~40.0 mL, 80.0 °C) of *N,N'*-bis(2-pyrazinecarboxamide)-2,3-pyridine (0.159 g, 0.00049 mol). An additional 20.0 mL of the ethanol/water solvent was used to transfer the $[Ru(NO)(Cl_3)(H_2O)_2]$. The reaction mixture became orange and a precipitate formed immediately. The reaction mixture was stirred at 80.0 °C for seven hours. A brown precipitate was removed from the reaction mixture by vacuum filtration. The filtrate volume was reduced under vacuum (rotary evaporator, 55 °C). The filtrate was stored at room temperature to allow for slow evaporation of solvent.

3.2.2 Results and Discussion

The labeling scheme for the ligand, *N*,*N*′-bis(2-pyrazinecarboxamide)-2,3-pyridine **(3.3)** is shown in Figure 3.3. ^{1}H and ^{13}C assignments are show in Tables 3.4 and 3.5, respectively. Chemical shift assignments were made based upon HH COSY, HMQC, and HMBC spectra. As for **2.4** the instruction of the pyridine into the backbone of the ligand differentiates the pyrazyl arms for **3.3**. Resonance forms of the pyridine ring in **3.3** places positive charge on the carbon atoms ortho and para to the pyridine nitrogen. For **3.3** C-10 exhibits more of a positive character than does C-6 as shown by the ^{13}C NMR data. The signal for C-10 is at 142.92 ppm while that for C-6 is at 127.85 ppm. The remaining ^{1}H and ^{13}C signals within **3.3** differ only slightly from each other.

The ^{1}H NMR spectrum of the aryl region of the **3.3** is shown in Figure 3.5. The tetradentate ruthemium nitrosyl complex **(3.4)** has not yet been isolated from the reaction mixture. ^{1}H NMR spectrum of the aryl region of the crude reaction mixture, shown in Figure 3.6, suggests that more than one product has formed.

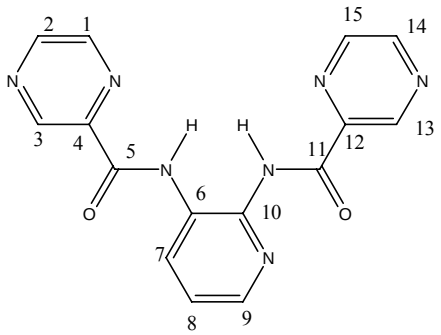

3.3

Figure 3.3- *N*,*N*′-bis(2-pyrazinecarboxamide)-2,3-pyridine

Table 3.4- ^{1}H Resonances for *N*,*N*′-bis(2-pyrazinecarboxamide)-2,3-pyridine

^{1}H	**1**	**2**	**3**	**7**	**8**	**9**	**13**	**14**	**15**	**N-H(1)**	**N-H(2)**
3.3	9.31	8.91	8.74	8.36	7.48	8.38	8.82	8.95	9.31	10.63	10.97

Table 3.5-^{13}C Resonances for *N*,*N*′-bis(2-pyrazinecarboxamide)-2,3-pyridine

^{13}C	**1**	**2**	**3**	**4**	**5**	**6**	**7**	**8**	**9**	**10**
3.3	143.82	148.26	143.50	144.06	161.66	127.85	133.48	122.50	145.26	142.92

3.3	**11**	**12**	**13**	**14**	**15**
	162.70	144.11	143.61	148.26	143.88

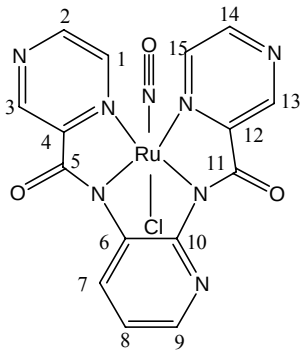

3.4

Figure 3.4-Tetradentate ruthenium nitrosyl compound

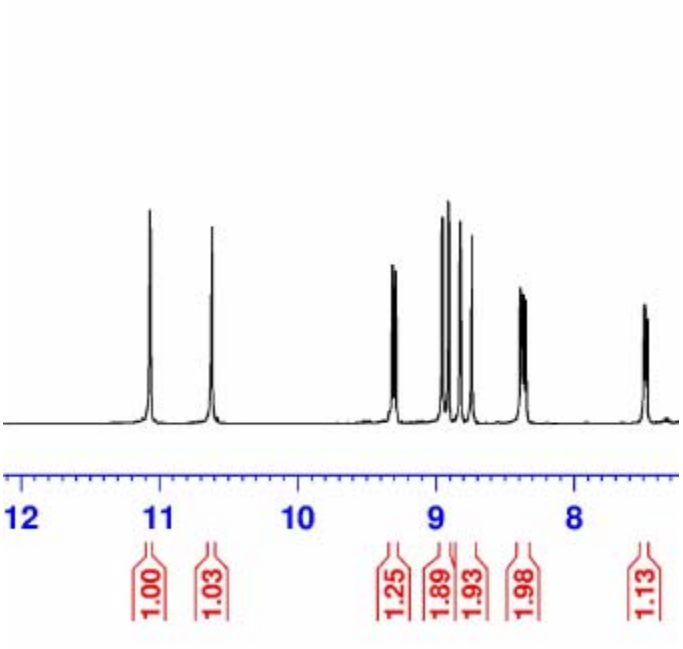

Figure 3.5- ^{1}H NMR spectrum of aryl region of 3.3

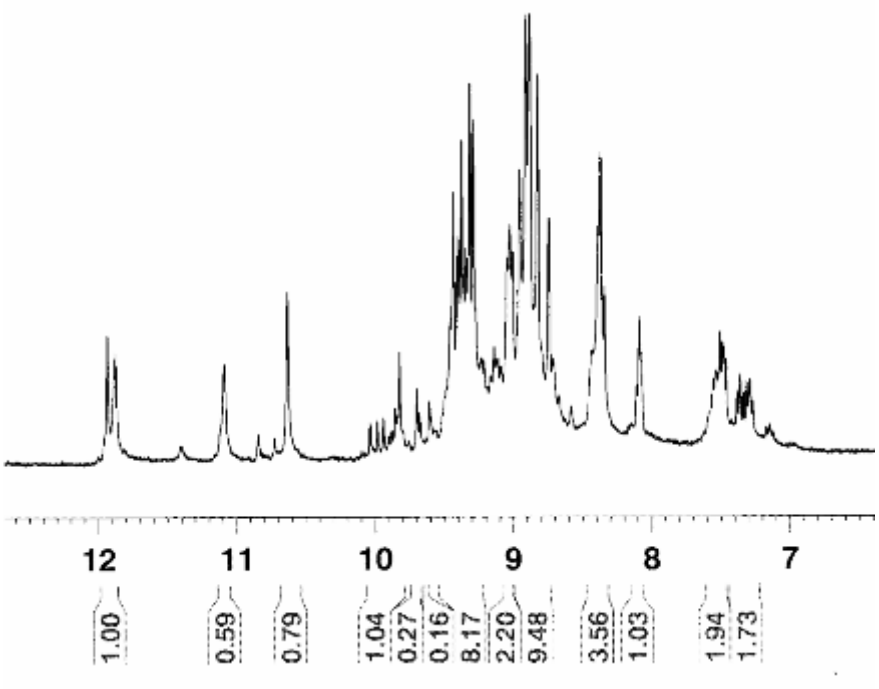

Figure 3.6-^{1}H NMR spectrum of aryl region after reaction of 3.3 with [Ru(NO)Cl$_3$(H$_2$O)$_2$]

3.2.3 Conclusion

The ligand, **3.3**, shows ^{1}H and ^{13}C NMR chemical shift patterns similar to those of **2.4**, the pyridine analogue. While no conclusion regarding the new compound(s) from the reaction between [Ru(NO)Cl$_3$(H$_2$O)$_2$] and **3.3**, can be drawn at this time, the ^{1}H NMR spectrum does indicate formation of more than one product. The signals near 12 ppm could correspond to the N-H protons; the presence of N-H resonances suggests that ligand **3.3** might chelate through the carbonyl oxygen and through one pyrazine nitrogen atom as did **2.4**.

3.3 *N,N′*-BIS(2-PYRAZINECARBOXAMIDE)-3,4-PYRIDINE

3.3.1 Materials and Methods

***N,N′*-bis(2-pyrazinecarboxamide)-3,4-pyridine (3.5)** was prepared according to a modified literature procedure.[68] Pyrazinecarboxylic acid (1.13 g, 0.009 mol) was dissolved in dry pyridine (~ 5.0 mL). To the picolinic acid solution was added 2,3-diaminopyridine (0.502 g, 0.005 mol) and triphenyl phosphite (d = 1.184 g/mL, 2.40 mL). The reaction mixture was stirred at 100 °C for four hours. Upon standing at room temperature for 1 day the reaction mixture produced crystals in a thick orange/brown mixture. ^{1}H After several days, the mixture was vacuum filtered and rinsed with chloroform. A viscous liquid remained on the frit. The filtrate volume was reduced under vacuum. The concentrated filtrate was left standing at room temperature. The viscous liquid from the frit was also dissolved with chloroform and stored in a separate beaker. After several days crystals formed in the filtrate and were isolated by vacuum filtration, rinsed and recrystallized from ethanol or chloroform. ESI-MS $M^{+\cdot}$ = 321. Preliminary 300 MHz ^{1}H NMR results suggest that formation of **3.5**. The ^{1}H NMR spectrum can be seen in Figure 3.8.

***N,N′*-bis(2-pyrazinecarboxamide)-3,4-pyridine reaction with [Ru(NO)Cl$_3$(H$_2$O)$_2$]** The reaction was run according to a modified literature procedure.[69] Trichloronitrosylruthenium (0.106 g, 0.00039 mol) in ethanol/water (95%, 10.0 mL) was added by pipette to an ethanol/water solution (95%, ~15.0 mL, 80.0 °C) of *N,N′*-bis(2-pyrazinecarboxamide)-3,4-pyridine (0.125 g, 0.00039 mol). The reaction mixture became orange and a precipitate formed upon addition of [Ru(NO)(Cl$_3$)(H$_2$O)$_2$]. The reaction mixture was stirred at 80.0 °C for six

hours. A brown precipitate was removed from the reaction mixture by vacuum filtration. The filtrate volume was reduced under vacuum (rotary evaporator, 55 °C). The filtrate allowed to evaporate slowly at room temperature to induce precipitation or crystallization. Eventually a tan solid was obtained. Comparison of the ^{1}H NMR spectrum with that of the starting material suggests the presence of one new species.

3.3.2 Results and Discussion

Mass spectral analysis confirmed the successful preparation of **3.5**. Final NMR assignments await 500 MHz two- dimensional data acquisition. However, preliminary 300 MHz ^{1}H NMR data indicates isolation of a single product with some NMR signals characteristic of similar *N,N′*-bis(2-pyridinecarboxamide)-3,4-pyridine and of *N,N′*-bis(2-pyrazinecarboxamide)-2,3-pyridine. The only signals that can be assigned with certainty at this time are the N-H(1) resonance at 11.04 ppm and the N-H(2) resonance at 10.72 (Figure 3.8).

The reaction between **3.5** and $[Ru(NO)Cl_3(H_2O)_2]$ yielded at least one new product. Comparison of the 300 MHz ^{1}H NMR spectrum of the new product to that of **3.5** indicates isolation of a single product. Unfortunately the mass spectral analysis was inconclusive and must be repeated.

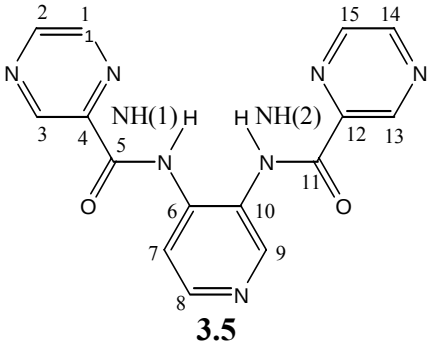

3.5

Figure 3.7-*N*,*N*′-bis(2-pyrazinecarboxamide)-3,4-diaminopyridine

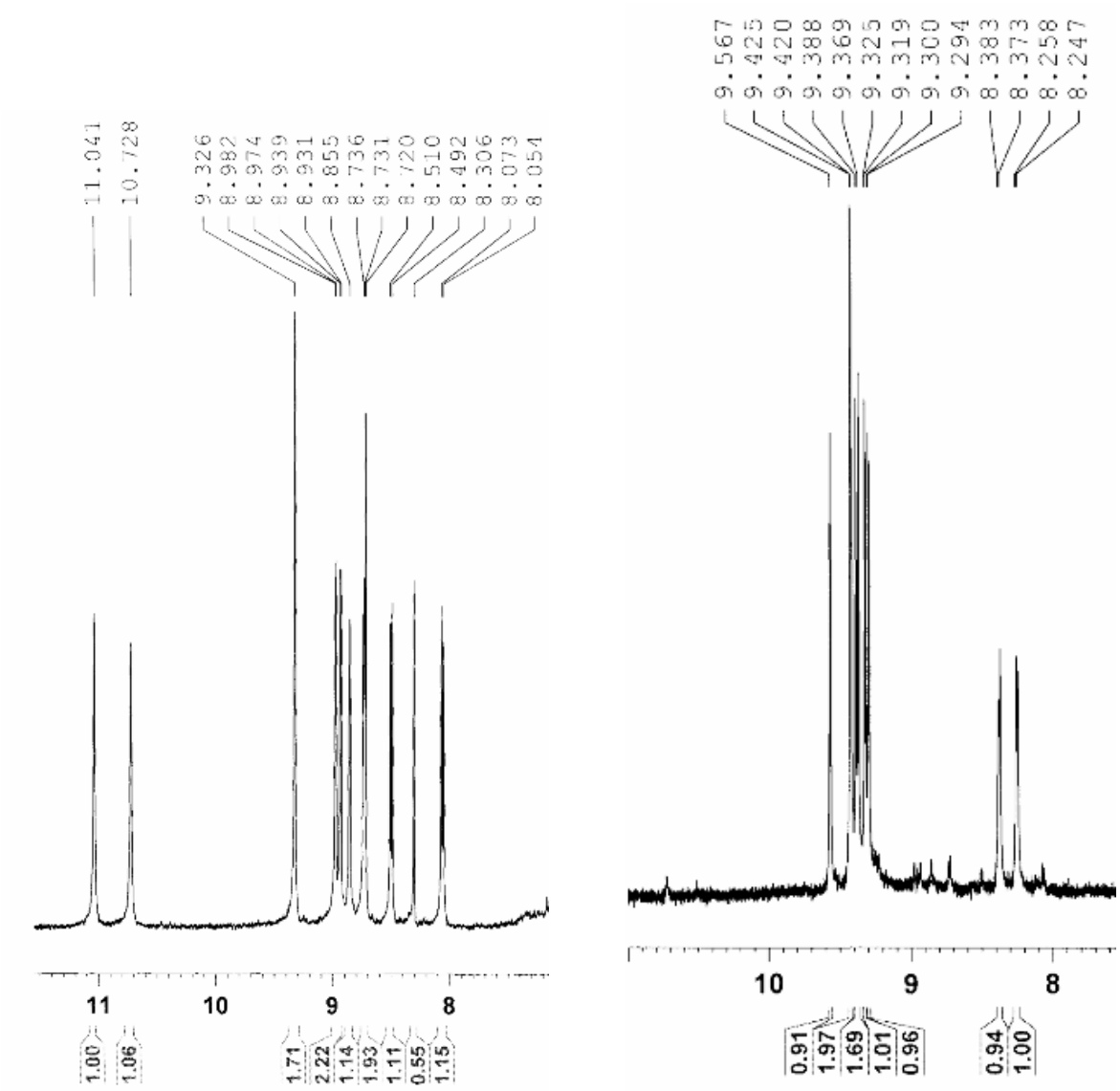

Figure 3.8-^{1}H NMR spectrum of aryl region of 3.5 and isolated product

3.3.3 Conclusion

Although characterization of the ruthenium nitrosyl compound isolated from the reaction between *N*,*N*′-bis(2-pyrazinecarboxamide)-3,4-diaminopyridine has not been completely characterized, comparison of the ^{1}H NMR spectrum of the isolated product to that of the ligand suggests that the ligand is coordinated in tetradentate fashion by the two carboxamido nitrogen atoms and the two pyridyl arms. Other spectra, not shown, suggest the presence of other coordination modes.

3.4 *N,N′*-BIS(2-PYRAZINECARBOXAMIDE)-1,2-ETHANE

3.4.1 Materials and Methods

***N,N′*-bis(2-pyrazinecarboxamide)-1,2-ethane (3.6)** was prepared according to a modified literature procedure.[68] A solution diaminoethane (d = 0.899 g/mL, 0.481 g, 0.540 mL, 0.008 mol) in dry dimethylformamide (~ 4.0 mL) was added to a solution of pyrazinecarboxylic acid (2.00 g, 0.016 mol), in dry dimethylformamide (~15.0 mL). A white precipitate formed upon addition of the diamine. The reaction mixture was stirred as triphenyl phosphite (d = 1.184 g/mL, 4.96 g, 0.016 mol) was added by pipette. The white precipitate did not dissolve after four hours of stirring at 110.0 °C. Additional dry dimethylformamide (~ 180 mL) was added. The precipitate dissolved after two more hours at 110.0 °C. The reaction mixture was stirred for four more hours at 110.0 °C. In total the reaction mixture required 200.0 mL dimethylformamide and eight hours of stirring at 110.0 °C. After solvent volume was reduced under vacuum the reaction mixture was allowed sit for a few days during which a solid formed. The white solid turned to a paste during vacuum filtration. The paste was taken up in dry chloroform. After the chloroform solution was dried over magnesium sulfate, slow evaporation of solvent produced crystals of *N,N′*-bis(2-pyrazinecarboxamide)-1,2-ethane. Repeated recrystallization from chloroform was required to obtain a pure product. Yield: 1.05 g, 48% yield; ^{1}H NMR (500 MHz, DMSO-d_6, δ): 9.16 (s, 2H, H-3, H-10), 9.09 (t, 2H, N-H(1), N-H(2)), 8.85 (d, 2H, H-1, H-12), 8.71 (d, 2H, H-2, H-11), 3.52 (m, 4H, H-6, 6′, H-7, 7′)^{13}C{H} (125 MHz, DMSO-$_{d6}$) δ): 163.16 (C=O), 147.41 (C-2), 144.73 (Pz-*ipso*), 143.26 (C-1), 38.73 (C-4, C-5); ESI-MS $M^{+\cdot}$ = 272.

Chloro-nitrosyl-*N,N′*-bis(2-pyrazinecarboxamido)-1,2-ethane (3.7) was prepared according to a modified literature procedure.[69] Trichloronitrosylruthenium (0.0018 mol, 0.502 g was added to ethanol/water solution (50%, ~100.0 mL, 80.0 °C) of *N,N′*-bis(2-pyrazinecarboxamide)-1,2-ethane (272.26 g/mol, 0.500 g, 0.0018 mol). After the reaction mixture was stirred for eight hours a fine brown precipitate was removed from the reaction mixture. The filtrate volume was reduced to ~ 15.0 mL under vacuum (rotary evaporator). After several days at ambient temperature the filtrate yielded red crystals of the product. Crystals have been submitted for X-ray analysis. ^{1}H NMR (500 MHz, DMSO-d_6, δ): 9.41 (m, 2H, H-1), 9.24 (bs, 2H, H-2), 9.23 (bs, 2H, H-3), 4.09 (m, 2H, H-4′, H-5), 3.92 (m, 2H, H-4, H-5′); ^{13}C{H} (125 MHz, DMSO-$_{d6}$) δ): 166.26 (C=O), 151.21 (pz-*ispso*), 149.63 (C-2), 147.07 (C-3), 146.89 (C-1), 52.18 (C-4, C-5); IR (KBr): $\bar{\nu}_{N\equiv O}$ = 1850 cm^{-1}; ESI-MS $M^{+\cdot}$ = 436.78

3.4.2 Results and Discussion

Figure 3.9 shows the labeling scheme for the ligand, *N,N′*-bis(2-pyrazinecarboxamide)-1,2-ethane **(3.6)** and its ruthenium nitrosyl complex, chloro-nitrosyl-*N,N′*-bis(2-pyrazinecarboxamido)-1,2-ethane ruthenium(II) **(3.7).** ^{13}C and ^{1}H NMR data are shown in Table 3.6. All chemical shift assignments were made based upon HH COSY, HMQC and HMBC spectra. The carboxamido N-H resonance disappears upon coordination to indicate that the ligand is coordinated to Ru^{II} through the amido protons. The Pyrazine ^{1}H and ^{13}C resonances shift downfield due to the electron withdrawing nature of the RuNO center. The downfield shift indicates that the pyrazine ring is coordinated through N-1 of each ring. Accordingly, H-1 is the

most downfield shifted resonance. The pyrazyl-*ipso* ^{13}C signal shifts downfield 7.0 ppm while C-1 shifts only 3.63 ppm.

For the free ligand, the ethylene protons, H-4 and H-5 produce one signal at 3.53 ppm. Upon coordination, the signal splits into two multiplets, one at 3.92 ppm, and the other at 4.09 ppm. The differentiation is attributed to the fact that the ethylene backbone is held in a fixed position upon coordination. The two H-5 and two H-4 protons become fixed in axial and equatorial positions on the chelate ring with Ru^{II}. Equatorial H-4 and axial H-5 are oriented toward the electron withdrawing RuNO, hence resonate at 4.09 ppm while the axial H-5 and equatorial H-4 are oriented away for the RuNO moiety and resonate at 3.53 ppm. The more complicated multiplets that appear upon coordination are due to additional geminal coupling.

The ligand's ^{1}H NMR spectrum is very similar to that of the pyridine analogue **2.9**. However, there are the slight differences introduced by the additional nitrogen atom of the pyrazine ring. All of the ^{1}H pyrazyl signals appear slightly more down field for **3.6** than for **2.9**. The ethylene protons for **3.6** appear at 3.53 ppm while those for **2.9** appear at 3.52 ppm. Upon coordination the ethylene protons exhibit almost exactly the same downfield shifts and the same splitting pattern. The ^{13}C resonances are not differentiated upon coordination for either **2.10** or **3.7**. The ligands **2.9** and **3.6** have an ethylene ^{13}C resonance at 38.48 and 38.78 ppm, respectively. Upon coordination ^{13}C resonance for each ligand shifts downfield about 13 ppm. C-1 for the pyrazine ring is also slightly less affected by coordination than C-1 for the pyridine ring. Infrared data show that donation from the ruthenium center to the π^* NO orbitals is less efficient for **3.7 (**$\bar{\nu}_{NO}$ = 1850 cm^{-1}**)** than for **2.10 (** $\bar{\nu}_{NO}$ = 1825 cm^{-1}).

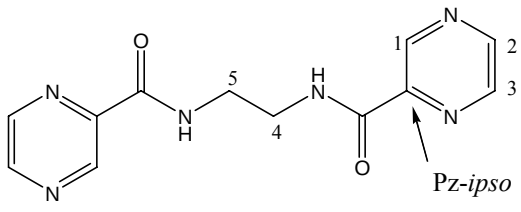

3.6

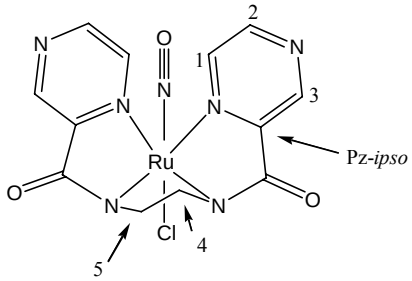

3.7

Figure 3.9-*N*,*N*′-bis(2-pyridinecarboxamide)-1,2-ethane and RuNO complex

Table 3.6-^{1}H and ^{13}C NMR Assignments for 3.6 and 3.7

^{1}H	**1**	**2**	**3**	**4**	**4′**	**5**	**5′**	**N-H**		
3.6	8.71	8.85	9.16	3.53	*	3.53	*	9.09		
3.7	9.41	9.23	9.24	3.92	4.09	4.09	3.92	*		
^{13}C									Pz-*ipso*	C=O
3.6	143.26	147.41	143.44	38.73	*	38.73	*	*	144.73	163.16
3.7	146.89	149.63	147.07	52.18	*	52.18	*	*	151.21	166.26

3.4.3 Conclusion

The ^{1}H and ^{13}C signals for **3.7** are downfield shifted with respect to those of **3.6.** The downfield shift is slightly greater than that observed upon coordination of the pyridine analogue, **2.9.** NMR data do not reveal any major differences due to the pyrazine ring. However, infrared data suggest that back-donation to NOπ* orbitals is less efficient for **3.7 (**$\bar{\nu}_{NO}$ = 1850 cm^{-1}) than for **2.10**($\bar{\nu}_{NO}$ = 1825 cm^{-1}). While $\bar{\nu}_{NO}$ for 3.8 is greater than that for **2.10**, it is still less than that for the benzene derivative, **2.3,** for which $\bar{\nu}_{NO}$ = 1867 cm^{-1}. Crystal structure data for **3.6** and **3.7** are pending and may help explain the difference in $\bar{\nu}_{NO}$ for **3.7** and **2.10.**

3.5 *N,N′*-BIS(2-PYRAZINECARBOXAMIDE)-1,3-PROPANE

3.5.1 Materials and Methods

***N,N′*-bis(2-pyrazinecarboxamide)-1,3-propane (3.8)** was prepared according to a literature procedure.[68] A solution of 1,3-diaminpropane (d = 0.88 g/mL, 0.593 g, 0.678 mL, 0.008 mol) in dry pyridine (~ 4.0 mL) was added to a solution of pyrazinecarboxylic acid (2.00 g, 0.016 mol), in dry pyridine (~20.0 mL). A white precipitate formed upon addition of 1,3-diaminopropane. The reaction mixture was stirred as triphenylphosphite (310.28 g/mol, d = 1.184 g/mL, 4.96 g, 0.016 mol, 2 equiv) was added by pipette. The white solid dissolved two hours after stirring for two hours at 100 °C. The reaction was stopped after four hours. White crystals were collected by vacuum filtration after the reaction mixture was to stand for three days at ambient temperature. X-ray quality crystals were obtained after several recrystallizations from ethanol and then from water. Yield: 1.18 g, 58 % yield; ^{1}H NMR (300 MHz, DMSO-d_6, δ): 9.17 (d, 2H, H-3), 9.07 (t, 2H, N-H(1), N-H(2)), 8.85 (m, 2H, H-2), 3.35 (q, 4H, H-4), 1.77 (m, 2H, H-5);^{13}C{H} (125 MHz, DMSO-$d6$, δ): 162.88 (C=O), 147.41(C-1), 144.74 (Pz-*ipso*), 143.43 (C-3), 143.25 (C-2), 36.33 (C-4), 29.07 (C-5); ESI-MS $M^{+\cdot}$ = 286.

Chloro-nitrosyl-*N,N′*-bis(2-pyrazinecarboxamido)-1,3-propane ruthenium(II) (3.9) was prepared according to a modified literature procedure.[69] Trichloronitrosylruthenium (273.4 g/mol, 0.478 g, 0.0017 mol) was added to ethanol/water solution (95%, ~40.0 mL, 85.0 °C) of *N,N′*-bis(2-pyrazinecarboxamide)-1,3-propane (286.29 g/mol, 0.500 g, 0.0017 mol). An additional 20.0 mL of the ethanol/water solvent was used to transfer the $[Ru(NO)Cl_3(H_2O)_2]$.

Upon addition of $[Ru(NO)Cl_3(H_2O)_2]$ the reaction mixture became orange and a precipitate formed. The reaction mixture was stirred for eleven hours. The brown/orange precipitate was removed by vacuum filtration. The filtrate volume was reduced under vacuum (rotary evaporator) and stored at ambient temperature for crystal formation. X-ray quality crystals were obtained from the filtrate. No yield was obtained. ^{1}H NMR (500 MHz, DMSO-d_6, δ): 9.34 (d, 4H, H-1, H-3), 9.20 (d, 2H, H-2), ^{13}C{H} (125 MHz, DMSO-$_{d6}$, δ): 168.04 (C=O), 148.55 (C-2), 147.12 (Pz-*ipso*), 146.64 (C-1), 144.25 (C-3), 46.07 (C-4), 30.14 (C-5).

3.5.2 Results and Discussion

Figure 3.10 shows the labeling schemes for **3.8** and **3.9.** The corresponding ^{1}H and ^{13}C NMR data are in Table 3.7. All resonances were assigned based upon 2-D NMR analysis. The HH COSY spectrum of **3.8** is shown in Figure 3.11. The broad triplet at 9.07 ppm is assigned to the N-H protons; the N-H protons exhibit a correlation with H-4. H-2 and H-1 correlate with each other but show a weak long range correlation with H-3 as well. ^{13}C assignments were made based upon HMQC and HMBC spectra.

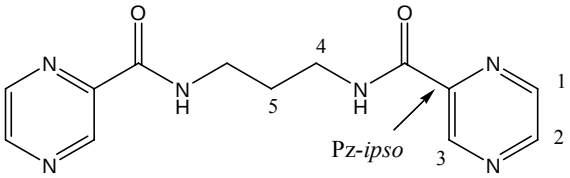

3.8

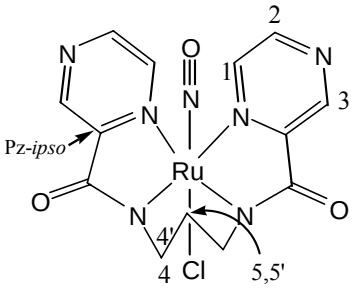

3.9

Figure 3.10-*N*,*N*′-bis(2-pyridinecarboxamide)-1,3-propane and RuNO complex

Table 3.7-^{1}H and ^{13}C NMR Assignments for 3.8 and 3.9

^{1}H	1	2	3	4	4′	5	5′	N-H		
3.8	8.71	8.85	9.17	3.35	*	1.77	*	9.07		
3.9	9.34	9.34	9.20	3.74	3.58	1.79	2.09	*		
^{13}C									**Pz-*ipso***	**C=O**
3.8	147.41	143.25	143.43	36.33	*	29.07	*	*	144.77	162.88
3.9	146.64	148.55	144.25	46.07	*	30.14	*	*	147.12	168.04

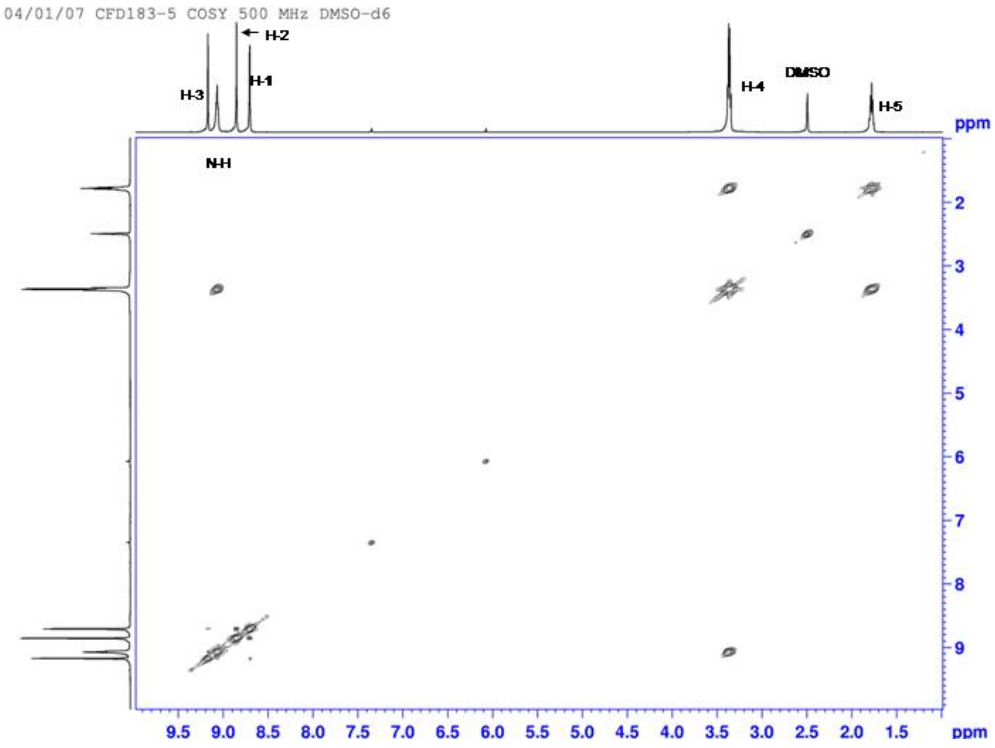

Figure 3.11- HH COSY spectrum of 3.8

All of the ^{1}H NMR signals shift downfield upon coordination to the RuNO center. The largest downfield shift occurs for H-1 which is adjacent to the coordinating nitrogen of the pyrazine group. The H-4 triplet splits into two multiplets that resonate downfield from the original signal at 3.35 ppm. One H-4 resonance appears at 3.58 ppm, the other at 3.74 ppm. The resonance at 3.58 ppm is assigned to the equatorial protons which are oriented more toward the RuNO side of the chelate ring than are the axial protons. The crystal structure in Figure 3.12 can be viewed for clarification, but be aware that the numbering system is different for the crystal structure. The H-5 multiplet is also split into two multiplets upon coordination. One multiplet, assigned to the equatorial proton, shifts very little, from 1.77 ppm to 1.79 ppm; the other multiplet, assigned to the axial proton which is oriented toward the RuNO moiety, shifts 1.07 ppm downfield to 2.09 ppm. The ^{13}C resonance for C-4, coordinating nitrogen atoms shifts downfield 9.74 ppm. The ^{13}C resonance for C-5 shifts only 1.07 ppm because it is one carbon atom removed from the coordinating nitrogen atoms. C-1, adjacent to the coordinating pyrazine nitrogen exhibits a very slight upfield shift compared to the free ligand while its corresponding proton shifts downfield. The carbonyl and pyrazyl-*ipso* carbons shift downfield 2.35 and 5.16 ppm, respectively.

Crystal intensity and collection data can be seen in Table 3.8. The crystal structure of **3.8** can be seen in Figure 3.12. Table 3.9 presents some selected bond distances and angles for **3.8**. The X-ray structure for **3.9** is in Figure 3.13; selected bond distances and angles are in Table 3.10. The most noticeable changes are in the bond angles.

The N(3)-C(3)-C(4) angle is 2° larger than the corresponding angle across from it, N(2)-C(1)-C(2) (121.0(2)°). In **3.8** those angles almost the same at 122.4(4)° and 121.9(4)°, respectively. Since N(1) and N(4) of the complex are bound and C(4) is bound to the carbonyl

group, the N(3)-C(3)-C(4) angle might distort to compensate for chelation. A similar distortion occurs in the other pyrazine ring on **3.9**. Angles N(4)-C(5)-C(4) and N(5)-C(9)-C(10) as well as N(2)-C(4)-C(5) and N(6)-C(10)-C(6) are 3-4° smaller than the corresponding angles of **3.8.** These angles are centered about the carbonyl and the ipso carbons.

The N(4)-C(6)-C(7) angle of **3.9** is the same as that of the ligand, 114°; however the corresponding angle of **3.9**, N(5)-C(8)-C(7) is 2° smaller. This difference and the increase in the C(6)-C(7)-C(8) angle upon coordination are attributed to the bite angle of the propanediamide and the fact that the one pyrazine ring has to tilt out of the equatorial plane to avoid in interaction between H-1 and H-13. The Ru-NO angle, 177.89 is typical of linear $\{RuNO\}^6$ complexes. The N(1)-Ru- N(5) and N(1)-Ru-N(4) angles are about the same at 95.71° and 94.55°. However, the angles between the nitrosyl nitrogen, ruthenium and the pyrazyl nitrogen atoms, N(1)-Ru-N(6) and N(1)-Ru-N(2), differ by a little over 3° as a result of the N(6) pyrazyl group's out of plane tilt. The equatorial angles that include a pyrazyl nitrogen and a carboxamide nitrogen, N(2)-Ru-N(4) and N(6)-Ru-N(5) are both close to 78°. The N(4)-Ru-N(5) angle which includes both carboxamido nitrogen atoms at 95.76° is 11.1° smaller than the N(2)-Ru-N(6) angle that includes the pyrazyl nitrogen atoms.

Table 3.8-Crystal data and refinements for 3.8 and 3.9

	3.8	**3.9**
Chemical Formula	$C_{13}H_{18}N_6O_4$	$C_{13}H_{12}ClN_7O_3Ru$
Formula Weight	322.33	450.82
Temperature (K)	150(2)	295(2)
Wavelength (Å)	0.71073	0.71073
Crystal system	Monoclinic	Triclinic
Space group	P-2(1)	P-1
a (Å)	5.2057(2)	7.4306(6)
b (Å)	19.060(7)	10.3562(9)
c (Å)	7.930(3)	11.2674(1)
α (°)	90	67.1930(1)
β (°)	106.079(7)	84.375(2)
γ (°)	90	79.042(2)
Volume ($Å^3$)	756.0(5)	784.41(1)
Z	2	2
Density (calculated) Mg/m^3	1.416	1.909
Absorption Coefficient (mm^{-1})	0.108	1.201
F(000)	340	448
Crystal Size (mm^3)	? x ? x ?	0.29 x 0.21 x 0.18
θ range for data collection (°)	2.14 to 27.49	1.96 to 32.46
Index Ranges	$-6 \le h \le 6$	$-11 \le h \le 11$
	$-24 \le k \le 24$	$-15 \le k \le 15$
	$-10 \le l \le 10$	$-16 \le l \le 16$
Reflections collected	7374	10418
Independent reflections	1789 [R(int) = 0.0735]	5400 [R(int) = 0.0174]
Completeness	100.0 % (θ=27.49°)	95.4 % (θ=32.46)
Data / restraints / parameters	1789/ 0 / 232	5400 / 0 / 226
Max. and min. transmissions	0.9856 and 0.9733	0.8129 and 0.7221
Refinement Method	Full-matrix least-squares on F^2	Full-matrix least-squares on F^2
Goodness-of-fit on F^2	0.828	1.187
Final R indices[$I > 2\sigma$ (I)]	R1 = 0.0488, wR2 = 0.1059	R1 = 0.0312, wR2 = 0.0780
R indices (all data)	R1 = 0.0922, wR2 = 0.1234	R1 =0.0348, wR2 = 0.0798
Largest diff. peak and hole (e $Å^3$)	0.218 and -0.168	0.821 and -0.323

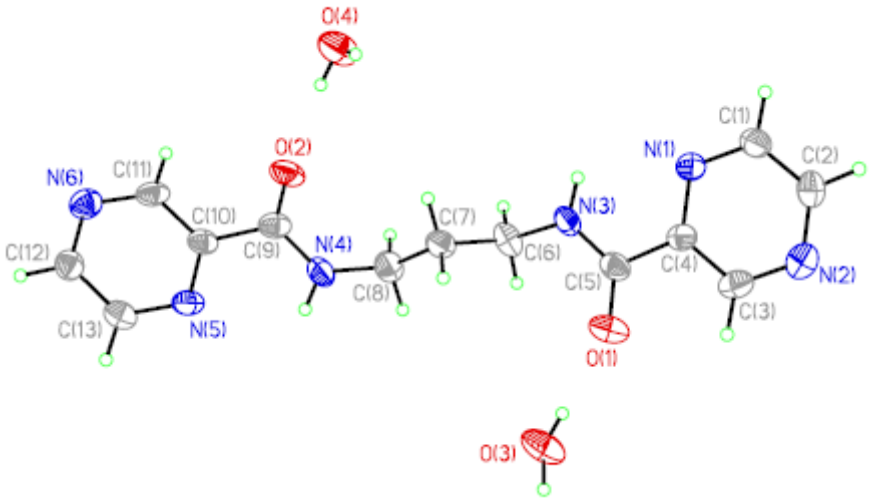

Figure 3.12-X-ray structure of 3.8

Table 3.9- Selected bond distances (Å) and angles (°) for 3.8

O(1)-C(5)	1.226(5)	C(10)-C(11)	1.384(6)
O(2)-C(9)	1.232(5)	C(3)-C(4)	1.394(6)
N(4)-C(8)	1.442(6)	N(5)-C(10)	1.339(5)
N(3)-C(6)	1.454(5)	N(6)-C(11)	1.338(6)
C(7)-C(8)	1.527(6)	N(2)-C(3)	1.331(6)
C(6)-C(7)	1.521(6)	N(6)-C(12)	1.335(5)
C(4)-C(5)	1.496(6)	N(2)-C(2)	1.318(6)
C(9)-C(10)	1.506(6)	C(12)-C(13)	1.386(6)
N(4)-C(9)	1.333(5)	C(1)-C(2)	1.371
N(3)-C(5)	1.325(5)	N(5)-C(13)	1.336(6)
N(4)-C(8)-C(7)	114.5(4)	N(6)-C(12)-C(13)	122.3(4)
N(3)-C(6)-C(7)	115.8(3)	N(2)-C(2)-C(1)	122.4(4)
C(6)-C(7)-C(8)	108.4(3)	N(5)-C(13)-C(12)	121.9(4)
N(3)-C(5)-C(4)	116.3(4)	N(1)-C(1)-C(2)	122.5(4)
N(4)-C(9)-C(10)	116.0(4)	C(1)-N(1)-C(4)	115.5(3)
N(5)-C(10)-C(11)	121.7(4)	C(13)-N(5)-C(10)	116.1(4)
N(1)-C(4)-C(3)	121.5(4)	N(5)-C(10)-C(9)	119.2(4)
N(6)-C(11)-C(10)	121.9(4)	N(1)-C(4)-C(5)	119.4(4)
N(2)-C(3)-C(4)	121.9(4)		

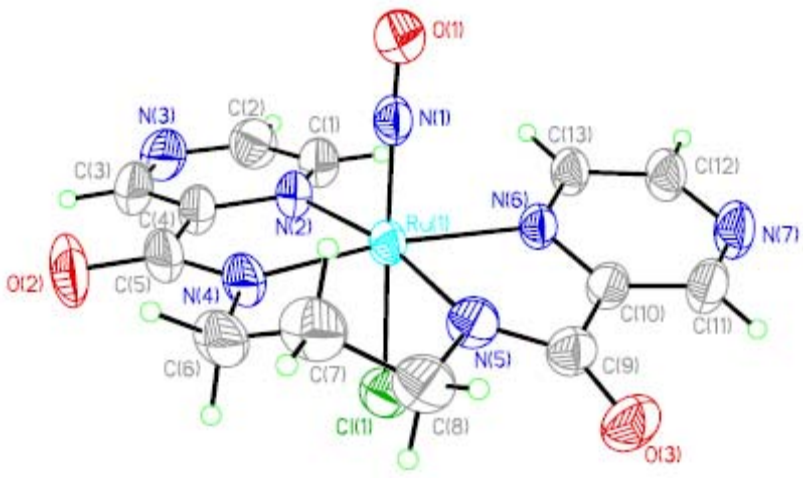

Figure 3.13-X-ray structure of 3.9

Table 3.10-Selected bond distances (Å) and angles (°) for 3.9

O(1)-N(1)	1.132(2)	O(2)-C(5)	1.235(2)
Ru-N(1)	1.7452(2)	O(3)-C(9)	1.231(2)
Ru-Cl	2.3439(6)	N(4)-C(5)	1.324(3)
Ru-N(2)	2.1248(2)	N(5)-C(9)	1.335(3)
Ru-N(6)	2.1415(2)	N(4)-C(6)	1.461(3)
Ru-N(4)	2.0143(2)	N(5)-C(8)	1.468(2)
Ru-N(5)	2.0201(2)	C(6)-C(7)	1.502(4)
C(1)-N(2)	1.334(3)	C(7)-C(8)	1.515(3)
C(1)-C(2)	1.376(3)	C(3)-C(4)	1.381(3)
C(2)-N(3)	1.327(3)	N(2)-C(4)	1.346(2)
N(3)-C(3)	1.332(3)	C(4)-C(5)	1.498(3)
O(1)-N(1)-Ru	177.89(2)	C(9)-C(10)	1.496(3)
N(1)-Ru-Cl	176.96(5)	N(5)-Ru-N(6)	78.02(6)
N(1)-Ru-N(2)	94.48(7)	N(5)-Ru-N(2)	168.61(7)
N(1)-Ru-N(6)	91.19(7)	N(4)-Ru-N(6)	171.95(6)
N(1)-Ru-N(5)	95.71(7)	N(4)-C(6)-C(7)	114.34(2)
N(1)-Ru-N(4)	94.55(7)	C(6)-C(7)-C(8)	115.0(2)
N(4)-Ru-N(5)	95.76(7)	C(8)-N(5)-Ru	123.08(1)
N(2)-Ru-N(6)	106.86(6)	C(6)-N(4)-Ru	123.21(1)
N(4)-Ru-N(2)	78.35(7)	N(5)-C(9)-C(10)	112.43(2)
N(2)-C(4)-C(5)	116.71(2)	N(4)-C(5)-C(4)	112.74(2)
N(6)-C(10)-C(9)	116.69(2)	N(5)-C(8)-C(7)	112.15(2)
C(1)-N(2)-C(4)	117.33(2)	C(13)-N(6)-C(10)	117.29(2)

3.5.3 Conclusion

The *N,N'*-bis(2-pyrazinecarboxamide)-1,3-propane ligand **(3.8)** was prepared and characterized by 2D NMR methods and by X-ray crystallography. The crystal structure of Chloro-nitrosyl-*N,N'*-bis(2-pyrazinecarboxamido)-1,3-propane ruthenium(II) **(3.9)** reveals a linear Ru-N-O bond of 177.89(15)° and an N-O bond distance of 1.132(2) Å. These values are similar to those for **2.12** which are 177.5(7) and 1.143(8) Å, respectively. There are some variations in the bite angles between **3.10** and **2.12.** For **3.9** **N**(4)-Ru-N(5) is 95.76(7)° is slightly larger than the corresponding angle for **2.12** at 95.4(3)°. The N(2)-Ru-N(6) angle for **3.9** is 106.86(6)° is slightly less than that for **2.12** which is 107.3(2)°. The N_{amide} Ru-$N_{py/pz}$ bond angles are all about the same at ~ 78°. The Ru-N pyrazine bond distances are about the same for **2.12** and **3.9**, however, the Ru-N carboxamido bonds are slightly shorter for **3.10** than for **2.12**. There are other slight differences in the N_{NO}-Ru-N*equat*. angles between the **3.9** and **2.12.** These variations are attributed to the degree to which the pyrazine or pyridine arms have to tilt out of plane to avoid an interaction between the pyridyl arms. Infrared data have not been obtained as of this report but will indicate the extent of back-donation to the NOπ^* orbitals. The shorter NO bond distance for **3.9** suggests that $\bar{\nu}_{NO}$ for **3.9** will be greater (back-donation will be less) for **3.9** than for **2.12**.

3.6 *N,N′*-BIS(2-PYRAZINECARBOXAMIDE)-1,4-PIPERAZINE

3.6.1 Materials and Methods

***N,N′*-bis(2-pyrazinecarboxamide)-1,4-piperazine (3.10)** was prepared according to a literature procedure.[68] Pyrazinecarboxylic acid (10.0 g, 0.0805 mol) was dissolved in dry pyridine (~40.0 mL). To the picolinic acid solution was added piperazine (3.47 g, 0.040 mol) and triphenyl phosphite (d = 1.184 g/mL, 21.0 mL, 0.0805 mol). The reaction mixture was stirred at 100 °C for four hours. After three days at room temperature the reaction mixture began to yield crystals. Recrystallization form DMSO produced X-ray quality crystals. ^{1}H NMR (500 MHz, DMSO-d_6, δ): 8.87 (d, 2H, H-3), 8.74 (d, 2H, H-2), 8.67 (d, 2H, H-1), 3.79 (s, 2H, H-6), 3.70 (m, 2H, H-7), 3.60 (m, 2H, H-4), 3.99 (s, 2H, H-5); ^{13}C{H} (125 MHz, DMSO-$_{d6}$, δ): 164.86 (C=O), 148.87 (Pz-*ipso*), 145.53 (C-2), 144.53 (C-3), 143.05 (C-1), 46.69 (C-5), 46.07 (C-4), 41.97 (C-7), 41.37(C-6); ESI-MS $M^{+\cdot}$ = 298.11

***N,N′*-bis(2-pyrazinecarboxamide)-1,4-piperazine reaction with [Ru(NO)Cl$_3$(H$_2$O)$_2$]** The reaction between *N,N′*-bis(2-pyrazinecarboxamide)-1,4-piperazine and [Ru(NO)Cl$_3$(H$_2$O)$_2$] was carried out according to a modified literature procedure.[69] Trichloronitrosylruthenium (0.594 g, 0.0021 mol) was added to ethanol/water solution (95%, ~20.0 mL, 85.0 °C) of *N,N′*-bis(2-pyrazinecarboxamide)-1,4-piperazine (0.648 g, 0.0021 mol). And additional twenty milliliters of 95% ethanol/water was used to completely transfer the [Ru(NO)Cl$_3$(H$_2$O)$_2$]. The reaction mixture was stirred at 85 °C for ten hours. A brown precipitate was removed from the reaction mixture via vacuum filtration. The filtrate volume was reduced under vacuum and stored at

ambient temperature for crystal formation. A precipitate was removed from the filtrate after several days. The precipitate was rinsed several times and was determined to be mostly the free ligand from ^{1}H NMR spectroscopic analysis. The orange ethanol wash was allowed to evaporate slowly at room temperature. After several days an orange precipitate formed. Preliminary NMR results indicate formation of a new species. The NMR spectrum of the new species and of the free ligand can be viewed in Figure 3.16.

3.6.2 Results and Discussion

The ligand *N,N'*-bis(2-pyrazinecarboxamide)-1,4-piperazine **(3.10)** was prepared as described and characterized by ^{1}H and ^{13}C NMR spectroscopy. ^{1}H and ^{13}C assignments were made based upon HH COSY, HMBC and HMQC spectra. The identity of the ligand was also confirmed by X-ray and mass spectral analysis. The labeling scheme for the NMR assignments is shown in Figure 3.14. The chemical shift values are listed in Table 3.11. The signals for the two pyrazine moieties are similar to those for other pyrazine compounds described in this section. There are separate signals for each carbon and each set of nitrogen atoms for the piperazine ring. The ^{1}H NMR spectrum is shown in Figure **3.16.**

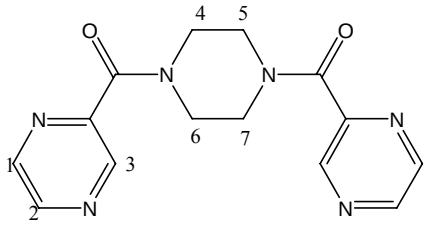

3.10

Figure 3.14-*N*,*N*′-bis(2-pyrazinecarboxamide)-1,4-piperazine

Table 3.11-^{1}H and ^{13}C NMR Data for *N*,*N*′-bis(2-pyrazinecarboxamide)-1,4-piperazine

^{1}H	**1**	**2**	**3**	**4**	**5**	**6**	**7**		
	8.87	8.74	8.67	3.60	3.99	3.79	3.70		
^{13}C								**Pz-*ipso***	**C=O**
	143.05	145.53	144.53	46.07	46.69	41.37	41.97	148.87	164.86

Crystal intensity and collection data are reported in Table 3.12. The X-ray crystal structure of **3.10** is shown in Figure 3.15. Selected bond distances and angles can be seen in Table 3.13.

Table 3.12-Crystal data and refinements for 3.10

	3.10
Chemical Formula	$C_{14}H_{14}N_6O_2$
Formula Weight	298.31
Temperature (K)	295(2)
Wavelength (Å)	0.71073
Crystal system	Monoclinic
Space group	P 21/n
a (Å)	5.8383(4)
b (Å)	18.2912(1)
c (Å)	6.8413(4)
α (°)	90
β (°)	109.2710(1)
γ (°)	90
Volume ($Å^3$)	689.64(7)
Z	2
Density (calculated) Mg/m^3	1.437
Absorption Coefficient (mm^{-1})	0.102
F(000)	312
Crystal Size (mm^3)	0.24 x 0.22 x 0.12
θ range for data collection (°)	2.23 to 32.54
Index Ranges	$-8 \le h \le 8$
	$-27 \le k \le 27$
	$-10 \le l \le 10$
Reflections collected	8985
Independent reflections	2450 [R(int) = 0.0241]
Completeness	97.8 % (θ=32.54°)
Data / restraints / parameters	2450/ 0 / 128
Max. and min. transmissions	0.9560 and 0.9464
Refinement Method	Full-matrix least-squares on F^2
Goodness-of-fit on F^2	1.414
Final R indices[$I > 2\sigma(I)$]	R1 = 0.0757, wR2 = 0.1960
R indices (all data)	R1 = 0.0890, wR2 = 0.2049
Largest diff. peak and hole (e $Å^3$)	0.408 and -0.267

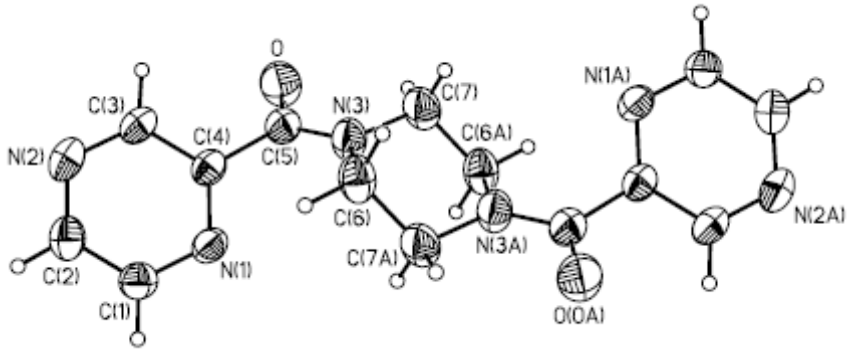

Figure 3.15-X-ray structure of *N*,*N'*-bis(2-pyrazinecarboxamide)-1,4-piperazine

Table 3.13 Selected bond distances (Å) and angles (°) for 3.10

O-C(5)	1.2195(2)	C(5)-N(3)-C(6)	126.52(1)
N(1)-C(1)	1.3353(2)	C(5)-N(3)-C(7)	119.45(1)
N(1)-C(4)	1.3364(2)	C(6)-N(3)-C(7)	113.71(1)
N(2)-C(2)	1.331(2)	O-C(5)-N(3)	123.21(1)
N(2)-C(3)	1.330(2)	O-C(5)-C(4)	117.87(1)
N(3)-C(5)	1.3434(2)	N(3)-C(5)-C(4)	118.91(1)
N(3)-C(6)	1.4594(2)	N(3)-C(6)-C(7A)	110.47(1)
N(3)-C(7)	1.4628(2)	N(3)-C(7)-C(6A)	109.75(1)
C(6)-C(7A)	1.499(3)	N(3)-C(6)-H(6A)	110.8(1)
C(7)-C(6A)	1.499(3)	N(3)-C(6)-H(6B)	106.0(1)
C(6)-H(6A)	0.979(9)	C(7A)-C(6)-H(6A)	106.7(1)
C(6)-H(6B)	1.05(2)	C(7A)-C(6)-H(6B)	105.3(1)
C(7)-H(7A)	1.01(3)	N(3)-C(7)-H(7A)	107.0(2)
C(7)-H(7B)	0.95(3)	N(3)-C(7)-H(7B)	105.8(2)

The reaction between **3.10** and $[Ru(NO)Cl_3(H_2O)_2]$ produced an orange precipitate from the filtrate. The NMR spectrum of the solid indicates the presence of some free ligand along with what appears to be one new product. The NMR spectra of the product and the free ligand can be seen Figure 3.16.

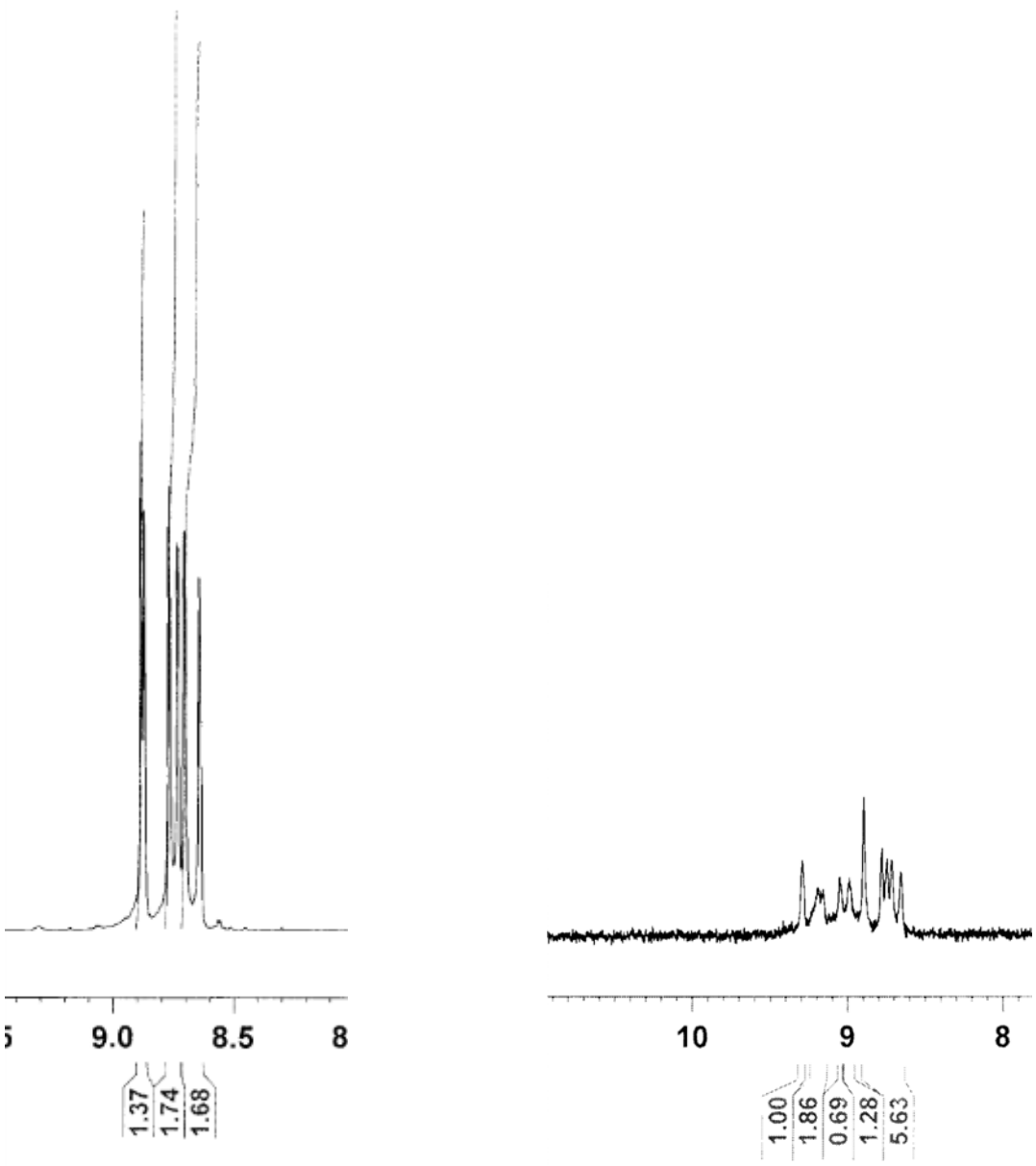

a. **b.**

Figure 3.16- a. ^{1}H NMR Spectrum of aryl region of 3.15 b. Reaction mixture

3.6.3 Conclusion

The ligand *N,N′*-bis(2-pyrazinecarboxamide)-1,4-piperazine was synthesized and characterized by NMR spectroscopy and X-ray crystallography. Preliminary results from a reaction between **3.10** and $[Ru(NO)Cl_3(H_2O)_2]$ suggest that one new species has been isolated from the reaction mixture. Complete analysis of the new complex awaits separation of the new complex from the ligand.

3.7 GENERAL CONCLUSION

The ligands *N*,*N′*-bis(2-pyrazinecarboxamide)-1,2-benzene, *N*,*N′*-bis(2-pyrazinecarboxamide)-2,3-diaminopyridine, *N*,*N′*-bis(2-pyrazinecarboxamide)-3,4-diaminopyridine, *N*,*N′*-bis(2-pyrazinecarboxamide)-1,2-ethane, *N*,*N′*-bis(2-pyrazinecarboxamide)-1,3-propane, and *N*,*N′*-bis(2-pyrazinecarboxamide)-1,4-piperazine were prepared and characterized by ^{13}C and ^{1}H NMR spectroscopy and/or X-ray crystallography. Although some of the complexes remain to be isolated, it seems that all pyrazine derivatives react with $Ru(NO)Cl_3(H_2O)_2]$ to form RuNO complexes. The complexes that have been prepared exhibit binding modes similar to the pyridine analogues.

The *N*,*N′*-bis(2-pyrazinecarboxamide)-1,2-benzene ligand has been characterized by X-ray crystallography. The reaction between the ligand and $[Ru(NO)Cl_3(H_2O)_2]$ yielded a complex similar to the prydine analogue but with expected variations in NMR data attributed to differences between the pyridine and pyrazine rings. Neither the crystal structure nor the infrared data for the complex are available at this time.

N,*N*′-bis(2-pyrazinecarboxamide)-2,3-diaminopyridine ligand was characterized by ^{1}H and ^{13}C NMR spectrosopy. Assignments were made based upon HH COSY, HMQC and HMBC data. No product from the reaction between $[Ru(NO)Cl_3(H_2O)_2]$ has been isolated at this time. However, preliminary NMR data suggest the formation of more than one product, one of which might exhibit a coordination mode similar to the pyridine analogue which binds through one pyridine arm and one carbonyl oxygen atom.

The *N*,*N*′-bis(2-pyrazinecarboxamide)-3,4-diaminopyridine ligand was characterized by ^{1}H NMR spectroscopy. Assignment of the signals awaits 2D analysis. However, at least one compound has been isolated from the reaction between the ligand and $[Ru(NO)Cl_3(H_2O)_2]$. The disappearance of the N-H signals and the downfield shift of all signals in the 300 MHz NMR spectrum of the product indicates that the ligand coordinates through the carboxamido and pyrazine arms. This promising result confirms that tetradentate coordination is possible with theses 2,3- and 3,4-diaminopyridine derivatives. It will be interesting to see which coordination mode is favored by each and how the RuNO moiety is affected.

The bis(2-pyrazinecarboxamide)-1,2-ethane ligand has been characterized by 2D NMR analysis and compared to pyridine analogue. Differences due to the pyrazine ring were noted. The RuNO complex with the ligand was also characterized by 2D analysis and shows features similar to the complex with the pyridine analogue. At 1850 cm^{-1}. $\bar{\nu}_{NO}$ for the pyrazine complex is higher than that for the pyridine analogue for which $\bar{\nu}_{NO}$ =1825 cm^{-1}. No other conclusions can be drawn until the crystal structure is obtained.

The N,N′-bis(2-pyrazinecarboxamide)-1,3-propane ligand **(3.9)** and chloro-nitrosyl-*N,N*′-bis(2-pyrazinecarboxamido)-1,3-propane ruthenium(II) **(3.10)** complex were prepared and characterized by 2D NMR analysis and X-ray crystallography. The RuNO complex exhibits a

linear nitrosyl group with and O(1)-N(1)-Ru angle of 177.89(15)° and N-O bond length of 1.132(2) Å. In comparison, the pyridine derivative exhibits a linear Ru-N-O angle of 177.5(7)° and an N-O bond distance of 1.143(8). Although infrared data have not been acquired, the longer N-O bond observed for **2.12** suggests that the stretching frequency for **3.10** should be greater than for **2.12**. That **3.7** exhibits $\bar{\nu}_{NO}$ that is greater than that of its pyridine analogue also suggests that a lower $\bar{\nu}_{NO}$ can be expected for **3.9**.

The *N,N'*-bis(2-pyrazinecarboxamide)-1,4-piperazine ligand **(3.10)** was prepared and characterized by NMR spectroscopy and X-ray crystallography. ^{1}H NMR data for the reaction between the ligand and [Ru(NO)$Cl_3(H_2O)_2$]suggest formation of at least one new product. This ligand like its pyridine analogue and the alkyl analogues should provide useful information about the magnetic anisotropy about the Ru-N-O moiety.

In summary, six bis-pyrazine bis-carboxamido and six bis-pyridine bis-carboxamido ligands were prepared. The ligands were designed with minor variations to adjust the ligand environment with the aim of producing ruthenium nitrosyl complexes that can withstand a physiological environment, lose NO by photolysis then stabilize the remaining Ru^{III} complex. Eventually photolysis data can be correlated with the changes in the ligand environment to arrive at the best ligand set for photolysis of NO. The change from pyridine to pyrazine, not only helps understand how changes in the ligand environment influence the RuNO moiety, but also introduces the possibility of coordination to another metal centers through the uncoordinated pyrazine nitrogen atom. Recently, pyrazine bridged ruthenium nitrosyl complexes have been shown to release NO under visible light.[80] The ligands with a 2,3- and 3,4-diaminopyridine backbone also introduce some promising additional coordination sites.

APPENDIX

REVIEW OF PROFESSOR SHEPHERD'S RESEARCH

Much of the Professor Shepherd's early work with ruthenium complexes, N-heterocyclic ligands and other biologically relevant ligands provided a foundation for the current applications to biochemistry. Therefore, a review of those investigations and others is provided in this appendix.

Under the direction of Professor Henry Taube, Professor Shepherd investigated the reaction between aquopentammineruthenium(II) ($[Ru^{II}(NH_3)_5(H_2O)]^{2+}$) and nitrogen-containing heterocyclic ligands including pyridine, pyrazine and imidazole, among others.[81] While a graduate student, Professor Shepherd[27,82,83] discovered that, although imidazoles are usually N-bound, they can coordinate through C-2 to $[Ru^{II}(NH_3)_5(H_2O)]^{2+}$ as imidazolium ylide. An imidazolium ylide is shown in Figure A.1. The ruthenium bound imidazolium ylide is shown in

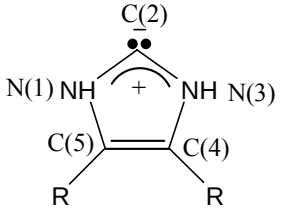

Figure A.1-Imidazloium Ylide

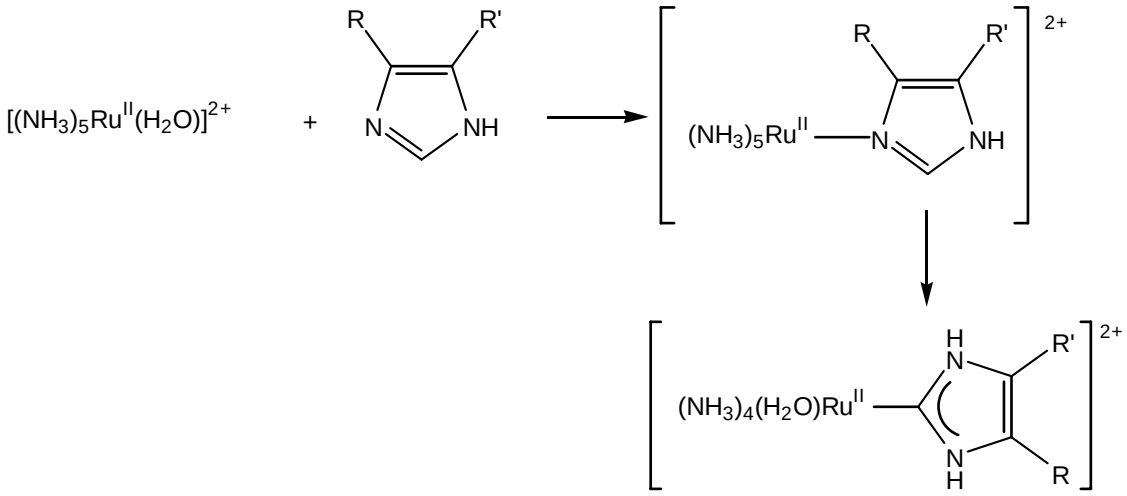

Scheme A.1-C-Bound ruthemium imidazole complex

The fact that imidazoles can bind through C-2, as well as through the pyridine nitrogen, might have important biological implications. Histidine (Figure A.2) a derivative of imidazole, binds to the metal ion centers in many metalloenzymes and heme proteins. Many[84-86] have pursued the possibility that linkage isomerization between N-3 and C-2 of histidine could trigger physiological functions. Today imidazolium ylides are used to improve catalyst performance, stability and recyclability and to provide sites for functional group introduction[16,87-89]

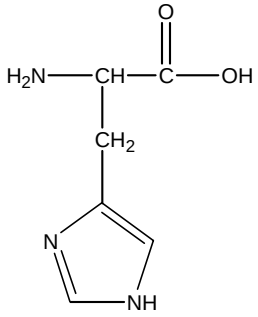

Figure A.2- Histidine

Investigations into the interaction of imidazoles, substituted imidazoles[90] and histidine with pentacyanoiron(II) and pentacyanoiron(III) moieties were initiated.[91,92] Electrochemical studies of $[(CN)_5FeL]^{2-/3-}$ and $[(NH_3)_5RuL]^{3+/2+}$ imidazole and pyrazole complexes illustrated that a ligand's π-acceptor ability has a stronger effect on reduction potential than does the ligand's π-donating character.[93] The influence of metal centers on the pK_a of the pyrrole hydrogen of imidazole complexes,[94,95] and of pyrazole complexes was also studied[96].

The role of imidazoles in physiological processes was examined by analyzing the ligand to metal charge transfer transitions (LMCT) of low-spin d^5 Fe^{III} and Ru^{III} pyrazole/imidazole and pyrazolato/imidazolato complexes.[97,98] The solvatochromism of the LMCT transition of $[Fe(CN)_5]^{2+}$ complexes[99,100] and the ^1H and ^{13}C NMR spectra of methylimidazole cobalt complexes. $[Co(NH_3)_5(Me\text{-}Im)]^{3+}$ (Me-Im = methylimidazole) was prepared to mimic histidyl moieties in Zn^{II} enzymes in which the histidyl side chain can be either adjacent to or remote from the coordination site. $[Co(NH_3)_5(Me\text{-}Im)]^{3+}$ complexes exhibiting adjacent and remote binding (Figures A.3 and A.4) were characterized by NMR spectroscopy. An X-ray crystal structure of the remote isomer (Figure A.5) allowed unambiguous chemical shift assignments. The NMR data illustrated that generalizations from other low-spin d^6 complexes with nitrogen heterocyles cannot be applied to tautomeric imidazoles.[101,102] NMR studies that followed the $[Co(NH_3)_5(Me\text{-}Im)]^{3+}$ experiments showed that the influence of temperature induced paramagnetic (TIP) on ^1H NMR chemical shift values for η-2 coordinated N-heterocycles is minimal in comparison to the σ withdrawing effect of the metal center and rehybridization upon coordination.[96]

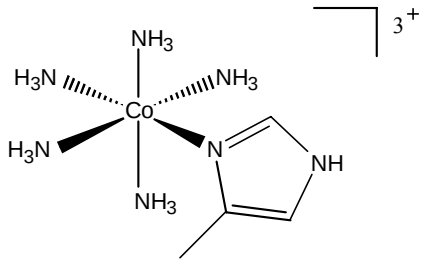

Figure A.3-Adjacent Isomer of (4-methylimidazole)pentaamminecobalt(III)
Reprinted with permission from *J. Am. Chem. Soc*., **1983** *22* 2693. Copyright 1983 American Chemical Society.

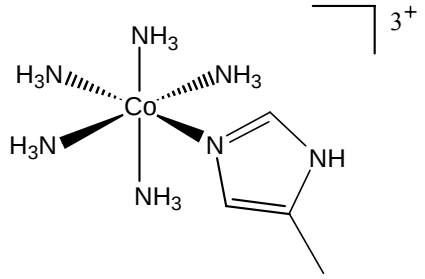

Figure A.4-Remote Isomer of (4-methylimidazole)pentamminecobalt(III)
Reprinted with permission from *J. Am. Chem. Soc*., **1983** *22* 2693. Copyright 1983 American Chemical Society.

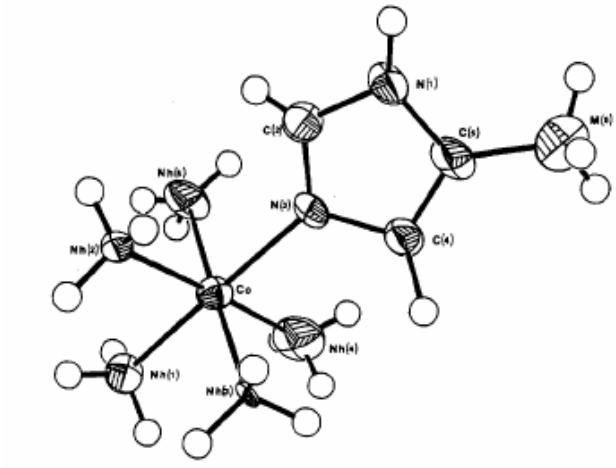

Figure A.5-Structure of the remote isomer of $[Co(NH_3)_5(4\text{-MeIm})]^{3+}$
Reprinted with permission from *J. Am. Chem. Soc*., **1986**, *25*, 3157. Copyright 1986 American Chemical Society.

Observations from the imidazole work helped elucidate the processes involved in immobilized metal affinity chromatography (IMAC). IMAC is a method developed by Porath

and coworkers[103,104] to purify proteins. In IMAC, a chelated metal ion which is attached to a solid support and interacts with proteins. Proteins that have a higher affinity for the chelated metal ion elute more slowly from the column than proteins that have lesser affinity for it. Until 1999 there was much debate about the nature of the coordination that occurs between a protein and the IMAC metal center. In collaboration with Richard Pasquinelli, Mohammad Ataai, and Richard Koepsel, definitive evidence of a three donor attachment was presented. Interactions between the six-mer peptide gly-his-pro-his-his-gly (GHPHHG) and Cu^{II} and Pd^{II} N-methyliminodiacetate complexes were used to model IMAC interactions. The model peptide tails were shown to attach at the first, third and fourth amino acid donors in order to approach the 90° bond angle favored for square planar coordination. The imidazole donors of histidine coordinate such that the three methylene linkers are adjacent, remote and adjacent to the coordinating nitrogen for the model GHPHHG.[105,106] Comprehensive NMR analysis of the model system helped identify another tag, his-pro-his-his-gly-gly (HPHHGG), that has affinity for purification from Zn^{II} iminodiacetate columns at pH 6.5-6.[107]

A molecular modeling study compared the energy-minimized structures of [Pd(mida)] complexes of peptide sequences used in IMAC chromatography. The small differences in the calculated energies of H_6, GHPHHG and ser-pro-his-his-gly-gly (SPHHGG) correlate with elution order. The most relaxed sequence, imH_6, is bound most strongly hence elutes most slowly from the column. The most relaxed ligand exhibits the strongest M^{II}-N because it is the least strained. The elution order does not have to be the same as the minimum energy order but it does suggest that the two values are based on similar factors.[108] Two related reviews were published in 2003. One review was on general chromatographic methods;[109] the other was on chromatographic and electrophoretic methods in the separation or transition metals.[110]

In 1983 the first series of low-spin Fe^{III} complexes, $[(CN)_5Fe^{III}(imidazoles)]^{2-}$ and $[(CN)_5Fe^{III}(pyrazoles)]^{2-}$, to exhibit the maximum 2.54 mm/s quadrupole splitting as predicted in 1967 by Golding[111] was reported. Two years later, in collaboration with Professor Sanford Asher, resonance Raman excitation profiles were used to distinguish between the π orbitals involved in the ligand to metal charge-transfer transitions for $[(CN)_5Fe^{III}(imidazole)]^{2-}$ and $[(NH_3)Ru^{III}(imidazole)]^{3+}$.[112] Evidence was presented for the proton-promoted chelate-ring opening of copper(II) polyamine complexes through the 3-centered electrophilic attack by H_3O^+ on the metal nitrogen bonds. This direct ligand substitution pathway was proposed initially by Wilkins as an alternative to simple dissociative cleavage.[113] A computational model based upon the infrared analysis of polyamine complexes with copper(II), including bis(ethylenediamine) and bis(trimethylenediamine), among others, was devised to help elucidate controversial vibrational assignments.[114,115] A water soluble porphyrin complex $[Ru(TPPS)CO]^{4-}$ (TPPS = tetraphenylporphyrinato) was prepared and shown to catalyze the water gas shift reaction without cluster- and hydride-forming side reactions. Such side reactions reduce the activity of mononuclear catalysts, $[Fe(CO)_5]$, $[Mo(CO)_6]$, $[W(CO)_6]$ and the trinuclear catalyst $[Ru_3(CO)_{12}]$.[116]

In the late 1980's experiments were initiated to dearomatize N-heterocycles. Concurrent with this work, the Taube group had dearomatized lutidine, pyrrole and N-methylpyrrole with $[(NH_3)_5Os]^{2+}$. An alternative approach was to use ruthenium(II)polyaminocarboxylates ($[Ru^{II}(pac)]$). $[Ru^{II}(pac)]$ complexes are much less toxic than the Os^{II} reagents, thus could have medicinal applications. Earlier it was shown that the stability of $[Ru(NH_3)_5(pyrazine)]^{2+}$ was due more to dπ-pπ backbonding than to pyrazine's basicity.[117,118] To estimate the extent of charge transfer from Ru^{II} into π-acceptor orbitals, a π-

acceptor scale was developed based upon photoelectron spectroscopy (PES). The π-acceptor order CH_3pz^+ > CO > dmad (dimethylacetylenedicarboxylate) > pz > CH_3CN > py, agrees with literature estimates based upon titration data and UV-vis data.[119] Later a method for measuring the π-donor capacity of Ru^{II} centers based upon the MLCT spectra of pyrazine and 4,4′-bipyridine was published.[120]

The similarities between $[W^0(CO)_5L]$ where L = pyridine, pyrazines, pyrimidines and pyridazine and analogous $[Ru(NH_3)_5L]^{2+}$ prompted an investigation for an isomerization pathway from N-1 to N-4 on the pyrazine ring for $[W(CO)_5]$. The solvents acetone and diglyme prohibited observation of the required η^2 intermediates by ^1H NMR studies. If the η^2 intermediates do exist they probably cannot survive long enough to be detected due to solvent displacement.[121] It was believed that a shorter path for migration might lead to the fluxionality observed for pyridazines. Therefore studies similar to the pyrazine studies were completed with pryimidine and 1,3,5-triazine and $M(CO)_5$ (M = W, Mo, Cr). Even with a two-bond path the barrier for migration was too large for migration to be observed.[122]

Since the π-base behavior of $[(NH_3)_5Ru]^{2+}$, and of $[(NH_3)_4Os]^{2+}$, toward π-acids such as pyridines and pyrazines had been well studied, this research was extended to include the affinity of $[(NH_3)_5Ru]^{2+}$ toward π-acids such as olefins, acetylenes and CO, which are of more interest to organic chemists. NMR data revealed that π donation from the metal center into olefinic π* orbitals, can affect atoms that are two and three bonds away from the coordination site.[123,124] The effect of $[(NH_3)_5Ru]^{2+}$ on the bend-back angles of dmad were examined by X-ray diffraction and compared to other $[(NH_3)_5Ru]^{2+}$ complexes with π-acceptor ligands.[125]

The experiments with $[(NH_3)_5Ru]^{2+}$, $[(NH_3)_5Os]^{2+}$, and Ru^{II} polyaminocarboxylates were extended to test the generality of the long range effect π-donation to π–acceptor ligands. Styrene

complexes of $[(NH_3)_5Ru]^{2+}$, $[(NH_3)_5Os]^{2+}$ and $[Ru^{II}(hedta)]^{-}$ were prepared and characterized by NMR spectroscopy. The styrene complexes exhibited the same changes in ^{1}H and ^{13}C chemical shifts as do linear olefins upon coordination. Another important conclusion from the styrene experiments is that disruption of aromaticity only occurs in the absence of alternate metal binding sites. For example, $[(NH_3)_5Ru]^{2+}$ and $[(NH_3)_5Os]^{2+}$ will only bind to the exo-vinylic donor of styrene.[126]

Since $[(NH_3)_5Ru]^{2+/3+}$ and $[(NH_3)_5Os]^{2+/3+}$ were known to bind to purine (Figure A.6) and pyrimidine (Figure A.7) bases in DNA and RNA the possibility that these nucleobases might also exhibit some dearomatizing π- bonding was investigated. Given from the styrene studies that no olefin-like binding will occur if alternate binding sites are available, 1,3-dimethyl uracil, (Figure A-8) in which the N-1 and N-3 ring locations are blocked with methyl groups, was selected as substrate. NMR and electrochemical studies indicated that coordination by 1,3-dimethyl uracil with $[(NH_3)_5Ru]^{2+}$ and with $[(NH_3)_5Os]^{2+}$ occurs through the C-5 and C-6 olefin bond.[127]

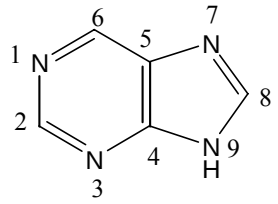

Figure A.6-Purine

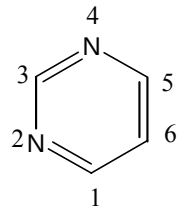

Figure A.7-Pyrimidine

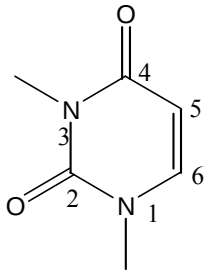

Figure A.8-1,3-dimethyluracil

Since metal complex binding to DNA and RNA nucleobases is pertinent to heavy metal labeling of DNA and the development of chemotherapeutics, the 1,3-dimethyl uracil study was followed with an investigation of methyl derivatives of uridine (Figure A.15) cytosine (Figure A.9) and cytidine (Figure A.10). Only C-5 C-6 olefinic coordination is observed for $[Ru^{II}(hedta)]^-$ complexes with 1,3-dimethyl uracil, (Figure A.8) uridine, 3-methyluridine, cytidine, and 3-methyl cytidine. The rehydbridization that accompanies η^2 coordination disrupts aromaticity and suggests that metallation of cytidine or uridine would likely be mutagenic during DNA replication because dearomatization would alter the ability of cytidine or uridine to match with guanosine and adenosine.

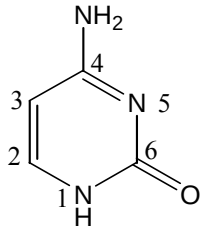

Figure A.9-Cytosine

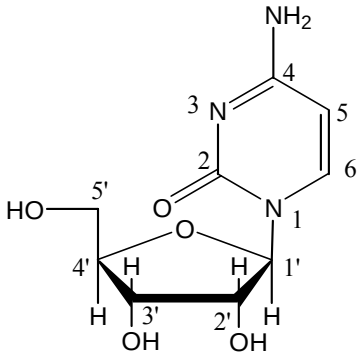

Figure A.10-Cytidine

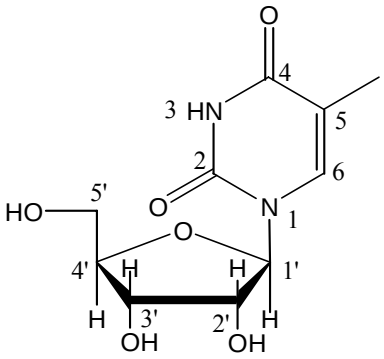

Figure A.11-Thymidine

Observation of C-5 and C-6 η^2 coordination to uridine by [Ru(hedta)]$^-$and not to thymidine (Figure A.11) suggested the possibility that steric hindrance by the C-5 methyl group might be preventing η^2 coordination.[128] Therefore the effects of C-5 substituents on uracil's and uridine's ability to participate in η^2 coordination through C-5 C-6 to [Ru^{II}(hedta)]$^-$ were studied. η^2 coordination was observed for uracil and uridine derivatives with electron withdrawing substituents at C-5, but not for derivatives with electron donating substituents such as a methyl group.[129] It was concluded that electronic factors are more important than steric factors. And that substituents at C-5 on thymidine don't necessarily preclude the possibility of an η^2 interaction with [Ru^{II}(hedta)]$^-$. Since the C-5 C-6 portion of C and T base residues of DNA reside in the major groove, an additional mode of DNA metallation seemed possible.

The propensity for ruthenium polyaminocarboxylate ligands to coordinate in an η^2 fashion to pyrimidine and pyrimidine derivatives was investigated. At pH 7 three isomers of [Ru(Hedta)L]$^-$ form three isomeric complexes with pyrimidine, 4-methylpyrimidine and 2-aminopyrimidine and five isomers with 4-aminopyrimidine.[130]

As previously mentioned and illustrated above, if a competing coordination site is available, coordination will occur there rather than at the olefinic site. However, migration from an N-bound site to an η^2 site is possible. The capacity of [Ru^{II}(hedta)]$^-$ to migrate from N-1 of pyrimidine to the η^2 position was observed. Another promising observation was that the exo carbonyl groups on nucleobases such as uracil ad cytosine enhance the stability η^2 ruthenium polymaminocarboxylates[131]

Results from the pyrimidine experiments prompted an interest in the tendency of [Ru^{II}(hedta)]$^-$ to form η^2 complexes with pyridazine (Figure A.12). The σ-basicity and

resonance energy of pyridazine closely match those of pyrimidine. However, due to the electron withdrawing nature of the adjacent nitrogen atom ortho to the coordination site, pyridazine is a better π-acceptor. In agreement with the fact that pyridazine is a better π-acceptor, the complex $[Ru^{II}(hedta)(pyd)_2]^-$ exhibits a stronger bond to ruthenium than does the analogous pyrimidine complex. The greater π-acceptor character creates a higher barrier for migration from a nitrogen lone pair to an η^2 site. In fact, no η^2 bound $[Ru^{II}(hedta)(pyd)_2]^-$ species were observed.[132]

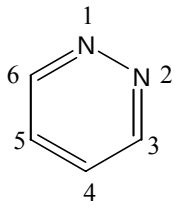

Figure A.12- Pyridazine

An examination of steric an electronic influences on the formation constants of sixteen $[Ru^{II}(hedta)]^-$ η^2 complexes of olefins and pyrimidines related to cytidine and uridine led to several conclusions, four of which are listed here. First, η^2 coordination is controlled more by electronic factors than by steric factors. Second, the three stereochemical isomers of $Ru^{II}(hedta)^-$ can determine, on the basis of size, which olefinic units may coordinate to each isomer. For example, the most crowded $[Ru^{II}(hedta)]^-$ isomer will bind only to the smallest olefins. Third, since some olefins can bind all three $[Ru^{II}(hedta)]^-$ isomers while others can't, it is difficult to get a good estimate of binding constants. Fourth, the sensitivity of the formation constant to ligand geometry, substituents, solvent, and the stereochemical isomers adopted by the metal center suggests that Ru^{II} agents can be tuned to form η^2 complexes with cytosine and thymine.[133]

In a related project the ruthenium(II) polyaminocarboxylate, Me_2-edda (Me_2-edda^{2-} = *N,N′*-dimethylethylenediaminediacetate), a derivative of [Ru^{II}(hedta)]$^-$ was prepared. [Ru^{II}(Me_2-edda)(H_2O)$_2$] exhibits axial binding sites, in contrast with the [Ru^{II}(hedta)]$^-$ complex which exhibits equatorial N trans bonding in the two isomers that bind to nucleobases. The axial binding sites [Ru^{II}(Me_2-edda)(H_2O)$_2$] present the same steric conditions as the most sterically hindered [Ru^{II}(hedta)]$^-$ that only binds to small substrates. It was thought that the enhanced π-donating capacity of [Ru^{II}(edda)] to might allow facile axial η^2 coordination with DNA nucleobases. For [Ru^{II}(Me_2-edda)(H_2O)$_2$], however, the glycinato rings migrate into axial positions. It was found that, like the sterically hindered [Ru^{II}(hedta)]$^-$ isomer, [Ru^{II}(Me_2-edda)(H_2O)$_2$] will not bind to pyrimidines and is selective for unhindered olefins. The new feature exhibited by [Ru^{II}(Me_2-edda)(H_2O)$_2$] is that bidentate dienes can promote isomerization into transaxial geometry which allows for η^4 coordination of olefins.[134]

An attempt to obtain η^2-coordination between [Ru^{II}(hedta)]$^-$ and pyrazine was complicated by protonation of the pyrazine nitrogen atoms. Three [Ru^{II}(hedta)(pz)]$^-$ species were detected, one with N-1 coordination, the other two with η^2-coordination.[135] To simplify the system the reaction was attempted with 2,3-dimethylpyrazine. It was hoped that steric conditions would force the formation of one η^2 isomer. In fact, two η^2 isomers were observed in very low abundance with respect to the pyrazinium ligand. The important result from this study was the observation of the binuclear [Ru^{II}(hedta)]$_2$-(2,3-Me_2pz)]$^{2-}$ complex in which the Ru^{II} centers exhibit non-equivalent coordination to the dimethylpyrazine bridging ligand.[136]

From the many literature reports on the capacity for Ru^{II} and Os^{II} to disrupt aromaticity and to bind to olefins, some criteria had become accepted as verification that an η-2 olefinic complex had been formed. Upfield shifts of 1.0-2.0 ppm for protons and 40-80 ppm for carbons

were accepted as evidence for the formation of an Os^{II} or an Ru^{II} η-2 olefin. Data were presented in 1996 to show that an overlooked influence on the ^1H chemical shift is the adjacent ring structure units when the Ru^{II} complex is $[Ru^{II}(hedta)]^-$. The ^1H NMR chemical shifts of N-heterocycles coordinated to d^6 metals had been rationalized by magnetic anisotropy, TIP, and π-back donation, among other effects based upon data from $[Os(NH_3)_5]^{2+}$ complexes and a limited number of Ru^{II} complexes.[137] In a paper regarding the effect of net charge and π-back bonding on the ^1H NMR chemical shifts of N-heterocycles coordinated to $M(NH_3)_5$ (M = Ru^{II}, Os^{II}, Co^{III} and Rh^{III}) and $M(CN)_5^{n-}$ (M = Co^{III}, Ru^{II}, and Fe^{II}) and Ru^{II} polyaminocarboxylates it was shown that the charge of the coordinating metal moiety also exerts a strong influence on the ^1H NMR chemical shifts of N-heterocycles coordinated to d^6 metals. α protons were seen to exhibit a downfield shift and β protons an upfield shift with an anionic ML_5 complexes; the opposite was observed for cationic ML_5 complexes.[138] The metal pentacarbonyl series $[M(CO)_5L]$ (M= Cr, Mo, W) was studied in C_6D_6 and $CDCl_3$ to observe solvent effects and the shift pattern with when ML_5L' is neutral.[139]

With the chemical shift variations that occur upon coordination N heterocycles to $W(CO)_5$ understood, the coordination sites preferred by $W(CO)_5$ were investigated. Photolysis of $W(CO)_6$ in dry acetone in the presence of guanosine (Figure A.13) and adenosine (Figure A.14) promotes coordination at N-7, N-1 and N-3. In support of similar results obtained with $[Ru^{II}(edta)(5'\text{-GMP})]^{4-}$ and discussed later, these results suggest that softer metal centers can bind to more nucleobase sites on than can the harder Pt^{II} complexes. The presence of multiple binding sites on guanosine and adenosine makes $W(CO)_5$ a viable candidate for heavy atom labeling of DNA. $W(CO)_5$ coordinates only at N-3 on cytidine (Figure A.10). Remarkably, $W(CO)_5$ attacks the ribose moiety at C-3′ to form a carbene instead a pyrimidine site on

thymidine (Figure A.11) or uridine (Figure A.15). Carbene formation occurs because thymidine and uridine lack suitable alternative binding sites.[140] The carbene forming reaction was used to form a $W(CO)_5$-furanosylidene complex from ribose.[141]

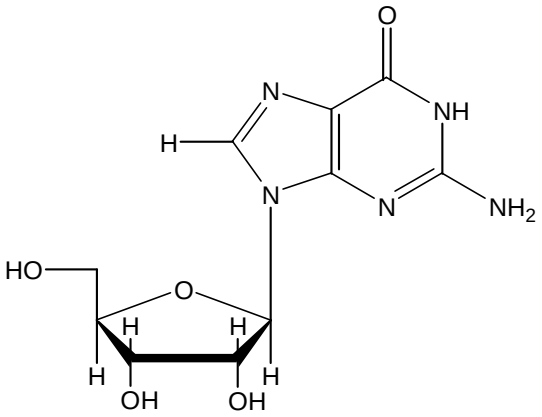

Figure A.13-Guanosine

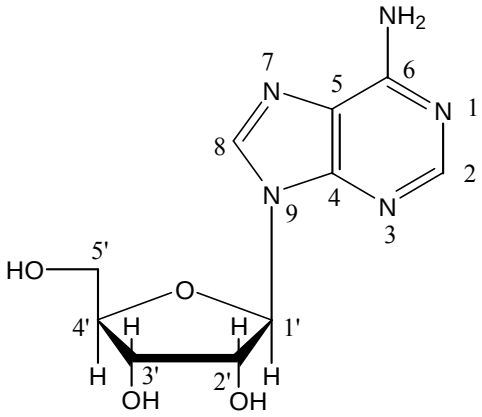

Figure A.14-Adenosine

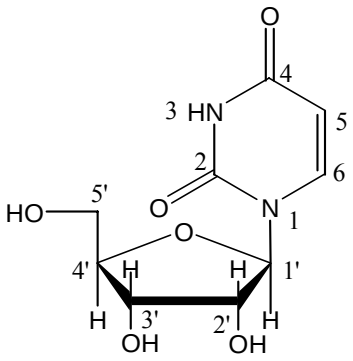

Figure A.15- Uridine

To determine the factors that guide the preference of $W(CO)_5$ for various coordination sites, 2-aminopyrimidine (2-ampym) and 4-aminopyrimidine (4-ampym), 2-aminopyridine (2-ampy), 4-aminopyridine, (4-ampy) and 4-dimethylaminopyridine were used to model coordination to the exo-amine or the endocyclic imino nitrogen of nucleobases. Non-labile coordination of 2-ampym and 4-ampym to $W(CO)_5$ through the exo-amine was observed. Secondary photoproducts of the 4-ampym complex were coordinated to $W(CO)_5$ either at N-1 or chelated via N-3 and the exocyclic amine. In agreement with a study completed by Darensbourg, 100 % of 2-aminopyridine coordinated to $W(CO)_5$ through the pyridine nitrogen and coordination by 4-aminopyridine through either the exo-amine or the pyridine nitrogen.[142] New information from this study was that 4-dimethylaminopyridine coordinates to $W(CO)_5$ exclusively by the exo-amine. Coordination to the exo-amine was favored by increasing its basicity, either by methylation or by placing it para to the pyridine nitrogen as in 4-ampym. Exo-amine coordination can also be favored by decreasing the basicity of the endocyclic imine. For example, the endocyclic nitrogens of 2-ampym and of 4-ampym are less basic that the

endocylic nitrogens on 2-ampy and 4-ampy.[143-146] Thus there is 100% coordination at the endocyclic pyridine of 2-ampy and 100% at the exocyclic nitrogen of 2-ampym.[147]

To test the validity of generalizing these observations, the reaction of $W(CO)_5$ with 4-dimethylaminopyridine (4-Me_2-ampy), 4-acetaminodpyridine (4-Acampy), 2-(methylamino) pyridine (2-Me-ampy) 2-(dimethylamino) pyridine (2-Me_2-ampy), adenosine (A) (Figure A.16), N^6-methyladenosine (N^6-Meado), and N^6,N^6-dimethyladenosine (Figure A.17) was investigated. The 2-ampy ligand coordinated to $W(CO)_6$ only through the pyridine nitrogen. Introduction of one methyl group on the amine substituent induced coordination at both the pyridine nitrogen and the amino nitrogen for 2-Me-ampy. Addition of another methyl substituent to the exo-nitrogen forced coordination exclusively at the amino nitrogen as it did for the 4-Me_2-ampy complex with $W(CO)_5$. It was thought that acetylation of the amino nitrogen on 4-aminopyridine would decrease the nitrogen atom's basicity and force coordination at the pyridine nitrogen. Instead, the amido lone pair increased the basicity of the carbonyl oxygen to such that the oxygen atom, rather than the pyridine nitrogen, coordinated to the $W(CO)_5$.[148]

Amino nitrogen coordination was observed neither for N^6-Meado nor for N^6,N^6-Meado. Instead, N-1 coordinates to $W(CO)_5$ albeit to a lesser extent in N^6,N^6-Meado and in N^6-Meado than in unsubstituted adenosine. The amino electrons of adensosine, N^6-methyladenosine, and N^6,N^6-dimethyladenosine are too involved in resonance with the purine ring to allow the exo-nitrogen to coordinate the $W(CO)_5$. Rather than increasing the basicity of the amino nitrogen, the methyl substituent(s) enhanced the hydrogen bonding capacity of N-3 with the ribose –OH group. The enhanced hydrogen bonding blocks coordination at N-3. N-7 and N-1, are also blocked by the methyl group(s), thus less N-1 coordination to $W(CO)_5$, is observed for N^6,N^6-Meado than for N^6-Meado. The conclusion was that, while the aminopyridine models do not

mimic the coordination behavior of nucleobases, exactly, comparison of their behavior and structural differences reveals important aspects of nucleobase coordination to transition metal complexes.[149]

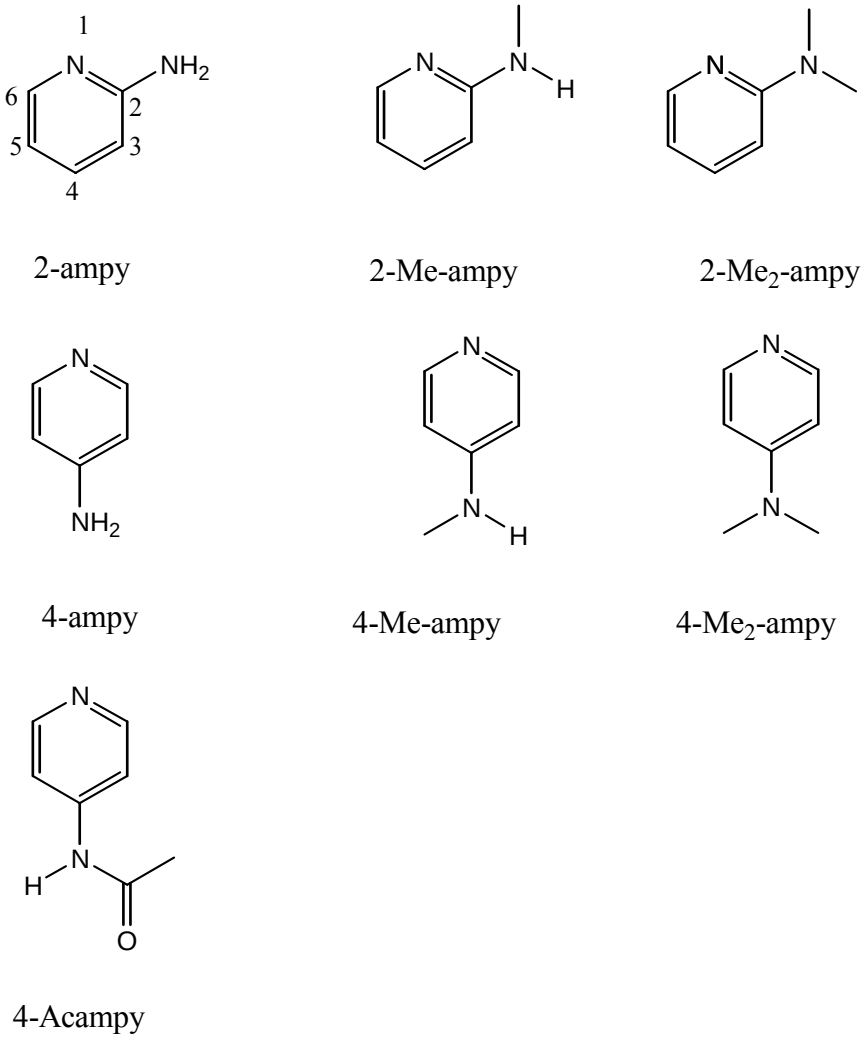

Figure A.16-2- and 4-Aminoyridine Derivatives and 4-Acetamidopyridine

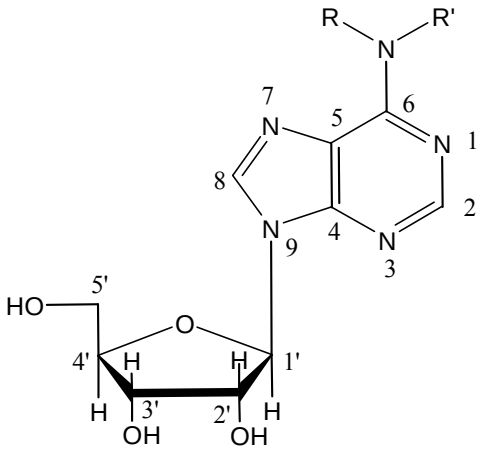

Figure A.17-N^6-methyladenosine (R=Me; R′=H); N^6, N^6-dimethyladenosine (R=R′=Me)

The reaction between $[Ru^{II}(hedta)]^-$ and 6-azauridine (Figure A.18) a leukemia drug and tumor inhibitor, also provided some interesting NMR data. The $[Ru^{II}(hedta)]^-$ moiety was shown to migrate among the three binding sites of 6-azauridine, the monodentate site at N-6, the bidentate site at N-3 and O-4 and the η^2 site between N-6 and C-5. This was the first good example of Ru^{II} η^2-N=CH- coordination. ^{13}C resonances for bound olefins usually shift upfield 40 to 80 ppm upon η^2 coordination. However, no shift in the ^{13}C resonance for C-5 was observed. Two possible explanations were presented. If olefinic π^* orbitals are closer in energy to the Ru^{II} $d\pi$ orbital than imine π^* orbitals are, then the imine ^{13}C chemical shift should be less affected by η^2 coordination. Another possibility is that the electronegative nitrogen is attracted to Ru^{II} to the extent that Ru^{II} begins to behave like Ru^{III}. The strong ionic attraction cause the ruthenium to reside closer to nitrogen than to carbon in the -N=CH- unit, thus decrease backbonding to C-5.[150] This unusual lack of ^{13}C chemical shift upon η^2 coordination prompted a follow-up experiment in which the η^2 isomer was isolated in quantitative yield below pH 3.0.[151]

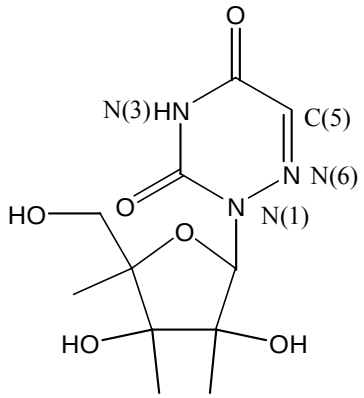

Figure A.18-6-azauridine

Electron transfer mechanisms and redox processes were of interest because of their relevance to biochemistry. In unpublished work, a stable Ru^{II} center was locked into a $[(CN)_5Ru^{II}LRu^{III}L']$ environment to show that lowering the potential energy well on one side of a binuclear complex results in a loss of the intervalence band.[27]

In published work it was reported that geometrical transformations change can trigger intramolecular electron transfer. Oxo-bridged binuclear ions containing V(III) or V(IV) at one metal site and Ru(II), Ti(III) or V(II) the reducing site were studied.[152-156] Some of the first major applications of EPR based spin trapping techniques to inorganic mechanistic studies[157-161] were reported. Secondary ligand effects on electron transfer and the intervalence transition band[161-163] were studied. The effects of changes in conjugation of the bridging ligand on metal coupling were also invstigated.[90]

Metal centers bound to a tethering backbone and bridged by a small molecule mimic nonheme iron mixed oxidation state species.[164] An iron group mixed oxidation state assembly to mimic the hydroxyl bridged $Fe^{II}Fe^{III}$ acid phosphatase enzyme[165,166] was developed. Research on the reduction of O_2 and H_2O_2 by $[Ru^{II}(NH_3)_6]^{2+}$, $[Ru^{II}(NH_3)_5OH_2]^{2+}$, and $[Ru^{II}(NH_3)_5$(1-

$CH_3imH)]^{2+}$ [167] as well as by $[(CN)_5Fe^{II}(imz)]^{3-}$ complexes[168] was completed. Binuclear V^{III} and Fe^{II} complexes were also prepared as models for metalloenzymes that reduce O_2 and H_2O_2. The reductions occur through O_2 coordination and cooperative reduction by the metal sites without the release of oxygen free radicals. The crystal structure of a novel seven coordinate alkoxy bridged binuclear V^{III} complex is shown in Figure A.19. The monomer-dimer equilibrium for the species was also studied.[169,170] For the reduction of O_2 by $[Fe_2^{II}(ttha)(H_2O)_2]^{2-}$ ($ttha^{6-}$ = triethylenetetraaminehexaacetate), evidence for reduction two-electron pathway via ferryl intermediates was presented. [171]

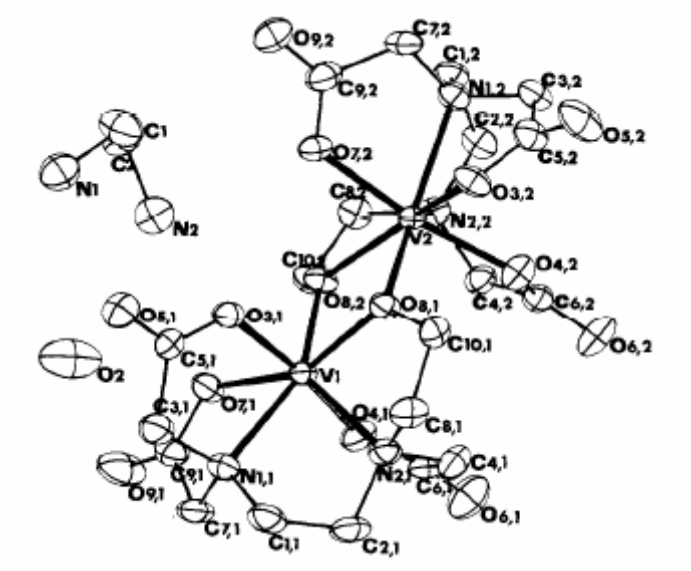

Figure A.19-Crystal Structure of $[enH_2][V(hedta\text{-}H)]_2 \bullet 2H_2O$

Reprinted with permission from *J. Am. Chem Soc*., **1981**, *103*, 5511. Copyright 1981, American Chemical Society.

$[Ru^{III}(hedta)]$ and $[Ru^{III}((CH_3)_2edda)]^+$ complexes were developed as epoxidation catalysts using *t*-butyl peroxide[172] and as oxidizing agents for alcohols bearing an α proton.[173] A review of ruthenium-oxo catalysts for stilbene oxidation was presented and explained how one could predict which catalysts would epoxidize with retention of configuration.[174] Formation of $[Ti(O_2)(edta)]^{2-}$ by peroxo displacement of the oxo moiety in $[TiO(edta)]^{2-}$ and by reduction of a superoxo transient $[Ti(O_2)(edta)]^{-}$ [175,176] was reported. The crystal structure of $[Ti(edta)(H_2O)]$ (Figure A. 20) revealed that at low pH the Ti(IV)-$edta^{4-}$ complex has an axial H_2O rather than an oxo group as previously believed. At higher pH the H_2O is deprotonated to form the π-donating oxo group.[177]

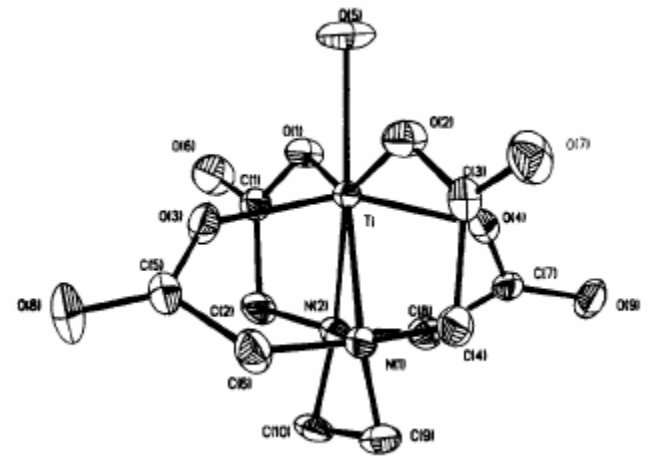

Figure A.20-Crystal Structure of $[Ti(edta)(H_2O)]$

Reprinted with permission from *J. Am. Chem Soc*., **1985**, *24*, 1857. Copyright 1985, American Chemical Society.

The chemistry and redox reactions of $[Ru(CN)_5]^{3+}$(II) complexes of several aromatic nitrogen heterocycles were developed.[178,179] The alcohol functionality of N-hydroxyethylethylenediaminetriacetate, which had been considered to be an innocent ligand was shown to accelerate ligand substitution reaction for $[Cr^{III}(hedta)]$.[180,181]

In collaboration with Professor Paul Dowd, the one electron reduction potentials of coenzyme B_{12} and alkyl cobalamins were measured. These results, along with literature molecular orbital treatments, suggest that the reduction potential varies with the energy of the lowest unfilled molecular orbital (the cobalt d_z^{2*} and the alkyl σ) and with Co-C distance.[182,183]

In 1987 development of complexes for antitumor use and for the control of free radical cell damage was begun. In collaboration with Thomas J. Lomis and Jerome F. Suida, the preparation of the dioxygen-activating metal head group analogue of the antitumor drug bleomycin, [Fe(HAPH)] (HAPH = N-[2-(imidazol-3-yl)ethyl-6-{[(2-(imidazol-3-yl)ethyl]amino}methyl]-2-pyridinecarboxamide) (Figure A.21) was reported. An axial imidazole in HAPH replaces the axial amine donor in bleomycin. A sulfur analogue which was also prepared $[Fe^{II}(SAPH)]$ (SAPH =2-pyridinecarboxamide,N-[2-(1H-imidazol-4-yl)ethyl]-6-[[[2-(methylthio)ethyl]amino]methyl]) (Figure A.22) did not cleave DNA.[184,185] $[Fe^{II}(HAPH)]$, however, even lacking the recognition tail of bleomycin, is approximately half as efficient as bleomycin at cleaving DNA and operates through the same ferryl pathway as bleomycin.[186] The $[Cu^{II}(HAPH)]$ complex was found to behave the same as $[Fe^{II}(HAPH)]$. [187] An X-ray crystal structure obtained for the Cu^{II} salt, $[Cu^{II}(HAPH)]ClO_4$ (Figure A.23) revealed that the imidazole moiety of HAPH binds in the axial position.[188] Much of the early imidazole and redox research laid the foundation for these bleomycin studies and for a review on O_2 activation by polyaminocarboxylates and imidazole based complexes.[189] A review was also prepared on the

use of Ru(II)-polyamniocarboxylate complexes for improved DNA probes for the American Chemical Society's Advances in Chemistry Series.[190]

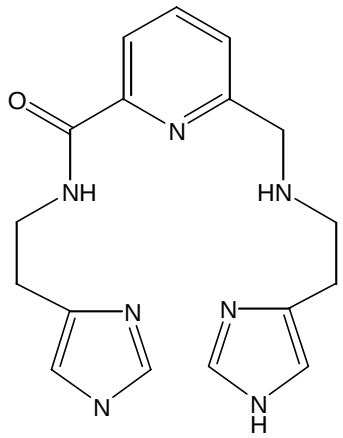

Figure A.21- HAPH Ligand

N-(2-(imidazol-3-yl)ethyl-6-(((2-(imidazol-3-yl)ethyl)amino)methyl)-2-pyridinecarboxamide
Reprinted from Inorganica Chimica Acta, 171 "The crystal structure of [Cu(HAPH)]ClO_4.1.6H_2O and the cleavage of DNA by analogs of the metal binding core of bleomycin" 139-149, Copyright Elsevier, 1990.

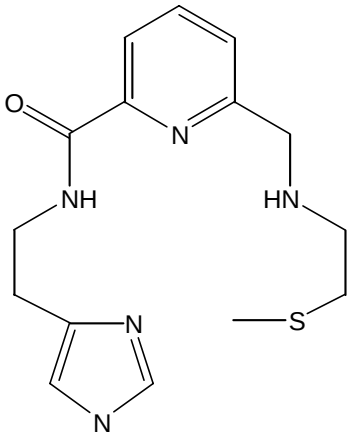

Figure A.22- SAPH Ligand

2-pyridinecarboxamide,N-[2-(1H-imidazol-4-yl)ethyl]-6-[[[2-(methylthio)ethyl]amino]methyl]
Reprinted from Inorganica Chimica Acta, 171 "The crystal structure of [Cu(HAPH)]ClO_4.1.6H_2O and the cleavage of DNA by analogs of the metal binding core of bleomycin" 139-149, Copyright Elsevier, 1990.

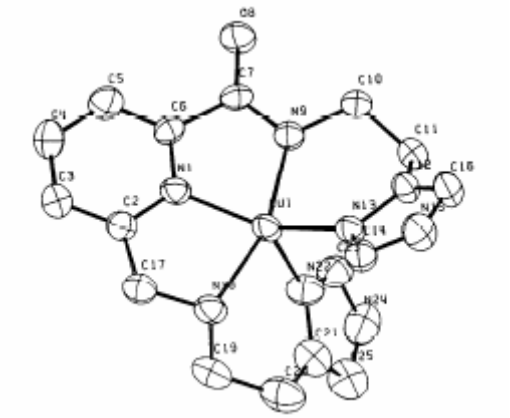

Figure A.23-ORTEP diagram of $[Cu(HAPH)]^+$

Reprinted from Inorganica Chimica Acta, 171 "The crystal structure of $[Cu(HAPH)]ClO_4.1.6H_2O$ and the cleavage of DNA by analogs of the metal binding core of bleomycin" 139-149, Copyright Elsevier, 1990.

In collaboration with Yisrael Isaccson, spin trapping was used to show that lactobionic acid, an active ingredient of transplant organ preservative, may prevent oxidation of free Fe^{II} and Fe^{III} by O_2 and H_2O_2 by forming $[Fe^{III}(lactobionate)]$.[191,192]

Early work on the illustrated the additivity effects of ligands when V^{IV} is used as a metalloenzyme in EPR studies.[193] Later the additivty effects were applied to show that the number of imidazole/histidyl units on a metalloenzyme may be estimated from comparison of the enzyme's EPR N-hyperfine structure to that of library spectra.[194]

Results from dearomatization of pyrimidine and DNA bases by Ru^{II} polyaminocarboxylates as described earlier were applied to designing Ru^{II} based antitumor agents that might attack different tumor lines that those attacked by the Pt^{II} agents in use.[128,131,133] A model for anchoring two Ru^{II} headgroups via pyrimidine base coordination was produced from dimethyluracil (Figure A.8). The methyl groups of dimethyl uracil prevent N-1 and N-3 in the same manner as N-3 coordination to pyrimidine bases is obstructed by hydrogen bonding to a purine base of DNA.[127] The ruthenium(II) polyaminocarboxylate, $[Ru^{II}(hedta)]^-$ was shown to

bind at the normal N-3 position of uridine (Figure A.15) and cytidine bases (Figure A.10) or to bind in an η^2 fashion through the C-5 C-6 olefinic site.[131] Further evidence for η^2-coordination was provided by the preparation and characterization of bis-$[Ru(hedta)(pym)_2]^-$ which exhibits one stereochemically-rigid η^2-bound pyrimidine and one fluxional N-bound pyrimidine. [195]

Platinum complexes with geometries other than the usual square planar geometry exhibited by most Pt^{II} complexes are of interest for their antitumor properties and for DNA labeling. The geometry variation may allow the complex to react more rapidly with or may select different base pairs along the DNA strand. Experiments with polyaminocarboxylates revealed their capacity to force Pt^{II} into 5-coorination. In particular the 2-pyridine-2-methylaminiediacetate ligand ($pida^{2-}$) was shown to react with K_2PtCl_4 to form a five-coordinate trigonal bipyramidal complex.[196] Formation of the five-coordinate $[Pt(uedda)Cl]^-$ and $[Pt(uedda)(H_2O)]$ upon reaction of K_2PtCl_4 with *N,N*-ethylenediaminediacetate (uedda) suggests that five coordinate Pt^{II} species may be more common with chelate ligands than has been realized. Similar observations were made for the reaction between nitrilotriacetic acid and K_2PtCl_4 Five coordindate Pt^{II} complexes are much like the well accepted stabilized five-coordinate intermediates that form during ligand substitution reactions.[197] A polyaminocarboxylate that can hold a potentially chelating ligand near the same site used during substitution it is likely to be more stable than the intermediate that forms during substitution.[198]

Hetero- and homo-binuclear complexes were also of interest. In 1979 the first $Fe^{II/III}$-imidazolato-$Cu^{I/II}$ bridged complexes which were models for complexes believed to be responsible for the magnetic coupling and electron transfer between heme iron and copper centers of cytochrome oxidase were prepared. The complexes $[(CH_3CN)(TIM)Fe(imep)Cu]^{3+}$ (TIM =2,3,9,10-tetramethyl-1,4,8,11-tetraazacyclotetradeca-1,3,8,10-tetraene; impeH = 2-[2-(4-

imidazolyl)ethyliminomethyl]-pyridine) and $[(CH_3CN)(TIM)Fe(bidH)Cu]^{3+}$ ($bidH_2$ = 2,3-bis(4-ethylimidazolyl)butanediimine) are shown in figures A.24 and A.25, respectively.[199]

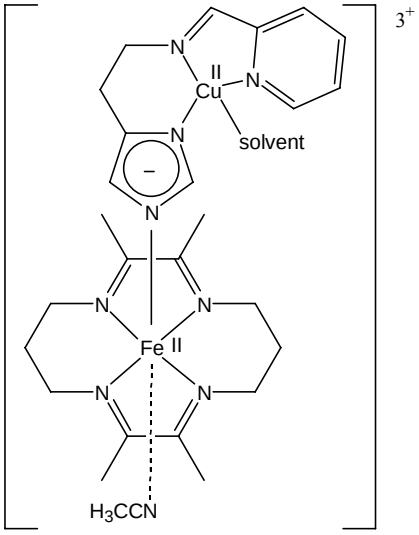

Figure A.24-$[(CH_3CN)(TIM)Fe(imep)Cu]^{3+}$

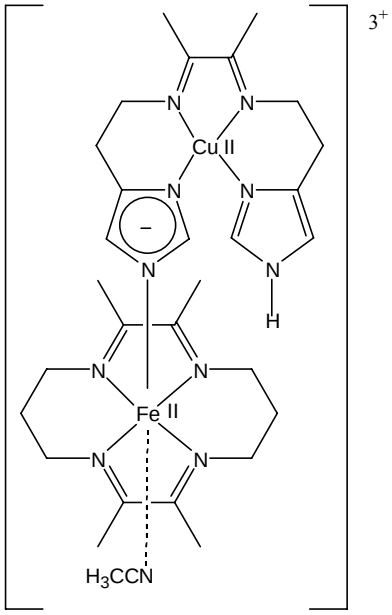

Figure A.25-$[(CH_3CN)(TIM)Fe(bidH)Cu]^{3+}$

Later the species responsible for magnetic coupling and electron transfer between heme iron and copper centers of cytochrome oxidase was shown to be a metal oxo chromophore. Models of the metal-oxo chromophore were prepared from the polyaminocarboxylate ligand, triethylenetetramininehexaacetate ($ttha^{6-}$).[166] Homo- and hetero-binuclear polyaminocarboxylates were also of interest for their potential to form Pd^{II} and Pt^{II} major groove-spanning chelates and act as cisplatin alternatives. The reactivity of a *cis*(R,S)-$[Pd(egta)]^{2-}$ ($egta^{4-}$ = glycine, *N*,*N*′-(1,2-ethanediyl*bis*(oxy-2,1-ethanediyl)*bis*[*N*-carboxymethyl])) complex with Cd^{II} was studied in an attempt to synthesize the heteronuclear Cd^{II}-Pd^{II} complex, [Cd(Pd)(egta)]. No [Cd(Pd)(egta)] was observed, although its existence as an intermediate was required to account for the observed $[Pd_2(egta)Cl_2]^{2-}$ product.[200] The Cd^{II}-Pd^{II} intermediate is bound by two pendant carboxylates. The 1:1 complex, *cis*(R,S)-$[Pd(egta)]^{2-}$ was shown to exhibit a temperature-dependent dynamic rearrangement which proceeds via five coordinate intermediates in aqueous solution.[201] Detailed ^{1}H, ^{13}C, and ^{15}N NMR studies were carried out on *cis*(R,S)-$[Pd(egta)]^{2-}$ and on $[Pd_2(egta)Cl_2]^{2-}$.[202]

The effect of Zn^{II} on the formation of 2,2′- and 2,3′-bipyridine complexes of $[Ru^{II}_2(ttha)]^{2-}$ ($ttha^{6-}$ = triethylenetetraminehexaacetate) was shown to be similar to that of Cd^{II} on *cis*(R,S)-$[Pd(egta)]^{2-}$ in that 2,2′-bipyridine displaces one in-plane glycinato donor per Ru^{II} which form a tight ion pair with $Zn(H_2O)_6^{2+}$. However, due to the strong Ru^{II}-N bonds as compared to the Pd^{II}-N bonds, the addition sequence for $[Ru_2(ttha)(H_2O)_2]^{2-}$/2,2′-bpy system is more complicated than that for the Cd^{II}/$[Pd(egta)]^{2-}$ reaction.[203]

Binuclear Pt^{II} complexes with metal binding sites connected by an organic tether form interstrand cross-links through N-7 attachments at GC sequences in DNA. Such cross-links may inhibit regulatory and repair proteins from reaching to the major groove of DNA. Displacement

of one chloride in $[Pt_2(hdta)Cl_2]^{2-}$ ($hdta^{4-}$ = 1,6-hexanediamine-*N*,*N*,*N*′,*N*′ -tetraacetate) by inosine to form $[Pt_2(hdta)Cl(ino)]^-$ occurs 3.4 times faster than DNA displacement of a chloride ion from cisplatin. The structures of $[Pt_2(hdta)Cl_2]^{2-}$ and inosine and the product, $[Pt_2(hdta)Cl(ino)]^-$ are shown in figures A.26, A.27 and A.28, respectively. Inosine, a purine base that lacks the 2 amino group of guanosine, is used as a representative purine base for reactions with Pt^{II} and Pd^{II} complexes because of its solubility.[204] In a later paper the crystal structure of $[MV][Pt_2(hdta)Cl_2]\bullet 4H_2O$ (MV =1,1′-dimethyl-4,4′-bipyridinium) was reported along with the formation the tetrasubstituted $[Pt_2(hdta)(Ino)_4]$. The Pd^{II} binuclear analogue of $[Pt_2(hdta)Cl_2]^{2-}$ and the heterobinuclear $[Pd^{II}(hdta)(H_2O)Pt^{II}Cl(hdta)]^-$ were later characterized by ^{13}C and ^{1}H NMR spectroscopy. Formation of $[Pd^{II}(hdta)(H_2O)Pt^{II}Cl(hdta)]^-$ suggests that other hybrids can be formed from $[Pd^{II}(hdta)]^{2-}$ and $[Pt^{II}(hdta)]^{2-}$. Only the formation of the mononuclear complex $[Pd^{II}(dhpta)]^{2-}$ ($dhpta^{4-}$ = 1,3-diamino-2-hydroxypropane-*N*,*N*,*N*′,*N*′-tertraacetate) was observed under conditions in which the $[Pt_2(hdta)Cl_2]^{2-}$ forms quickly. Formation of only the mononuclear $[Pd^{II}(dhpta)]^{2-}$ complex was attributed to the fact that there are only three linker units in $dhpta^{4-}$ as opposed to six linkers in $hdta^{4-}$.[205]

A mechanistic study of the substitution of inosine on $[Pd(mida)Cl]^-$, $[Pd(mida)(D_2O)_2]$, $[Pd(egta)(D_2O)_2]$ and of guanosine 5′-monophosphate (5′-GMP) on $[Pd_2(egta)(D_2O)_2]$ highlighted some of the differences between the chemistry of Pd^{II} and Pt^{II}.[206] N-3 and N-7 coordinated $[Ru^{II}(edta)(5'\text{-GMP})]^{4-}$ complexes were studied in collaboration with Debabrata Chatterjee. The N-3 site of 5′-GMP-H is in the minor groove when GMP is incorporated into DNA. Coordination at N-3 suggests that soft donors might preferentially seek N-3 rather than N-7 which projects into the major groove.[207]

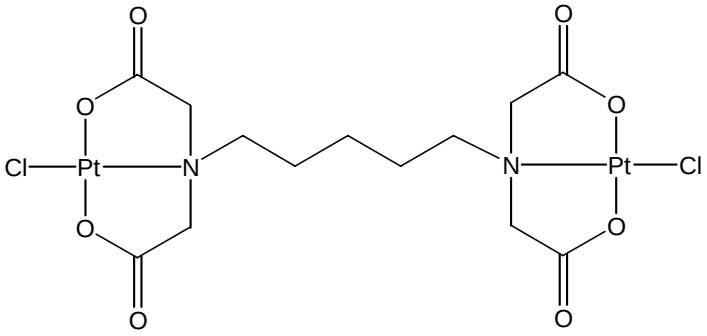

Figure A.26-$[Pt_2^{II}(hdta)Cl_2]^{2-}$

Reprinted with permission from Inorganica Chimca Acta, 271, Lin Fu-Tyan, Shepherd, Rex E. Substitution of inosine for chloride in $[Pt_2(hdta)Cl_2]^{2-}$ ($hdta^{4-}$ = 1,6-hexanediamine-N,N,N',N'-tetraacetate) 124-128, copyright Elsevier.

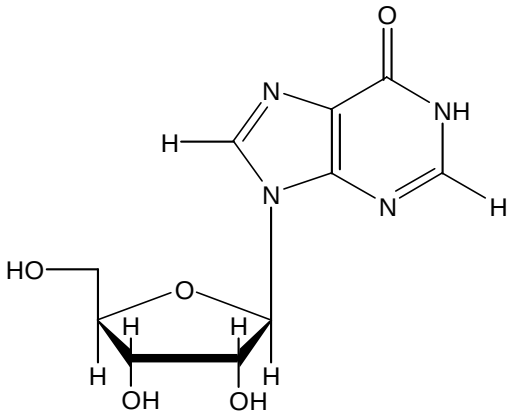

Figure A.27-Inosine

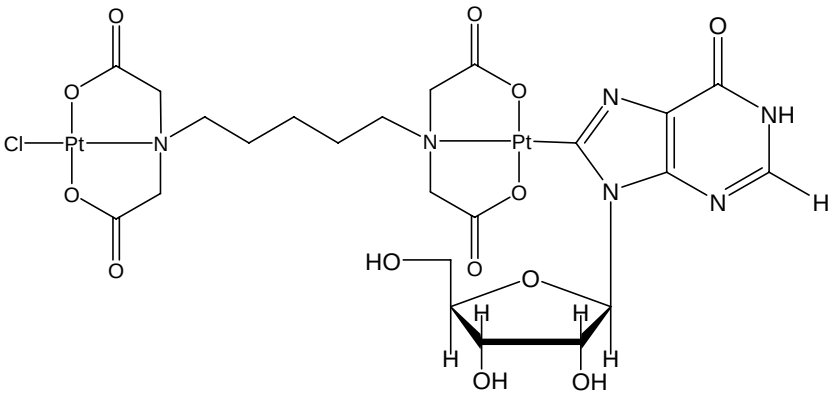

Figure A.28- $[Pt_2(hdta)Cl(ino)]^-$

The polyaminocarboxylate *N*,*N*′-bis-(pyridylmethyl)ethylenediamine-*N*,*N*′-diacetate ($edampda^{2-}$) ligand (Figure A.29) was used in the development of the nitric oxide scavenger $[Fe^{II}(edampda)(H_2O)]$. The $edampda^{2-}$ ligand is a derivative of $edta^{4-}$ in which two carboxylate groups have been replaced by pyridyl groups. The pyridyl groups increase the ligand field strength with respect to $edta^{4-}$. The stronger ligand field strength is evidenced by the spin state character of a series of polyaminocarboxylate complexes of $Fe^{II}NO$. $[Fe(edta)(NO)]^{2-}$ [208,209] the weakest field of the series exhibits S=3/2. The [Fe(edampda)(NO)] exhibits spin crossover behavior.[210] Finally, $[Fe(tpen)(NO)]^{2+}$ (tpen = *N*,*N*,*N*′,*N*′-tetrakis(2-pyridylmethyl)ethylenediamine), which has the strongest ligand field exhibits S = 1/2.[211] See Figure A.30 for the structure of tpen. The solution behavior of $[Cu^{II}(edampda)]$ and $[Zn^{II}(edampda)]$ was also investigated.[212]

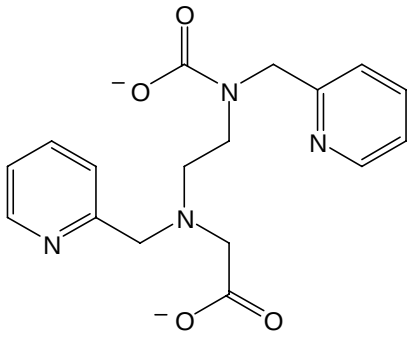

Figure A.29-*N*,*N*′-bis-(pyridylmethyl)ethylenediamine-*N*,*N*′-diacetate

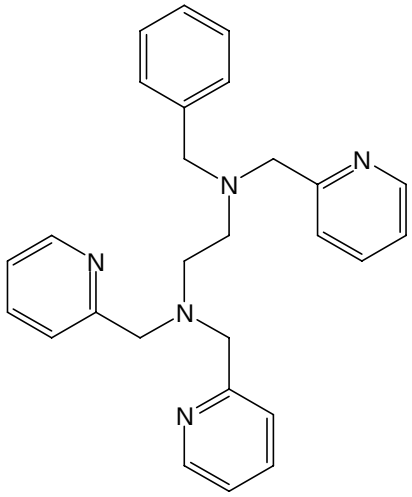

Figure A.30-*N*,*N*,*N′*,*N′*-tetrakis(2-pyridylmethyl)ethylenediamine

Two ligands related to edampda, 2,2′-dipyridyl amine (dpaH) shown in Figure A.31 and *N*,*N*,*N′*,*N′*-tetrakis(2-pyridyl)adipamide (tpada) shown in Figure A.32 were studied. At the time this work was published there were few reports of dpaH complexes of Pt^{II}, Pd^{II} and Ru^{II}. Some of the few that had been synthesized exhibited and antitumor activity comparable to cisplatin.[213,214] Pt^{II}, Pd^{II} and Ru^{II} complexes of the tpada ligand might serve as a crosslinker toward DNA. $[Ru^{II}(hedta)]^-$ complexes with dpaH and tpada allowed their π-acceptor ability to be determined as bpy > 1/2tpada > dpaH > dpa^-. Further studies with tpada as a multidentate chelate toward one metal center such as Cu^{II}, Ni^{II}, Fe^{II}, or Ru^{II} with and NO or CO ligand in an were in development as antitumor agents.[215]

Fe^{II} aminocarboxylate and pyridyl based complexes were also developed for use as NO scavengers. The ttha ligand ($ttha^{6-}$ = triethyenetetraminehexaacetate) forms the binuclear $[Ru_2^{III}(ttha)(H_2O)_2]$ complex which reacts readily with NO to form $[(Ru^{II}(NO^+))_2(ttha)]$. The asymmetric mononitrosyl derviative $[(Ru_2^{II}(NO^+)(bpy)(ttha)]^{2-}$ has potential to bind to DNA.[216]

While the complexes do bind NO their reactivity to oxygen limits their use as NO scavengers in blood. The TIM ligand (TIM = 2,3,9,20-tetrmethyl-1,4,8,11-tetraazacyclodeca-1,3,8,10-tetraene) is a water soluble unsaturated macrocycle similar to porphyrins. The reversible coordination of NO to $[Fe(TIM)(CH_3CN)_2]^{2+}$ was found to be similar to Fe^{II}porphyrin nitrosyls.[217]

The first reported set of NO^+, NO, and NO^- complexes for the same metal center in same oxidation state and a constant ligand environment was prepared from Ru^{II} and $hedta^{3-}$. The NO complex exists as cis- and trans-equatorial isomers which have ^{15}N NMR resonances at 609.4 and 607.4 ppm, respectively. That these singlet NO^- complexes absorb in the infrared at 1383 cm^{-1} suggests that there is some backbonding from Ru^{II}. Typically NO^- absorbs around 1650 cm^{-1}. The NO^+ complex which exists as the cis-equatorial species absorbs in the infrared at 1846 cm^{-1} and exhibits a resonance at 249.6 ppm in its ^{15}N NMR spectrum. The $NO^\bullet$ complex has an infrared absorbance at 1858 cm^{-1}. The lower stretching frequency for NO^+ than for $NO^\bullet$ indicates that there is more Ru^{II} to NO^+ than for $NO^\bullet$. A molecular orbital analysis was presented to rationalize the existence of singlet as well as triplet NO. Whether NO^- is singlet or triplet depends upon the energy of orbitals with respect to the energy of the d_{z^2} and $d_{x^2-y^2}$ orbitals. If the π^* NO orbitals are lower in energy than the metal d_{z^2} and $d_{x^2-y^2}$ orbitals as they are with Ru^{II} in this case, then singlet NO^- is favored. The lower charge of $[Ru(hedta)(NO^+)]$ compared to $[Ru(edta)(NO^+)]^-$ may allow more facile biological transport. Related mixed pyridyl, mixed carboxylate ligands were studied.[14]

Studies of binuclear complexes which have applications to electron transfer reactions as well as medicinal applications were continued. The mixed-valence Ru^{IV}-Fe^{II} complex

$[Ru^{IV}(edtaH)(NC)Fe^{II})(CN)_5]^{4-}$, analogous to Taube's $[Ru^{IV}(NH_3)_5(NC)Fe^{II})(CN)_5]$ complex, was prepared and characterized in collaboration with Debabrata Chatterjee.[218]

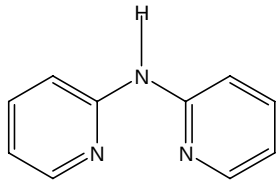

Figure A.31-2,2′-dipyridylamine (dpaH)

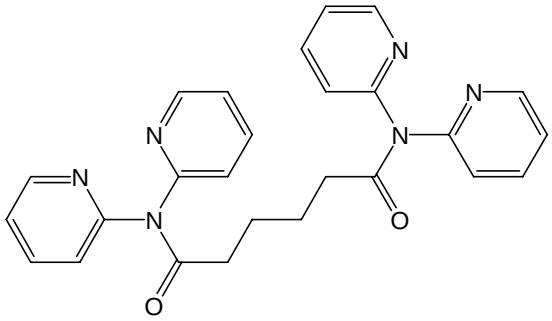

Figure A.32-*N*,*N*,*N′*,*N′*tetrakis(2-pyridyl)adipamide (tpada)

BIBLIOGRAPHY

(1) Schreiner, A. F.; Lin, S. W.; Hauser, P. J.; Hopcus, E. A.; Hamm, D. J.; Gunter, J. D. *Inorg. Chem.* **1972**, *11*, 880-888.

(2) Bobkova, E. Y.; Borkovskii, N. B.; Svetlov, A. A.; Novitskii, G. G. *Russ. J. Inorg. Chem.* **1994**, *39*, 796-798.

(3) Pipes, D. W. *Inorg. Chem.* **1984**, *23*, 2466-2472.

(4) Ford, P. C. *Coord. Chem. Rev.* **1970**, *5*, 75-99.

(5) Enemark, J. H.; Feltham, R. D. *Coord. Chem. Rev.* **1974**, *13*, 339-406.

(6) Bottomley, F. In *Reactions of Coordinated Ligands*; Braterman, P. S., Ed.; Plenum Press: New York, 1986; Vol. 2, p 115.

(7) Silva, W. C.; Castellano, E. E.; Franco, D. W. *Polyhedron* **2004**, *23*, 1063-1067.

(8) Bremard, C.; Nowogrocki, G.; Sueur, S. *J. Am. Chem. Soc.* **1979**, *79*, 1549-1555.

(9) Huheey, J. E. *Inorganic Chemistry Principles of Structure and Reactivity*; Second ed.; Harper & Row: New York, 1978.

(10) Ford, P. C.; Bourassa, J.; Miranda, K.; Lee, B.; Lorkovic, I.; Boggs, S.; Kudo, S.; Laverman, L. *Coord. Chem. Rev.* **1998**, *171*, 185-202.

(11) Stochel, G. y.; Wanat, A.; Kuliœ, E.; Stasicka, Z. *Coord. Chem. Rev.* **1998**, 203-220.

(12) Ackroyd, R.; Kelty, C.; Brown, N.; Reed, M. *Photochem. Photobiol.* **2001**, *74*, 656-669.

(13) Shepherd, R. E. In *35th Central Regional Meeting of the American Chemical Society*; American Chemical Society: Pittsburgh, PA, 2003.

(14) Chen, Y.; Lin, F. T.; Shepherd, R. E. *Inorg. Chem.* **1999**, *38*, 973-983.

(15) Chen, Y.; Shepherd, R. E. *Inorg. Chim. Acta* **2003**, *343*, 281-287.

(16) Shepherd, R. E.; Stringfield, T. W.; Somayajula, K. V.; Muddiman, D. C.; Flora, J. W. *Inorg. Chim. Acta* **2003**, *343*, 317-328.

(17) Lujan, S.; Slocik, J. M.; Chatterjee, D.; Mitra, A.; Shepherd, R. E. *Inorg. Chim. Acta* **2004**, *357*, 785-796.

(18) Shepherd, R. E.; Slocik, J. M.; Kortes, R. A. *Met. Based Drugs* **2000**, *7*, 67-75.

(19) Slocik, J. M.; Somayajula, K. V.; Shepherd, R. E. *Inorg. Chim. Acta* **2001**, *320*, 148-158.

(20) Shepherd, R. E.; Slocik, J. M.; Ward, M. S.; Somayajula, K. V. *Trans. Met. Chem.* **2001**, *26*, 351-364.

(21) Slocik, J. M. S., Rex E. *Inorg. Chim. Acta* **2000**, *311*, 80-94.

(22) Shepherd, R. E.; Slocik, J. M.; Ward, M. S. *Inorg. Chim. Acta* **2001**, *317*, 290-303.

(23) Ward, M. S.; Lin, F.-T.; Shepherd, R. E. *Inorg. Chim. Acta* **2003**, *343*, 231-243.

(24) Shepherd, R. E.; Slocik, J. M.; Stringfield, T. W.; Somayajula, K. V.; Amoscato, A. A. *Inorg. Chim. Acta* **2004**, *357*, 965-979.

(25) Fortney, C. F.; Shepherd, R. E. *Inorg. Chem. Commun.* **2004**, *7*, 1065-1070.

(26) Patra, A. K.; Rose, M. J.; Murphy, K. A.; Olmstead, M. M.; Mascharak, P. K. *Inorg. Chem.* **2004**, *43*, 4487-4495.

(27) Shepherd, R. E., Personal Communication.

(28) Comba, P.; Goll, W.; Nuber, B.; Varnagy, K. *Eur. J. Inorg. Chem.* **1998**, 2041-2049.

(29) Gajda, T.; Henry, B.; Delpuech, J.; Aubrey, A. *Inorg. Chem.* **1996**, *35*, 586.

(30) Hay, R. W.; Hassan, M. M.; You-Quan, J. *J. Inorg. Biochem.* **1993**, *52*, 17.

(31) Pickart, L.; Freedman, J. H.; Loker, W. J.; Peisach, C. J.; Perkins, C. M.; Stenkamp, R. E.; Weistein, B. *Nature* **1980**, *288*, 715.

(32) Kasselflouri, S.; Laussac, J. P.; Hadjiliadis, N. *Inorg. Chim. Acta* **1989**, *166*, 239.

(33) Camerman, N.; Camerman, A.; Sarkar, B. *Can. J. Chem.* **1976**, *54*, 1309.

(34) Lang, D. R.; Davis, J. A.; Lopes, L. G. F.; Ferro, A. A.; Vasconcellos, L. C. G.; Franco, D. W.; Tfouni, E.; Wieraszko, A.; Clarke, M. J. *Inorg. Chem.* **2000**, *39*, 2294-2300.

(35) Tfouni, E.; Krieger, M.; McGarvey, B. R.; Franco, D. W. *Coord. Chem. Rev.* **2003**, *236*, 57-69.

(36) Ignarro, L. J. *Nitric Oxide*; Academic Press: New York, 2000.

(37) Clarke, M. J.; Zhu, F.; Frasca, D. *J. Am. Chem. Soc.* **1999**, *99*, 2511-2533.

(38) Clarke, M. J. In *Platinum, Gold and Other Chemotherapeutic Agents*; Lippard, S. J., Ed.; ACS: Washington, D. C., 1983, p 335.

(39) Vilaplana, R. A.; Gonzalez-Vilchez, F.; Gutierrez-Puebla, E.; Ruiz-Valero, C. *Inorg. Chim. Acta* **1994**, *224*, 15-18.

(40) Peti, W.; Pieper, T.; Sommer, M.; Keppler, B. K.; Geister, G. *Eur. J. Inorg. Chem.* **1999**, *9*, 1555.

(41) Sava, G.; Pacor, S.; Bregant, F.; Ceschia, A. *Anticancer Res.* **1991**, *11*, 1103.

(42) Keppler, B. K.; Rupp, W.; Juhl, U. M.; Endres, H.; Niebel, R.; Balzer, W. *Inorg. Chem.* **1987**, *26*, 4366.

(43) Chapman, R. L.; Stephens, F. S.; Vagg, R. S. *Inorg. Chim. Acta* **1981**, *52*, 161-168.

(44) Freeman, H. C. *Adv. Protein Chem.* **1967**, *22*, 257.

(45) Fabbrizzi, L.; Kaden, T. A.; Perotti, A.; Seghi, B.; Siegfried, L. *Inorg. Chem.* **1986**, *25*, 321-327.

(46) Upadhyay, M. J.; Bhattacharya, P. K.; Ganeshpure, P. A.; Satish, S. *J. Mol. Catal.* **1994**, *88*, 287-294.

(47) Collins, T. J.; Powell, R. D.; Slebodnick, C.; Uffelman, E. S. *J. Am. Chem. Soc.* **1990**, *112*, 899.

(48) Margerum, D. W. *Pure Appl. Chem.* **1983**, *55*, 23.

(49) Coe, B.; McDonald, C. I.; Couchman, S. M.; John, J. C.; Rees, L. H.; Coles, S. J.; Gelbrich, T.; Hursthouse, M. B. *Polyhedron* **2000**, *19*, 1193-1203.

(50) Tomizawa, H.; Miki, E.; Mizumachi, K.; Ishimori, T. *Bull. Chem. Soc., Jpn.* **1994**, *67*, 1816-1824.

(51) Shepherd, R. E. In *Metal-Medicine CourseMetal-Medicine Course*, 2003.

(52) Marcondes, F. G.; Ferro, A. A.; Souza-Torsoni, A.; Sumitani, M.; Clarke, M. J.; Franco, D. W.; Tfouni, E.; Krieger, M. *Nitric Oxide* **2000**, *4*, 181.

(53) Franco, D. W.; Tfouni, E.; Krieger, M.; Toledo, J. C.; Barros, B. *Nitric Oxide* **2000**, *4*, 254.

(54) Batista, A. A.; Pereira, C.; Queiroz, S. L.; de Oliveira, L. A. A.; de Almeida Santos, R. H.; do P. Gambardella, M. T. *Polyhedron* **1997**, *16*, 927-931.

(55) Tomizawa, H.; Miki, E.; Mizaumachi, K.; Ishimori, T. *Bull. Chem. Soc., Jpn.* **1994**, *67*, 1809-1815.

(56) Enemark, J. H.; Fetham, R. D.; Huie, B. T.; Johnson, P. L.; Swedo, K. B. *J. Am. Chem. Soc.* **1977**, *99*, 3285-3292.

(57) Feltham, R. D.; Enemark, J. H. In *Topics in Inorganic and Organometallic Stereochemistry*; Geoffroy, G., Ed.; John Wiley & Sons: New York, 1981; Vol. 12, pp 155-215.

(58) Haller, K. J.; Johnson, P. L.; Feltham, R. D.; Enemark, J. H.; Ferraro, J. R.; Basile, L. J. *Inorg. Chim. Acta* **1979**, *33*, 119-130.

(59) Westcott, B. L.; Enemark, J. H. In *Inorganic Electronic Spectroscopy*; Solomon, E. I., Lever, A. B. P., Eds.; John Wiley & Sons, Inc.: New York, 1999; Vol. II, pp 403-450.

(60) Raynor *Inorganica Chimica Acta* **1972**, *6*, 347-348.

(61) Sidgwick, N. V.; Bailey, R. W. *Proc. Roy. Soc. London* **1934**, *A144*, 521-537.

(62) Eisenberg, R. *Acc. Chem. Res.* **1975**, *8*, 26-34.

(63) Hodgson, D. J.; Payne, N. C.; McGinnety, J. A.; Pearson, R. G.; Ibers, J. A. *J. Am. Chem. Soc.* **1968**, *90*, 4486-4488.

(64) Hodgson, D. J.; Ibers, J. A. *Inorg. Chem.* **1968**, *7*, 2345-2352.

(65) Shepherd, R. E. **2002**.

(66) Fortney, C. F.; Geib, S. J.; Lin, F.-T.; Shepherd, R. E. *Inorg. Chim. Acta* **2005**, *358*, 2921-2932.

(67) Fletcher, J. M.; Jenkins, I. L.; Lever, F. M.; Martin, F. S.; Powell, A. R.; Todd, R. *J. Inorg. Nucl. Chem.* **1955**, *1*, 378-401.

(68) Barnes, D. J.; Chapman, R. L.; Vagg, R. S.; Watton, E. C. *J. Chem. Eng. Data* **1978**, *23*, 349-350.

(69) Chapman, R. L.; Vagg, R. S. *Inorg. Chim. Acta* **1979**, *33*, 227-234.

(70) Lin, J.; Zhang, J.-Y.; Xu, Y.; Ke, X.-K.; Guo, Z. *Acta Cryst.* **2001**, *C57*, 192-193.

(71) Bottomley, F. *J. Chem. Soc., Dalton Trans.* **1974**, *15*, 1600-1605.

(72) Tomizawa, H.; Harada, K.; Miki, E.; Mizaumachi, K.; Ishimori, T.; Urushiyama, A.; Nakahara, M. *Bull. Chem. Soc., Jpn.* **1993**, *66*, 1658-1663.

(73) Coleman, P. B. *Practical Sampling Techniques for Infrared Analysis*; CRC Press: Boca Raton, 1993.

(74) HMBC Spectrum can be seen in the supplementary information

(75) Jones, M. *Organic Chemistry*; W. W. Norton & Compay: New York, 2000.

(76) Gupta, R. R.; Kumar, M.; Gupta, V. *Heterocyclic Chemistry*; Springer-Verlag: Heidelberg, 1998; Vol. 1.

(77) Bottomley, F. *Coord. Chem. Rev.* **1978**, *26*, 7-32.

(78) Bordini, J.; Hughes, D.; da Motta Neto, J. D.; da Cunha, C. J. *Inorg. Chem.* **2002**, *41*, 5410-5416.

(79) Richter-Addo, G. B.; Legzdins, P. *Metal Nitrosyls*; Oxford University Press: New York, 1992.

(80) Sauaia, M. G.; de Lima, R. G.; Tedesco, A. C.; da Silva, R. S. *J. Am. Chem. Soc.* **2003**, *125*, 14718-14719.

(81) Shepherd, R. E.; Taube, H. *Inorg. Chem.* **1973**, *12*, 1392-1401.

(82) Shepherd, R. E.; Taube, H.; Sundberg, R. J. *J. Am. Chem. Soc.* **1972**, *94*, 6558-6559.

(83) Cotton, F. A.; Wilkinson, G. *Advanced Inorganic Chemistry*; Fifth ed.; John Wiley & Sons: New York, 1988.

(84) Clarke, M. J.; Taube, H. *J. Am. Chem. Soc.* **1974**, *97*, 1397-1403.

(85) Sundberg, R. J.; Bryan, R. F.; Taylor, I. F.; Taube, H. *J. Am. Chem. Soc.* **1974**, *98*, 381-392.

(86) Tweedle, M. F.; Taube, H. *Inorg. Chem.* **1982**, *21*, 3361-3371.

(87) Weigl, K.; Kohler, K.; Dechert, S.; Meyer, F. *Organometallics* **2005**, *24*, 4049-4056.

(88) Sini, G.; Eisenstein, O.; Crabtree, R. *Inorg. Chem.* **2002**, *41*, 602-604.

(89) Thayer, A. *Chem. Eng. News* **2006**, 26.

(90) Sabo, E. M.; Shepherd, R. E.; Rau, M. S.; Elliot, M. G. *Inorg. Chem.* **1987**, *26*, 2897-2907.

(91) Shepherd, R. E. *J. Am. Chem. Soc.* **1976**, *98*, 3329-3335.

(92) Johnson, C. R.; Shepherd, R. E.; Marr, B.; O'Donnell, S.; Dressick, W. *J. Am. Chem. Soc.* **1980**, *102*, 6227-6235.

(93) Johnson, C. R.; Shepherd, R. E. *Synth. React. Inorg. Met.-Org. Chem.* **1984**, *14*, 339-353.

(94) Hoq, M. F.; Shepherd, R. E. *Inorg. Chem.* **1984**, *23*, 1851-1858.

(95) Winter, J. A.; Caruso, D.; Shepherd, R. E. *Inorg. Chem.* **1988**, *27*, 1086-1088.

(96) Elliot, M. G.; Shepherd, R. E. *Trans. Met. Chem.* **1989**, *14*, 251-257.

(97) Elliot, M. G.; Shepherd, R. E. *Inorg. Chem.* **1987**, *26*, 2067-2073.

(98) Johnson, C. R.; Henderson, W. W.; Shepherd, R. E. *Inorg. Chem.* **1984**, *23*, 2754-2763.

(99) Warner, L. W.; Hoq, M. F.; Myser, T. K.; Henderson, W. W.; Shepherd, R. E. *Inorg. Chem.* **1986**, *25*, 1911-1914.

(100) Shepherd, R. E.; Hoq, M. F.; Hoblack, N.; Johnson, C. R. *Inorg. Chem.* **1984**, *23*, 3249-3252.

(101) Hoq, M. F.; Johnson, C. R.; Paden, S.; Shepherd, R. E. *Inorg. Chem.* **1983**, *22*, 2693-2700.

(102) Henderson, W. W.; Shepherd, R. E.; Abola, J. *Inorg. Chem.* **1986**, *25*, 3157-3163.

(103) Porath, J.; Carlson, I.; Olsson, G. *Nature* **1975**, *258*, 591-591.

(104) Hemdan, E. S.; Zhoa, Y. J.; Sulkowski, E.; Porath, J. *Proc. Natl. Acad. Sci. USA* **1989**, *86*, 1811.

(105) Shepherd, R. E.; Chen, Y.; Pasquinelli, R. S.; Ataai, M. M.; Koepsel, R. R.; Stringfield, T. W. *Inorg. Biochem.* **1999**, *76*, 211-220.

(106) Chen, Y.; Pasquinelli, R. S.; Attai, M. M.; Koepsel, R. R.; Kortes, R. A.; Shepherd, R. E. *Inorg. Chem.* **2000**, *39*, 1180-1186.

(107) Pasquinelli, R. S.; Shepherd, R. E.; Koepsel, R. R.; Zhao, A.; Ataai, M. M. *Biotechnol. Prog.* **2000**, *16*, 86-91.

(108) Ward, M. S.; Shepherd, R. E. *Inorganica Chimica Acta* **2000**, *311*, 57-68.

(109) Shepherd, R. E. In *Comprehensive Coordination Chemistry II*; Lever, A. B. P., Meyer, T. J., Eds.; Pergamon Press: New York, 2003, pp 567-577.

(110) Shepherd, R. E. *Coord. Chem. Rev.* **2003**, *247*, 147-184.

(111) Johnson, C. R.; Shepherd, R. E. *Inorg. Chem.* **1983**, *22*, 3506-3513.

(112) Jones, C. M.; R., J. C.; Asher, S. A.; Shepherd, R. E. *J. Am. Chem. Soc.* **1985**, *107*, 3772-3780.

(113) Siddiqui, S.; Shepherd, R. E. *Inorg. Chem.* **1983**, *22*, 3726-3733.

(114) Fleming, G. D.; Shepherd, R. E. *Spectrochim. Acta* **1987**, *43A*, 1141-1146.

(115) Díaz, G.; Bustos, C.; Shepherd, R. E. *Inorg. Chim. Acta* **1987**, *133*, 23-25.

(116) Pawlik, M.; Hoq, M. F.; Shepherd, R. E. *J. Chem. Soc., Chem. Commun.* **1983**, 1467-1468.

(117) Malin, J. M.; Shepherd, R. E. *J. Inorg. Nucl. Chem.* **1972**, *34*, 3203-3207.

(118) Ernhoffer, R. E.; Shepherd, R. E. *J. Chem. Soc., Chem. Commun.* **1978**, 859-861.

(119) Shepherd, R. E.; Proctor, A.; Henderson, W. W.; Myser, T. K. *Inorg. Chem.* **1987**, *26*, 2440-2444.

(120) Zhang, S.; Shepherd, R. E. *Trans. Met. Chem.* **1992**, *17*, 199-203.

(121) Shepherd, R. E.; Chen, Y.; Ernhoffer, R. E. *Trans. Met. Chem.* **1998**, *23*, 375-385.

(122) Shepherd, R. E.; Stringfield, T. W. *Inorg. Chim. Acta* **1999**, *292*, 225-230.

(123) Elliot, M. G.; Shepherd, R. E. *Inorg. Chem.* **1988**, *27*, 3332-3337.

(124) Grubbs, R. H.; McGrath, D. V. *J. Am. Chem. Soc.* **1991**, *113*, 3611-3613.

(125) Henderson, W. W.; Bancroft, B. T.; Shepherd, R. E.; Fackler, J. P. J. *Organometallics* **1986**, *5*, 506-510.

(126) Elliot, M. G.; Zhang, S.; Shepherd, R. E. *Inorg. Chem.* **1989**, *28*, 3036-3043.

(127) Zhang, S.; Shepherd, R. E. *Inorg. Chim. Acta* **1989**, *163*, 237-243.

(128) Zhang, S. H., Lori A.; Shepherd, Rex E. *Inorg. Chem.* **1990**, *29*, 1012-1022.

(129) Shepherd, R. E. Z., Songsheng; Lin, Fu Tyan; Kortes, Richard A. *Inorg. Chem.* **1992**, *31*, 1457-1462.

(130) Shepherd, R. E.; Zhang, S. *Trans. Met. Chem.* **1994**, *19*, 146-150.

(131) Chen, Y.; Lin, F.-T.; Shepherd, R. E. *Inorg. Chem.* **1997**, *36*, 818-826.

(132) Chen, Y.; Shepherd, R. E. *Inorg. Chim. Acta* **1998**, *279*, 85-94.

(133) Shepherd, R. E. Z., Songsheng; Lin, Fu Tyan; Kortes, Richard A. *Inorg. Chim. Acta* **1992**, *191*, 271-278.

(134) Zhang, S.; Chen, Y.; Shepherd, R. E. *Inorg. Chim. Acta* **1995**, *230*, 77-84.

(135) Shepherd, R. E.; Chen, Y. *Inorg. Chem.* **1998**, *37*, 1249-1256.

(136) Chen, Y.; Shepherd, R. E. *Inorg. Chim. Acta* **1998**, *268*, 279-285.

(137) Shepherd, R. E.; Zhang, S.; Chen, Y. *Inorg. Chim. Acta* **1996**, *253*, 65-70.

(138) Shepherd, R. E.; Chen, Y.; Johnson, C. R. *Inorg. Chim. Acta* **1998**, *267*, 11-18.

(139) Shepherd, R. E.; Stringfield, T. W.; Chen, Y. *Inorg. Chim. Acta* **1999**, *285*, 157-169.

(140) Shepherd, R. E.; Stringfield, T. W. *Trans. Met. Chem.* **1999**, *24*, 571-576.

(141) Stringfield, T. W. S., Rex E. *Inorg. Chim. Acta* **2001**, *325*, 51-57.

(142) Darensbourg, D. J.; Frost, B. J.; Larkins, J. H. *Inorg. Chem.* **2000**, *40*, 1993.

(143) Undheim, U.; Benneche, T. In *Comprehensive Heterocyclic Chemistry II*; Pergamon: New York, 1996.

(144) Chen, D. L.; McLaughlin, L. W. *J. Org. Chem.* **2000**, *65*, 7468.

(145) Jakupca, M. R.; Dutta, P. K. *J. Org. Chem.* **1992**, *65*, 953.

(146) Castle, N. A.; Fadus, S. *Pharmacol.* **1994**, *45*, 1242.

(147) Shepherd, R. E.; Strignfield, T. W. *Inorg. Chem. Commun.* **2001**, *4*, 760-765.

(148) Major, D. T.; Avital, A.; Fischer, B. *J. Org. Chem.* **2002**, *67*, 790.

(149) Shepherd, R. E.; Strignfield, T. W. *Inorg. Chim. Acta* **2003**, *343*, 156-168.

(150) Shepherd, R. E.; Chen, Y. *Inorg. Chim. Acta* **1998**, *277*, 46-54.

(151) Chen, Y.; Shepherd, R. E. *Inorg. Chim. Acta* **1999**, *293*, 123-126.

(152) Kristine, F. J.; Gard, D. R.; Shepherd, R. E. *J. Chem. Soc., Chem. Commun.* **1976**, 994-995.

(153) Nelson, J.; Shepherd, R. E. *Inorg. Chem.* **1978**, *17*, 1030-1034.

(154) Kristine, F. J.; Shepherd, R. E. *J. Am. Chem. Soc.* **1978**, *100*, 4398-4404.

(155) Kristine, F. J.; Shepherd, R. E. *Inorg. Chem.* **1978**, *17*, 3145-3152.

(156) Kristine, F. J.; Shepherd, R. E. *Inorg. Chem.* **1981**, *20*, 215-222.

(157) Myser, T. K.; Shepherd, R. E. *Inorg. Chem.* **1987**, *26*, 1544-1555.

(158) Shepherd, R. E.; Myser, T. K.; Elliot, M. G. *Inorg. Chem.* **1988**, *27*, 916-923.

(159) Johnson, C. R.; Myser, T. K.; Shepherd, R. E. *Inorg. Chem.* **1988**, *27*, 1089-1095.

(160) Zhang, S.; Shepherd, R. E. *Inorg. Chem.* **1988**, *27*, 4712-4719.

(161) Johnson, C. R.; Shepherd, R. E. In *Proceedings of Inorganic Mechanisms Conference*: Wayne State University, 1981.

(162) Siddiqui, S.; Henderson, W. W.; Shepherd, R. E. *Inorg. Chem.* **1987**, *26*, 3101-3107.

(163) Shepherd, R. E.; Henderson, W. W. *Inorg. Chem.* **1985**, *24*, 2398-2404.

(164) Zhang, S.; Shepherd, R. E. *Trans. Met. Chem.* **1992**, *17*, 97-103.

(165) Zhang, S.; Shepherd, R. E. *Inorg. Chem.* **1994**, *33*, 5262-5270.

(166) Zhang, S.; Dahl, W. R.; Shepherd, R. E. *Trans. Met. Chem.* **1995**, *20*, 280-287.

(167) Kristine, F. J.; Johnson, C. R.; O'Donnell, S.; Shepherd, R. E. *Inorg. Chem.* **1980**, *19*, 2280-2284.

(168) Bowers, M. L.; Kovacs, D.; Shepherd, R. E. *J. Am. Chem. Soc.* **1977**, *99*, 6555-6561.

(169) Shepherd, R. E.; Hatfield, W. E.; Ghosh, D.; Stout, D. C.; Kristine, F. J.; Ruble, J. R. *J. Am. Chem. Soc.* **1981**, 5511-5517.

(170) Kristine, F. J.; Shepherd, R. E. *J. Am. Chem. Soc.* **1977**, *99*, 6562-6570.

(171) Zhang, S.; Snyder, K. S.; Shepherd, R. E. *Inorg. Chim. Acta* **1992**, *201*, 223-238.

(172) Zhang, S.; Shepherd, R. E. *Inorg. Chim. Acta* **1992**, *193*, 217-227.

(173) Zhang, S.; Holl, L. A.; Shepherd, R. E. *Trans. Met. Chem.* **1992**, *17*, 390-396.

(174) Shepherd, R. E. *Inorg. Chim. Acta* **1993**, *209*, 201-206.

(175) Kristine, F. J.; Shepherd, R. E. *J. Chem. Soc., Chem. Commun.* **1980**, 132-133.

(176) Kristine, F. J.; Shepherd, R. E.; Siddiqui, S. *Inorg. Chem.* **1981**, *20*, 2571-2579.

(177) Fackler, J. P. J.; Kristine, F. J.; Mazany, A. M.; Moyer, T. J.; Shepherd, R. E. *Inorg. Chem.* **1985**, *24*, 1857-1860.

(178) Johnson, C. R.; Shepherd, R. E. *Inorg. Chem.* **1983**, *22*, 2439-2444.

(179) Johnson, C. R.; Shepherd, R. E. *Inorg. Chem.* **1983**, *22*, 1117-1123.

(180) Guardalabene, J.; Gulnac, S.; Keder, N.; Shepherd, R. E. *Inorg. Chem.* **1979**, *18*, 22-27.

(181) Hatfield, W. E.; MacDougall, J. J.; Shepherd, R. E. *Inorg. Chem.* **1981**, *20*, 4216-4219.

(182) Shepherd, R. E.; Zhang, S.; Dowd, P.; Choi, G.; Wilk, B.; Choi, S. C. *Inorg. Chim. Acta* **1990**, *174*, 249-256.

(183) Dowd, P.; Choi, G.; Wilk, B.; Zhang, S.; Choi, S. C. In *Chemical Aspects of Enzyme Biotechnology: Fundamentals*; Scott, A. I., Rauschel, F. M., Baldwin, T. O., Eds.; Plenum Press: New York, 1990.

(184) Lomis, T. J.; Siuda, J. F.; Shepherd, R. E. *J. Chem. Soc., Chem. Commun.* **1988**, 290-292.

(185) Lomis, T. J.; Martin, J.; McCloskey, B.; Zhang, S.; Siddiqui, S.; Shepherd, R. E.; Studa, J. F. *Inorg. Chim. Acta* **1989**, *157*, 99-116.

(186) Shepherd, R. E.; Lomis, T. J.; Koepsel, R. R. *J. Chem. Soc., Chem. Commun.* **1992**, 222-224.

(187) Lomis, T. J.; Elliot, M. G.; Siddiqui, S.; Moyer, M.; Koepsel, R. R.; Shepherd, R. E. *Inorg. Chem.* **1989**, *28*, 2369-2377.

(188) Shepherd, R. E.; Lomis, T. J.; Koepsel, R. R.; Hegde, R.; Mistry, J. S. *Inorg. Chim. Acta* **1990**, *171*, 139-149.

(189) Shepherd, R. E. *Trends Inorg.* **1993**, *2*, 503-530.

(190) Shepherd, R. E.; Chen, Y.; Zhang, S.; Lin, F.-T.; Kortes, R. A. A. i. C. S., 253(Electron Transfer Reactions), 367-397. In *Advances in Chemistry Series*; American Chemical Society: Washington, D. C., 1997; Vol. 253, pp 367-397.

(191) Shepherd, R. E.; Isaacson, Y.; Chensny, L.; Zhang, S.; Kortes, R. A.; John, K. *J. Inorg. Biochem.* **1993**, *49*, 23-48.

(192) Isaacson, Y.; Salem, O.; Shepherd, R. E.; Van Thiel, D. H. *Life Science* **1989**, *45*, 2372.

(193) Johnson, C. R.; Shepherd, R. E. *Bioinorg. Chem.* **1978**, *8*, 115-132.

(194) Siddiqui, S.; Shepherd, R. E. *Inorg. Chem.* **1986**, *25*, 3869-3876.

(195) Shepherd, R. E.; Chen, Y.; Lin, F.-T. *Inorg. Chim. Acta* **1998**, *268*, 287-295.

(196) Winter, J. A.; Lin, F. T.; Shepherd, R. E. *Inorg. Chim. Acta* **1989**, *155*, 155-159.

(197) Kortes, R. A.; Lin, F. T.; Shepherd, R. E.; Maricondi, C. *Inorg. Chim. Acta* **1996**, *245*, 149-156.

(198) Shepherd, R. E.; Zhang, S.; Kortes, R. A.; Lin, F. T.; Maricondi, C. *Inorg. Chim. Acta* **1996**, *244*, 15-23.

(199) Kovacs, D.; Shepherd, R. E. *J. Inorg. Biochem.* **1979**, *10*, 67-88.

(200) Kortes, R. A.; Shepherd, R. E. *Trans. Met. Chem.* **1997**, *22*, 68-73.

(201) Lin, F. T.; Kortes, R. A.; Shepherd, R. E. *Trans. Met. Chem.* **1997**, *22*, 243-247.

(202) Shepherd, R. E.; Kortes, R. A.; Lin, F. T.; Ward, M. S. *Trans. Met. Chem.* **2000**, *25*, 251-259.

(203) Chen, Y.; Zhang, S.; Shepherd, R. E. *Trans. Met. Chem.* **1997**, *22*, 338-346.

(204) Lin, F. T.; Shepherd, R. E. *Inorg. Chim. Acta* **1998**, *271*, 124-128.

(205) Shepherd, R. E.; Kortes, R. A.; Stringfield, T. W.; Ward, M. S.; Lin, F. T.; Shepherd, R. E. *Inorg. Chim. Acta* **2000**, *304*, 60-71.

(206) Stringfield, T. W. S., Rex E. *Inorg. Chim. Acta* **2000**, *309*, 28-44.

(207) Chatterjee, D.; Ward, M. S.; Shepherd, R. E. *Inorg. Chim. Acta* **1999**, *285*, 170-177.

(208) Salerno, J. C.; Siedow, J. N. *Biochim. Biophys. Acta* **1979**, *579*, 247.

(209) Westre, T. E.; DiCicco, A.; Filipponi, C. R.; Natoli, C. R.; Hedman, B.; Solomon, E. I.; Hodgson, K. O. *J. Am. Chem. Soc.* **1994**, *116*, 6757.

(210) Shepherd, R. E.; Ward, M. S. *Inorg. Chim. Acta* **1999**, *286*, 197-206.

(211) Shepherd, R. E.; Sweetland, M. A.; Junker, D. E. *J. Inorg. Biochem.* **1997**, 1-14.

(212) Shepherd, R. E.; Ward, M. S.; Borisenko, G. *Trans. Met. Chem.* **1999**, *24*, 224-232.

(213) Paul, A. K.; Mansuri-Torshizi, H.; Srivastava, S. J.; Chavan, M.; Chitnis, J. *J. Inorg. Biochem.* **1993**, *50*, 9.

(214) Paul, A. K.; Srivastava, T. S.; Chitnis, J.; Desai, K. K.; Rao, J. *J. Inorg. Biochem.* **1996**, *61*, 179.

(215) Shepherd, R. E.; Chen, Y.; Kortes, R. A.; Ward, M. S. *Inorg. Chim. Acta* **2000**, *303*, 30-39.

(216) Chen, Y. S., Rex E. *J. Inorg. Biochem.* **1997**, *68*, 183-193.

(217) Shepherd, R. E.; Chen, Y.; Sweetland, M. A. *Inorg. Chim. Acta* **1997**, *260*, 163-172.

(218) Shepherd, R. E.; Chatterjee, D.; Ward, M. S. *Polyhedron* **2000**, *19*, 1339-1346.